MODELING, SIMULATION AND MATHEMATICAL ANALYSIS OF QUANTUM PLASMAS

The Schrödinger Equation

Ravello summer school 2016

On Mathematical Physics

Claudia NEGULESCU

UNIVERSITÉ Paul Sabatier, Toulouse III

Institut de Mathématiques de Toulouse

Mathématiques pour l'Industrie et la Physique

Unité Mixte de Recherches CNRS - Université Paul Sabatier Toulouse 3 - INSA Toulouse - Université Toulouse 1

UMR 5640

UFR MIG, Université Paul Sabatier Toulouse 3, 118 route de Narbonne, 31062 TOULOUSE cédex 4, France

Foreword

These lecture notes summarize a succession of works of the author (with exception of the last chapter) dealing with the numerical resolution of the linear respectively non-linear Schrödinger equation, arising in different physical contexts. In particular the author is interested in the construction as well as mathematical and numerical study of multi-scale schemes, as for ex. *Asymptotic-Preserving* schemes, for the resolution of the Schrödinger equation in several regimes, as the semi-classical regime. The lectures are based on articles, which were chosen to illustrate different techniques in the design of efficient numerical schemes for singular perturbation problems. However, the here developped techniques can also be applied for various other singular perturbation problems.

The author would like to thank here her co-authors for the fruitful collaboration during the preparation of all the here cited articles, in particular *R. Adami, A. Arnold, N. Ben Abdallah, R. Carlone, R. Figari, M. Hauray*. Furthermore, the author is especially thankful to *L. Barletti*, for helpful discussions and suggestions as well as having corrected the introductory part of this work.

This work has been supported by the CNRS-PICS project “MANUS” (Modelling and numerics of Spintronics and Graphenes, 2016-2018).

CONTENTS

INTRODUCTION

The central theme of this course deals with the presentation of several numerical schemes for the discretization of the linear/non-linear Schrödinger equation occurring in various application fields.

The non-linear Schrödinger equation (NLSE) furnishes a general model permitting to describe, briefly speaking, a large class of wave propagation phenomena in non-linear media, more precisely it provides a description of the envelope dynamics of waves in a weakly non-linear dispersive medium, when dissipative processes are negligible. In particular, the Schrödinger equation involves a dynamical balance between a linear dispersion or spreading (generated by the Laplacian term $\Delta\psi$) and a non-linear (focusing or defocusing) self-interaction of the wave (generated by the non-linear term $\alpha|\psi|^\sigma\psi$). This equation (in its several forms) arises in apparently rather different fields of application, such as quantum mechanics, nanotechnology, nonlinear optics, hydrodynamics, plasma physics, biology and so on. As it permits to capture the physics of some interesting and stimulating non-linear phenomena and incorporates some specific mathematical and numerical difficulties and curiosities, the Schrödinger equation has had and still has more than its share of attention in the scientific community. All this shall be specified in a few words in this introduction and we shall pick up in the next chapters some typical applications of the Schrödinger equation to examine its distinguishing behaviours. But firstly, let us concisely overview the fields where the non-linear Schödinger equation occurs. I will give here only some examples, the list being really not exhaustive, and I will leave the most important example, which is the quantum mechanics, for the end.
Let us mention at this point, that the physical domains where the Schrödinger equation occurs, can be divided into two categories. In the first category enter the problems which manifest some kind of quantum behaviour, as for example interference effects, such that the most appropriate model for their description is the Schrödinger equation, which is the fundamental model of quantum mechanics. In the second category can be put the problems (classical), whose complex description requires some simplifications for a sketchy investigation and for which the Schrödinger equation offers an uninvolved approach. However one cannot justify rigorously in this latter cases the use of the Schrödinger equation from first principles, as for example from a microscopic quantum description. The Schödinger equation can be seen in this case as a sort of phenomenological model.

Non-linear optics [10, 49]

The field of non-linear optics is an active area of research since several years, with some important applications in communication systems, high power laser technology, optical tomography, fiber-optic sensor devices and so on. Optical fibers, made of pure glass, as well as optical amplifiers are used as waveguides to transmit light-waves (signals) over large distances without losses and attenuation (see Fig. 1). To model nonlinear phenomena in fiber optics, it is necessary to consider the field of electromagnetic wave propagation in dispersive media, the wave-propagation being governed by Maxwell's equations. These equations provide a general framework to study the nonlinear effects in optical fibers, however, because of their complexity, it is often necessary to make some simplifying approximations, which lead finally to the nonlinear equation

$$\mathbf{i}\partial_z A + \beta\partial_{tt} A - \mathbf{i}\alpha A + \gamma|A|^2 A = 0\,, \qquad \alpha\,,\beta\,,\gamma \in \mathbb{R}\,, \tag{1}$$

which coincides with the non-linear Schrödinger equation (NLSE) for $\alpha = 0$. The focusing case corresponds to $\beta\gamma > 0$, otherwise we are in the defocusing case. This equation describes the evolution of the (slowly varying) pulse-envelope $A(t,z)$ of a monochromatic plane-wave electric field $E(t,\mathbf{r}) = \Re\left[A(t,z)e^{\mathbf{i}(k_0 z-\omega_0 t)}\right]$, where z is here the longitudinal propagation direction, t the time and k_0 resp. ω_0 represent the pilot wavenumber resp. the frequency of the plane-wave. The term $\mathbf{i}\alpha A$ includes the effects of the fiber losses, $\beta\partial_{tt} A$ the chromatic dispersion and $\gamma|A|^2 A$ represents the fiber nonlinearity. In fiber optics, the soliton solutions of (1) (with $\alpha = 0$) are essential solutions, as they represent traveling wave-pulses with a remarkable stability, due to the balance between two forces: the linear dispersive force and the nonlinear, focusing force. This inbuilt stability property enables in principle solitons to travel over rather long distances without changes, such that they can be used to carry information in communication systems.

It is meaningful to remark here that in this case, the NLSE is only an approximate, simplified model for the investigation of nonlinear phenomena in fiber optics, and cannot be rigorously justified from microscopic models.

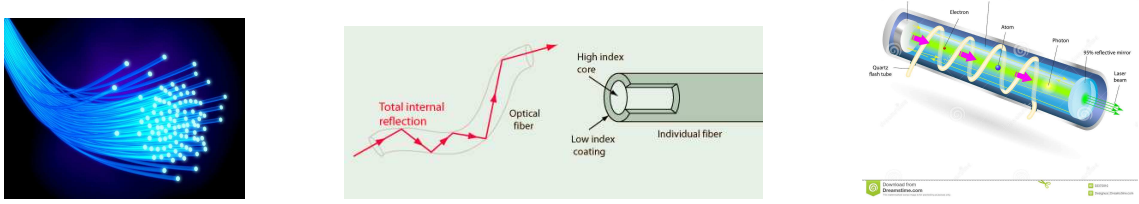

Figure 1: Optical fibers and lasers

Hydrodynamics [59, 76, 77]

Waves of extremely large size (giant or rogue waves, height over 10 m) are essentially non-linear objects. These deep-water waves are very steep and high and can appear right away from a relatively calm sea (see Fig. 2), due to the non-linear Benjamin-Feir instability and wave focusing; important damage can be caused consequently on ships and oil platforms. The dynamics of such surface gravity waves is usually described by the Navier-Stokes equations (or Euler equations under some suitable approximations and assumptions). Due to their complexity, it could be however advantageous to find a simpler approximation model, in order to investigate some particular features of these waves. In this context, the nonlinear Schödinger equation of focusing type

$$\mathbf{i}\partial_t A + \alpha\partial_{xx} A + \beta|A|^2 A = 0\,, \qquad \alpha\,,\beta \in \mathbb{R}\,, \tag{2}$$

provides a good description of the envelope dynamics of these surface giant waves. The function $A(t,x)$ represents the complex wave envelope, connected to the surface elevation $\eta(t,x)$ via the formula

$$\eta(t,x) = \Re\left[A(t,x)e^{\mathbf{i}(k_0 x-\omega_0 t)}\right], \qquad (t,x)\in\mathbb{R}^+\times\mathbb{R},$$

with k_0 the wave-number, ω_0 the frequency of the carrier wave, and the coefficients given by $\alpha = \frac{\omega_0}{8k_0^2}$, $\beta = \frac{\omega_0 k_0^2}{2}$. The Schrödinger equation is in this case just the first term in a hierarchy of envelope equations, describing such surface waves. It is clear however that such giant non-linear wave phenomena cannot be correctly modeled in terms of only envelope equations, but this description gives some valuable information about the formation of such waves, in particular it contains the two basic ingredients of surface dynamics: non-linearity and dispersion. One particular class of solutions of (2), so-called "breather"-type solutions, are considered as prototypes of rogue waves in oceans.
As in the case of non-linear optics, we would like to observe here again that the use of the NLSE cannot be justified in this field from microscopic quantum principles.

Figure 2: Rogue waves and their big distructive power

Plasma physics [32, 79, 81, 85]
Fusion plasmas are an inherently non-linear medium and far from being in thermodynamical equilibrium, due to the high temperatures needed to maintain the plasma. A

certain amount of energy is thus stored in a plasma, under different forms, which may be converted one into another through violent, non-linear phenomena, for example instabilities, turbulences. Several types of non-linear waves develop hence in a fusion plasma, as a manifestation of such abundant dynamical processes, even waves which cannot be found in other media as neutral gases. To mention an archetype of such waves, one can cite the Langmuir waves (electrostatic electron waves), where the energy is converted or oscillating between the kinetic particle energy and the electric field energy. These waves correspond to rapid oscillations of the electron density around a perturbed equilibrium state, thus also called electron plasma waves. At the basis of the description of Langmuir waves are the fluid equations (continuity and momentum equations, coupled to Poisson equation), however, the simplest model for the description of the propagation of the low frequency Langmuir wave-envelope is the NLSE for the electric field $E(t,x)$

$$\mathbf{i}\partial_t E + \frac{v_{th}^2}{2\,\omega_{pe}}\Delta E + \frac{\omega_{pe}\epsilon_0}{8\,k_B\,T_e}|E|^2\,E = 0\,, \qquad E = -\nabla\phi\,, \tag{3}$$

where v_{th} is the electron thermal velocity, T_e the electron temperature, ω_{pe} the electron plasma frequency (related to the Langmuir oscillations), ϵ_0 the permitivity of vacuum and k_B the Boltzmann constant.

Another typical specimen of plasma waves are the Alfvén waves (electromagnetic ion waves), where the converted energy forms are the kinetic particle energy and the magnetic field energy (see Fig. 3). Using the MHD model (Magneto-Hydrodynamics), it is possible to describe the propagation of these low frequency electromagnetic modes in a plasma. But, as for the former waves, due to the considerable complexity of the multi-dimensional MHD equations, an approximate, simpler model for their partial description is provided by the NLSE, which is similar to (3), with the electric field E replaced by the magnetic field $B(t,x)$ and other constants, depicting the evolution of the magnetic-field envelope-function, propagating in the medium.

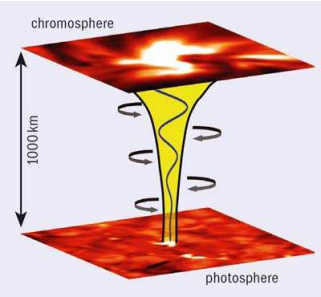

Figure 3: Creation of an Alfvén wave, propagating between two levels of the solar atmosphere

To bring up finally a third example, let us mention the zonal flow, which is an important phenomenon in fusion plasmas and consists in a $E \times B$ sheared flow, produced by toroidally and poloidally symmetric fluctuations of the electrostatic potential. Due to its shearing property, it attenuates turbulence in fusion plasmas and thus enforces its confinement, permitting to increase the reactor operation time. One possibility to generate zonal flows is by means of the drift-wave instability. Drift-waves are low frequency electrostatic ion waves, which are set into motion through a pressure gradient perpendicular to the external magnetic field. Drift-waves are described via the Hasegawa-Mima equations, which, under suitable assumtions, can be simplified to obtain again the Nonlinear Schrödinger equation, for the description of the slowly-varying drift-wave envelope.

Biology [69–71]

The cubic NLSE furnishes also an approximate description of various pulse-propagation phenomena in biological systems. In Bioenergetics for example, the question is how cells generate and transfer their supply energy. In this context the NLSE gives a simplified model for the α-Helix protein dynamics. In Neuroscience, the NLSE describes the electric pulse propagation, or simply the electrical activity, in nerve cells (neurons), permitting thus the investigation and understanding of the brain functioning. In Cardiology the NLSE serves as a model for the description of a traveling pulse, representing for example a heartbeat, or simply the propagation of an excitation in the human heart. Standard (classical) models for the description of the spatial propagation of potential pulses along nerve-systems are the Hodgkin-Huxley or the FitzHugh-Nagumo models, the NLSE however furnishes a simplified model for the description of the envelope propagation of the wave-front only and has the form

$$\mathbf{i}\partial_t u + \partial_{xx} u - 2|u|^2 u + \Phi(t,x,u)\, u = 0\,,$$

where $u(t,x)$ represents the action potential response of cells/neurons and Φ is a given (potential) function.

To understand better the relation between neurons and electricity, let us bring up here some words for clarity. The brain and the central nervous system control the organs via two distinct mechanisms: the hormonal system (which releases chemicals into the bloodstream, influencing thus particular organs) and the nervous system (which works via the very fast transmission of electrochemical pulses down specific paths between the brain and the organs). These pathways are called nerves and are constituted of thousands of neurons. A typical neuron (cell) can be seen in Fig. 4. The electric activity in nerve cells, as well as in heart muscle cells (myocyte), is generated by means of a simple mechanism, in particular via the motion of sodium ions (Na^+) and potassium ions (K^+) across the cell membranes (see Fig. 4). The imbalance in ion concentration (between the surrounding medium and the interiour of the axon) generates then the so-called action potential, which is then propagated as a wavefront down the axon.

Quantum mechanics

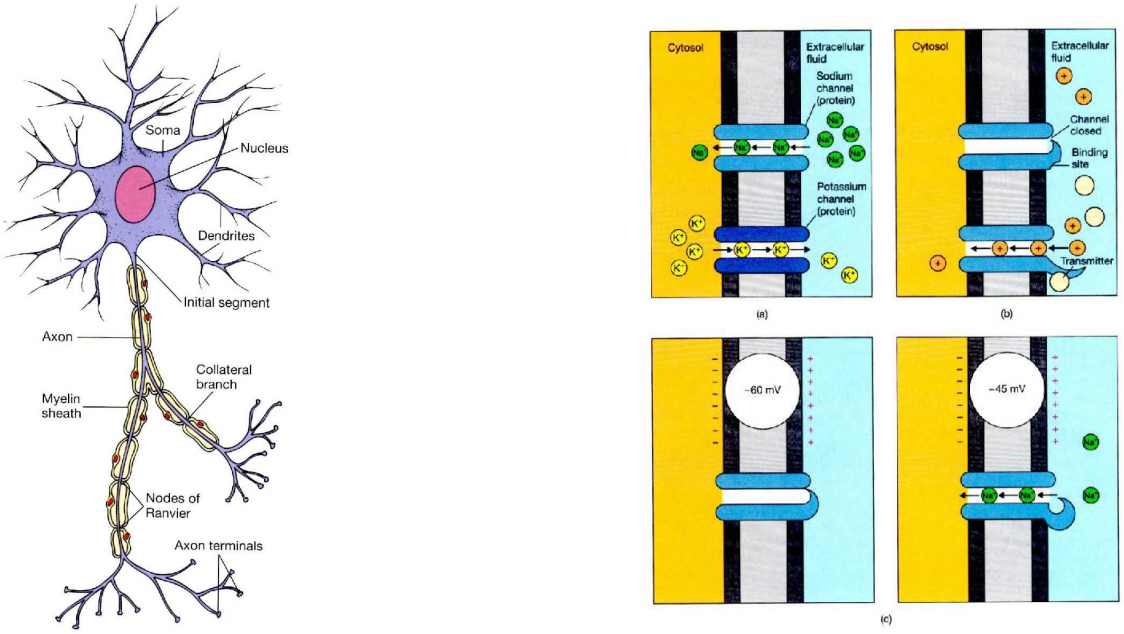

Figure 4: Left: A neuron. Right: Ions crossing the membran through protein pores (ion channels) and creating hence the action potential.

Let us come now to the main applications of this course. At the heart of quantum mechanics stands the Schödinger equation, describing the particles as waves (particle-wave dualism) propagating through space and time. The manner in which the Schrödinger equation describes the behaviour of the particles is very different from the corresponding description in classical mechanics. In classical mechanics a particle is characterized by its position $x \in \mathbb{R}^3$, which evolves in time $t \in \mathbb{R}^+$. The thus obtained trajectory of a classical particle $x(t)$ obeys Newton's law

$$m\,\ddot{x}(t) = F(t, x, \dot{x}), \quad t \in \mathbb{R}^+, \tag{4}$$

with F a force term (gravitational force, electromagnetic force, *etc*). In quantum mechanics, a particle has no longer a well-defined trajectory $x(t)$. Instead, each particle is considered as a wave, in particular it is described by means of a wave-function $\psi(t, x)$, where $|\psi(t, x)|^2\, dx$ represents the probability of finding the particle at time t in the space-volume dx around x. The equation which describes the evolution of this wave-function is the Schrödinger equation, which is the quantum analogue of Newton's laws (4). For a single particle of mass m, moving in a given external potential V this linear Schrödinger equation reads

$$\mathbf{i}\hbar\partial_t\psi = -\frac{\hbar^2}{2m}\Delta\psi + eV\psi, \quad (t, x) \in \mathbb{R}^+ \times \mathbb{R}^3, \tag{5}$$

where $\hbar$ is the rescaled Planck constant and e the particle elementary charge. The Hamilton operator $H := -\frac{\hbar^2}{2m}\Delta + eV$ is the observable of the total energy of the quantum-

mechanical particle, consisting of a kinetic energy operator (free Hamiltonian $H_0 := -\frac{\hbar^2}{2m}\Delta$) and a potential energy operator. The wave-function $\psi(t,x)$ contains all the necessary information to determine completely the state of a physical system. In particular, the macroscopic quantities, so-called observables, are then calculated via this wave-function, for example the density of the (single) particle $n(t,x)$ and the current density $j(t,x)$ are given by

$$n(t,x) := |\psi(t,x)|^2\,, \qquad j(t,x) := \frac{\hbar}{m}\Im(\overline{\psi(t,x)}\,\nabla\psi(t,x))\,.$$

If the potential is created selfconsistently, the Schrödinger equation (5) has to be coupled with the Poisson equation

$$-\Delta V = n(t,x)\,, \qquad (t,x) \in \mathbb{R}^+ \times \mathbb{R}^3\,.$$

The statistical interpretation of the wave-function $\psi(t,x)$ introduces however a sort of indeterminacy into quantum mechanics, which is different from the completely determined classical picture, where the exact position and momentum of a particle are entirely known by the initial conditions. In quantum mechanics you have only a statistical information about the position and momentum of the particle. In fact, Heisenberg's uncertainty principle

$$\Delta x\,\Delta p \geq \hbar/2\,,$$

where Δx and Δp are the uncertainties in space and momentum, gives a theoretical limitation on the accuracy of a simultaneous measurement of the position and momentum of a particle, or other pairs of observables with operators which do not commute (time and energy for example). It is a fundamental principle, which has nothing to do with technical imperfections of the measurement apparatus. One can remark now that the Planck constant is a fundamental parameter which enables to pass from the quantum-mechanical picture to the classical picture, as $\hbar \to 0$. This simply means that the limitation predicted by Heisenberg's principle is not remarkable at the macroscopic level, where $\hbar \ll 1$ meaning that $\hbar$ is small with respect to other variables. The limit $\hbar \to 0$ is the so-called "semi-classical" limit and is related to the high-frequency limit of the Schrödinger equation. In reality one has $\hbar = 10^{-34}\,Js$.
In this sense, the Schrödinger equation is an appropriate model to describe physical phenomena which exhibit some sort of quantum behaviour with no classical explanations. Such typical quantum effects, are for example:

- Energy-level quantization, visible for ex. in low-dimensional systems;
- Tunneling through a thin insulating region (RTDs, MOSFETs);
- Interference effects between two different wave-packets (electron paths);
- Quantum Hall effects, which are Landau levels formed via a high magnetic field;
- Superconductivity in hetero-structures, obtained by phase-coherent effects.

This course will be mainly concerned with the following three applications:

Particle transport in nanoscale semiconductor devices [66–68]
Semiconductor devices are today's most essential components in electronic industry. Some examples of such devices are photodiodes, laserdiodes, resonant-tunneling diodes (RTD), field-effect transistors (MOSFET) *etc*, generally employed as detectors, amplifiers, modulators, electronic switches and so on. The increasing need of new reliable devices, which are more functional, less energy-consuming and high speed, requires a better comprehension of the multitude of physical phenomena arising in such structures. One of the reasons for the great success of semi-conductor devices is their very small, nano-scale size, allowing higher electron mobilities. At this nano-metric scales, quantum effects start to play an important role, such that the most appropriate model to describe the electron transport is a fully quantum, ballistic model, based on the Schrödinger equation.
Chapter 2 will be concerned with an application in this field, namely the modeling of the electron transport through a RTD (Resonant Tunelling Diode) via stationary, one-particle Schrödinger equations. Despite their simple structures, RTDs are still intensively studied because they constitute a good prototype for electron-wave tests, which permit to investigate several manifestations of quantum transport in semi-conductor structures. Besides, RTDs enable to proceed to study more complex and advanced quantum systems, such as for example MOSFET-transistors, and have potential applications in very high-speed devices and circuits. For all these reasons, we shall concentrate in Chapter 2 on an RTD-example to treat numerically highly oscillating, linear and stationary Schrödinger equations with an appropriate multi-scale scheme.

Quantum chemistry [28, 65]
One of the goals of quantum chemistry is to understand matter at its most fundamental level, for example by investigating the electronic structures of atoms and study thus the properties of molecules, like stability, atom arrangements, magnetization, *etc*.
At the atomic level, the force governing the system is the Coulomb interaction force (Coulomb potential V) between the charged particles. The whole N-particle system (electrons+nuclei) can then be described by means of the time-dependent, linear many-body Schrödinger equation of the form

$$\mathbf{i}\hbar\partial_t\Psi(t,x,X) = -\frac{\hbar^2}{2m}\Delta_x\Psi - \frac{\hbar^2}{2M}\Delta_X\Psi + V(x,X)\,\Psi\,, \qquad \forall (t,x,X)\in\mathbb{R}^+\times(\mathbb{R}^3)^{N_e}\times(\mathbb{R}^3)^{N_n}\,,$$

where $\Psi(t,x,X)$ is here the wave-function describing the evolution of the whole system, consisting of N_e electrons, with mass m and positions $x_i\in\mathbb{R}^3$, and N_n nuclei, with mass M and positions $X_j\in\mathbb{R}^3$. For many-particle system ($N := N_e + N_n \gg 1$) a numerical resolution of this equation is very expensive or even out of reach. Several approximations can then be considered.
Let us mention here the Born-Oppenheimer approximation, which corresponds to assuming that the nuclei are much more heavier than the electrons, such that they are

considered as stationary, forming a frozen charged background, while the electrons are evolving. Doing so, the rapid electron dynamics is separated from the rest of the system, and these electrons are governed by one N_e-body Schrödinger equation, which is coupled to the nuclei dynamics via the interaction potential V.
The new electronic many-body problem can still be too expensive to be solved numerically. This time, a different approximation can render the problem simpler. In particular, the Hartree-Fock approximation corresponds to the approximation of the N_e-body electron system by several (N_e) single-particle Schrödinger equations, each particle evolving now in an averaged (mean-field) potential, determined by the position of the other particles. In this contexte, Chapter 3 will be concerned with the numerical resolution of a two-body Schrödinger equation in the aim to better understand the so-called *decoherence* phenomenon.

Condensed matter physics [24, 80]
The study of Bose-Einstein condensates (BEC) has become a very active research field, first of all for its importance in basic research. A BEC is a macroscopic, purely quantum mechanical phenomenon, being related to the way of how particles interact to each other. In more details, a BEC consists of a macroscopic ensemble of atoms, confined in a potential trap and occupying the same one-particle quantum-state (bosons). At very small temperatures (beyond some critical temperature T_c) the BEC is well-described by a single-particle wave-function $\psi(t,x)$ whose evolution is governed by the NLSE, also called in this context "Gross-Pitaevskii" equation (GPE)

$$\mathbf{i}\hbar\partial_t\psi = -\frac{\hbar^2}{2m}\Delta\psi + V\psi + \gamma|\psi|^2\psi\,, \qquad (t,x)\in\mathbb{R}^+\times\mathbb{R}^3\,, \quad \gamma\in\mathbb{R}\,.$$

This equation is a mean-field approximation of the many-body Schrödinger equation, describing the collection of a multitude of interacting bosons. The study of a BEC is so interesting, as after the cooling processes, the condensate acquires some special, typical quantum-mechanical properties, as for example the superfluidity or the creation of vortices. These features have certain quantum mechanical pecularities (quantization for vortices for example), which can be seen as a manifestation of quantum effects on a macroscopic scale.
The BEC are also the object of intense studies, due to possible (future) applications, as for example in precision measurement (replacing the lasers?), or in quantum information processes (vortices as bits?). However, we are still far away from seeing clearly, what for BEC can be used. Chapter 5 shall present a numerical scheme for an efficient resolution of a one-dimensional Gross-Pitaevskii equation, suitable for this context.

Mathematical and numerical particularities [30, 31, 93]
The nonlinear Schrödinger equation (NLSE) belongs to the family of nonlinear dispersive equations of Hamiltonian type, such as the Sine-Gordon, the Klein-Gordon equations, the KdV equations, the Gross-Pitaevskii equation and so on. It can take slightly different forms, however all these forms share common characteristics, as for example

the conservation of mass, energy and other specific features. In particular, the following mathematical questions are crucial in the study of the nonlinear Schrödinger equation as well as more generally in the study of nonlinear wave phenomena, and raised a lot of interest in the last years:

- well-posedness: existence/uniqueness results as well as stability criteria for solutions (blow up); IST-methods;
- conservation of several macroscopic quantities (mass/energy);
- study of solitons, which are particular solutions of the NLSE emerging due to a balance between the nonlinearity and the dispersion property;
- study of the semi-classical regimes (asymptotic analysis) as $\hbar \to 0$; quantum-to-classical transition;
- study of the many-body asymptotics (Born-Oppenheimer, Hartree-Fock, mean-field limits).

Special attention is paid often to soliton solutions or simply solitons, which are local traveling wave-structures with remarkable stability properties. Soliton-like behaviours have been observed in fiber optics, water waves, biological systems *etc*, which explains somehow the appearance of the Schrödinger equation as a model in all the above mentioned fields.

One of the goals of a numerical scientist is to develop efficient as well as precise numerical schemes (accurate, not time- and not memory-consuming) for the discretization of a given mathematical problem, arising from the modeling of a physical/biological/chemical phenomenon. The numerical simulation is an important tool, additional to the theoretical study, for getting deep insight into a given problem, for example understanding better a certain phenomenon, as an instability or turbulences *etc*. Furthermore simulations have many advantages as compared to experiments, for example the advantage of being secure, design-flexible, having controllable environments, high reproducibility, high efficiency when thinking of the cost-benefit ratio. However, experiments will always be needed, in order to validate the mathematical models and the numerical schemes.

It is usually a big challenge to develop numerical schemes which balance well the two rather contradictory requirements of "efficiency" and "precision". Usually one has to make a compromise between these two quantities, meaning that one has to avoid unnecessary computations to be performant, however trying at the same time to attain the required accuracy. Another difficulty in the numerical science is the treatment of multi-scale problems. Multi-scale problems arise very often in nature, and are characterized by the fact that the solution contains multiple dynamics or behaviours, which have to be captured in an adequate manner by the scheme without so much numerical effort. We shall go into more details on multi-scale problems and their numerical

treatment in the next chapter. For the moment, let us only mention here the typical numerical difficulties one encounters when dealing with the numerical resolution of the (non-linear) Schödinger equation in one of the above mentioned applications:

- the high dimensionality of the problems (many-body problems);
- the balance or competition between dispersive effects and non-linearity (soliton solutions);
- the occurrence of highly oscillating wave-functions (semi-classical limit);
- the numerical preservation of various properties (mass/energy conservation);
- the prescription of appropriate boundary conditions (avoiding spurious, non-physical effects).

I OUTLINE

The present work is a review of several numerical schemes (in particular multi-scale and Asymptotic-Preserving schemes), constructed for the resolution of the linear/ non-linear Schödinger equation in different contexts or applications. Inevitably, the choice of the model problems is related to the author's knowledge and to the concept of providing the reader with the most important features of multi-scale and AP-schemes. Such schemes are not specific for the here presented equations, but can be designed for several other singularly perturbed problems, that admit asymptotic regimes.

An overview of the subject of this manuscript is:

- Chapter 1 introduces the concept of multi-scale problems and numerical schemes;
- Chapter 2 deals with the stationary, linear Schödinger equation in the semi-classical regime; the concerned application is the simulation of the electron transport in a RTD;
- Chapter 3 discusses the time-dependent, linear Schödinger equation in an anisotropic two-dynamics or two-body framework; aim is to study the so-called "decoherence-effect";
- Chapter 4 considers a time-dependent Schrödinger equation with Delta-Dirac point interactions to describe the so-called "beating-effect" in an ammonia molecule;
- Chapter 5 deals finally with the cubic non-linear Schödinger equation, applied to the modeling of BECs.

CHAPTER 1

MULTI-SCALE PROBLEMS

Before embarking on a detailed description of numerical schemes for the linear/nonlinear Schrödinger equation, it may be useful to take a wider look at the so-called multi-scale problems, which are at the basis of all the mathematical problems investigated in the sequel.

Multi-scale problems arise very often in nature. When we say that a problem is multi-scale, we broadly mean that it involves phenomena at disparate spatial and/or temporal scales, spanning over several orders of magnitude. More importantly, these phenomena all play key roles in the problem, so that we cannot correctly model the problem under study without explicitly accounting for all these different scales.

To mention only some examples, we can think of fluid dynamics, which is a broad field, emerging in aeronautics, medicine, biology, meteorology, electronics, astrophysics *etc* and which is characterized by the existence of several length and temporal scales, ranging over a wide spectrum. Indeed, turbulent flows (high Reynolds numbers flows) can be defined as multi-scale, dynamic and chaotic phenomena, where vortices of various sizes appear chaotically. Multiple scales exist also in laminar flows (low Reynolds numbers), for example in the occurrence of boundary layers at the interface with a wall. Furthermore, in shear flows (laminar or turbulent) a big discrepancy exists between the "diffusive" length scale across the flow and the "convective" length scale along the flow, discrepancy which leads to interesting approximations as well as difficulties in numerics.

Biological systems involve also a large variety of spatial as well as temporal scales. Looking upon from the lowest to the highest scales, we can mention at the atomic/molecular level the DNA-processes (described via quantum mechanics and evolving on time-scales of approx. $10^{-6}\,s$), at the cellular scale one has the metabolism-processes ($10^{-3} - 10^{0}\,s$), at the tissue scale the cell-migration and cell-division ($10^{0} - 10^{3}\,s$), at the organ-scale the familiar heart-beating, breathing, the neuronal signaling processes ($10^{0} - 10^{6}\,s$) and finally at the macroscopic level, the population dynamics, social interactions and epidemics ($10^{3} - 10^{9}\,s$). In Fig. 1.1 one can get a look at the different scales present in biological systems, as for example the human body.

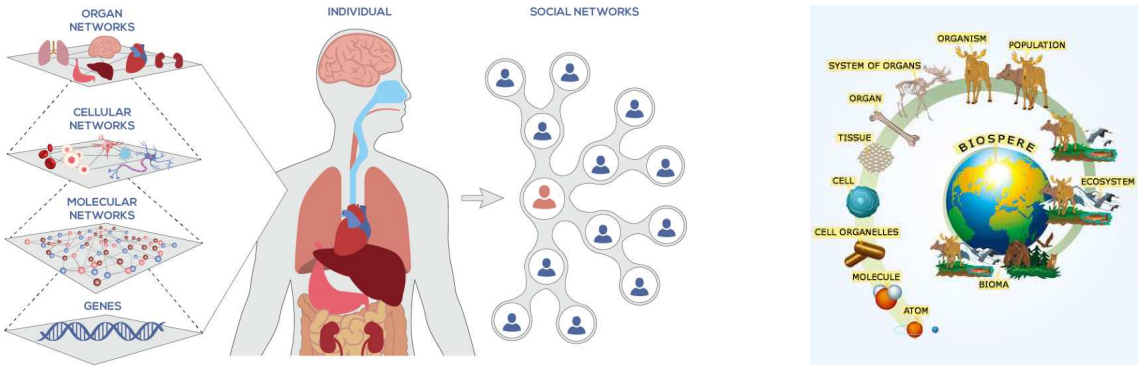

Figure 1.1: Different time and space scales in biological systems

Plasma dynamics reveals on its turn a vast range of time and space scales. Indeed, magnetism creates anisotropy, which means that the properties of the plasma are rather different when considered in the parallel or in the transverse direction with respect to the magnetic field lines. This anisotropy contributes, jointly with other phenomena, to the multi-scale dynamics of the plasma. As an example, concerning the temporary scales, one can pass from the fast electron plasma frequency ω_p, to the fast Larmor gyromotion ω_c, further to the collisional frequencies $\nu_{i,e}$ and finally to the confinement time τ_E, as observed in Fig. 1.2. Concerning the spatial scales, it ranges from the small Debye length λ_D, to the electron Larmor radius ρ_e, further to the mean free path of the particles and finally to the spacial extent of the tokamak L.

In chemistry, the chemical reactions can take seconds or hours, while the vibrations of atoms and molecules occurs in femto-seconds. In wave-mechanics, propagation of wave-packets contains short wave-lengths (corresponding to the underlying fast plane-wave modes) and the slowly-varying scale of the envelope-evolution. A multitude of other problems in nature exhibit multi-scale behaviours, which can be rather different in character. One can divide these problems in two categories. On one hand we have problems which exhibit local singularities, like for example boundary or internal layers, shocks, dislocations and so on. On the other hand we have problems, where microscopic and macroscopic scales coexist in the whole domain, as for example porous media flows, turbulent flows, highly oscillating problems *etc.* A general, unified treatment of all these problems is impossible, such that a lot of techniques have been developed in literature, each one being adapted to a particular situation.

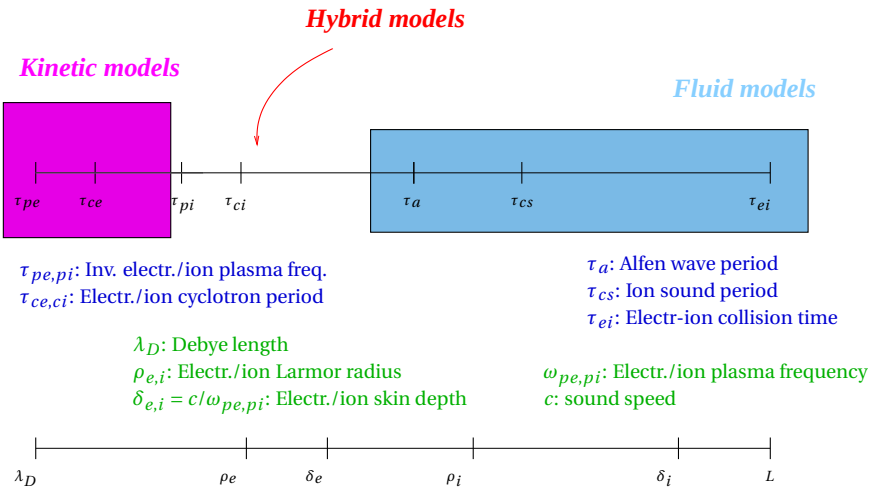

Figure 1.2: Different time and space scales occurring in a fusion plasma

I SINGLE-SCALE AND MULTI-SCALE APPROACHES

When several scales occur in a physical problem, it is no more adequate to use the so-called "traditional approaches" which describe the phenomenon on a single scale. Describing the problem on a microscopic level is physically very accurate, however from a computational point of view unfeasible. Using a macroscopic description, which means a model which uses explicit equations for the macroscopic scale, eliminating the other scales, is also inappropriate. Indeed, this procedure uses often empirical closures for the elimination/description of the microscopic scales, that are not justified nor well understood, as for example the viscosity tensor terms in turbulent flows. In all these cases, one has to proceed to multi-scale modeling, for example using different models, which describe the various phenomena on their different scales; and all this by taking care to achieve a balance between accuracy of the numerical results and efficiency of the numerical method. Briefly, the main goal of multiscale techniques is to design microscopic-macroscopic numerical methods, which are more efficient than solving the full microscopic model and at the same time furnish the desired accuracy.

To be more precise, suppose we are interested in the evolution of a macroscopic quantity, say U, but we do not have an explicit macroscopic model for the description of U, which is valid everywhere. This can be either because we lack the constitutive relation or because the macroscopic model is invalid due to the presence of localized singularities for example. However, we dispose of a microscopic model, describing the dynamics of a microscopic quantity u, which is related to U by a relation $F(u) = U$. Our goal is to accurately approximate the variable U, using a macroscopic grid, in order to be efficient from a computational point of view. A standard method would require to use a fine grid, in order to resolve the small scales of the problem, obtaining thus u,

and computing then the correct macroscopic solution via the function $F(\cdot)$. However, this is usually a computationally phenomenal and unfeasible work. And moreover, for most engineering purposes, it is even unnecessary to know all the details of u. Engineers are often contented with accurate time-averaged properties of the flow, as the averaged velocities, pressures *etc*.

Multi-scale methods were thus introduced in literature, based on different ideas, however with the same aim, which is to capture the macroscopic evolution, using the necessary/required microscopic information, without however having to resolve in detail the microscopic behaviour. Some analytical techniques to cope with multi-scale problems are for example the "matched asymptotics method", used for problems which undergo rapid variations in localized regions, or the "homogenization methods", employed in the case of problems with oscillating coefficients and based on asymptotic expansions. Among the numerical approaches can be counted the multigrid methods and the adaptive mesh refinements, which are efficient techniques for the resolution of the small-scale behaviour of the solution. Furthermore, domain decomposition methods aim to couple different mathematical descriptions, corresponding to different regions of the domain, where the physics is distinct. And finally, multiscale finite element methods employ basis functions, which incorporate the small-scale information, permitting thus the use of coarse grids. For a detailed description of all these methods, we refer to the textbooks [40, 50, 62] as well as all the references therein.

To summarize briefly the advantages of multi-scale techniques, let us mention here, that for the fine-scale scientist, a multi-scale approach allows to study much larger systems or longer times, than could be studied using the fine-scale model. For the coarse-scale scientist, the multi-scale model is viewed as a way to establish the constitutive laws of the problem from first principles, or at least from the coarse-scale alone.

II ASYMPTOTIC-PRESERVING SCHEMES

The solutions of singularly perturbed problems reveal a typical multiscale character, and their numerical resolution presents some major difficulties. Singular perturbation problems are mathematical problems characterized by the occurrence of one or several small parameters, denoted in this section by $0 < \varepsilon \ll 1$, and where mathematical as well as numerical difficulties arise due to a change in type of the equation as $\varepsilon \to 0$. The solutions of a singularly perturbed problem show a non-uniform behaviour as the parameter tends to zero, for instance the character of the limiting solution is different in nature from that of the solutions for finite values of $\varepsilon > 0$. Examples of such singularly perturbed problems are viscous flows with large Reynolds numbers, convective heat transport with large Peclet numbers, low Mach number flows, diffusive relaxation in kinetic models and so on.

Asymptotic-Preserving schemes are efficient procedures for solving singularly perturbed problems, denoted here by P^ε. The solution of P^ε is supposed to converge, as the perturbation parameter tends to zero, towards the solution of a limit problem P^0, which is a well-posed problem. However, the fact that the singular limit $P^\varepsilon \to_{\varepsilon\to 0} P^0$ leads to a change in the type of the equation, explains somehow the difficulties encountered when trying to solve P^ε for too small ε-values. The use of standard numerical schemes for the resolution of singularly perturbed problems requires, due to stability reasons, very restrictive time and space dicretization step conditions, of the type $\Delta t, \Delta x \sim \mathcal{O}(\varepsilon)$ or $\Delta t, \Delta x \sim \mathcal{O}(\varepsilon^2)$. This becomes rapidly too costly from a numerical point of view and consequently a numerical asymptotic study and even numerical simulations for small ε-values, are out of reach. Moreover, standard implicit schemes (even if computationally heavy) may be uniformly stable for $0 < \varepsilon < 1$, but yet provide a wrong solution in the limit $\varepsilon \to 0$, which means the scheme is not consistent with the limit problem P^0. Thus the design of robust numerical methods for singularly perturbed problems, whose accuracy does not depend on the parameter ε (hence on the local scales of the singularity), allowing even to capture the limit $\varepsilon \to 0$, becomes an important task.

In order to tackle such problems, several methods were introduced in literature. One approach can be to solve directly the limit problem P^0 instead of P^ε, if ε is small. However, in some situations, the parameter ε can vary within the simulation domain, making thus this approach unusable. Indeed, ε is the ratio of two characteristic lengths, which can vary in space as well as in time. In this case, hybrid techniques can be employed, solving P^ε there where $\varepsilon \sim \mathcal{O}(1)$ and P^0 where ε is rather small. Several difficulties can be encountered with this approach, for example how to locate the interface between P^ε and P^0 and what type of interface conditions to use. Thus, this approach can be difficult to implement in practice.

Asymptotic-Preserving schemes were introduced the first time by S. Jin [57] with the aim to cope with such singularly perturbed problems, in particular in the framework of kinetic models in a diffusive regime. The construction of these AP-schemes necessitates the existence of a well-posed limit problem P^0, which has to be identified beforehand. The main feature of these schemes is that they permit a precise, ε-independent, resolution of the problem P^ε as well as of its limit problem P^0, with no huge computational effort. The main idea for the construction of AP-schemes is based on asymptotic arguments and consists in a mathematical reformulation of the singularly perturbed problem P^ε into an equivalent problem $(AP)^\varepsilon$, which is a regular perturbation of the limit problem P^0. The equivalent reformulation of P^ε into $(AP)^\varepsilon$ is a sort of "reorganization" of the problem into a form which is better suited for the numerical discretization, and permits to approach for $\varepsilon \to 0$ the limit model in a mathematically regular manner. The same numerical scheme is then used for the discretization of $(AP)^\varepsilon$ as well as for P^0, which means that they allow for an automatic numerical transition from P^ε to P^0. Remark that the AP-reformulation is by no means unique, and several AP-schemes can be conceived/designed for the same problem. It

is necessary to underline here that the asymptotic preserving techniques are not used to derive a simplified "macroscopic" model, which is then solved numerically. Rather the objective is to construct a numerical scheme, using asymptotic techniques, whose solution does not deteriorate as the singular limit is approached.

To summarise, the essential properties of AP-schemes are (see diagram 1.3):

- for fixed $\varepsilon > 0$, the AP-scheme, denoted in this diagram $P^{\varepsilon,h}$, is a consistent discretization of the continuous problem P^{ε}, where $h = (\Delta t, \Delta x)$
- the stability condition is independent of ε
- for fixed discretization parameters $h = (\Delta t, \Delta x)$, the AP-scheme $P^{\varepsilon,h}$ provides in the limit $\varepsilon \to 0$ a consistent discretization of the limit problem P^0

Thus, the asymptotic-preserving approach consists somehow in trying to mimic on the discrete level the asymptotic behaviour of the singularly perturbed problem solutions. It is thus very important to have a full understanding of the solutions behaviour. Remark that the AP-techniques have to be distinguished from the multiscale techniques, as the former solve the micro-scales when the (spacial or/and temporal) mesh-sizes resolve these scales and automatically switch to the macroscopic behaviour when the mesh-sizes do not resolve the micro-scales. In other words, the AP-schemes catch the numerical transition from microscopic to macroscopic scales, in some difficult situations as for singularly perturbed problems, however their primary focus is not to reduce the computational costs, as the multiscale methods do.

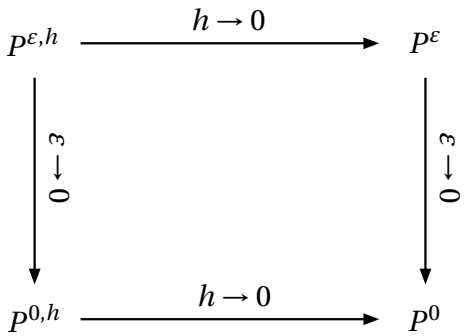

Figure 1.3: Properties of AP-schemes

CHAPTER 2

STATIONARY SCHRÖDINGER EQUATION IN THE SEMI-CLASSICAL LIMIT

Chapter based on the articles:
C. Negulescu [1]
A. Arnold, N. Ben Abdallah, C. Negulescu [2]
A. Arnold, C. Negulescu [3]

Highly oscillating phenomena occur in several fields of application, as for example quantum mechanics, electro-magnetics, fluid dynamics, acoustics, electrodynamics, plasma transport, molecular dynamics and so on. The difficulty with high oscillations becomes immediately visible if one attempts to produce accurate numerical results. In principle, increasing the resolution of the computation by choosing finer and finer grids, improves the precision of the results. However this procedure requires hugh computational resources and long simulation times, which become rapidly unacceptable. An adequate treatment of such problems requires hence a multi-scale approach, as will be seen in this chapter.

In the focus of this chapter stands the stationary linear Schrödinger equation in the semi-classical regime

$$\varepsilon^2\psi''(x) + a(x)\psi(x) = 0\,, \quad x \in \mathbb{R}\,, \tag{2.1}$$

where $0 < \varepsilon \ll 1$ is a very small parameter and $a(x)$ a piecewise, sufficiently smooth function. This equation describes the ballistic electron transport through nanoscale devices like resonant tunnel diodes (RTD) or MOSFET transistors. The here introduced multi-scale treatment of the problem is based on WKB-basis functions, permitting to filter out the oscillations and transform the problem into a smoother one.

[1] "Numerical analysis of a multiscale finite element scheme for the resolution of the stationary Schroedinger equation", Numerische Mathematik 108 (2008), no. 4, 625–652.

[2] "WKB-based schemes for the oscillatory 1D Schroedinger equation in the semi-classical limit", SINUM (SIAM J. on Numerical Analysis) 49 (2011), no. 4, 1436–1460.

[3] "Stationary Schrödinger equation in the semi-classical limit: numerical coupling of the oscillatory and evanescent regions", submitted.

I THE MATHEMATICAL PROBLEM

The application we are interested in here, stems from the electron transport in nanoscale semiconductor devices. In a 1D model setting, which is appropriate for RTDs or for the longitudinal dynamics in each transversal mode in MOSFETs, the governing equation is the stationary Schrödinger equation:

$$\begin{cases} -\varepsilon^2\psi''(x) + V(x)\psi(x) = E\psi(x)\,, \quad x \in (0,1)\,, \\ \varepsilon\psi'(0) + i\sqrt{a(0)}\,\psi(0) = 0\,, \quad \text{if } a(0) > 0\,, \\ \varepsilon\psi'(0) - \sqrt{|a(0)|}\,\psi(0) = 0\,, \quad \text{if } a(0) < 0\,, \\ \varepsilon\psi'(1) - i\sqrt{a(1)}\,\psi(1) = -2i\sqrt{a(1)}\,. \end{cases} \qquad a(x) := E - V(x)\,, \tag{2.2}$$

This equation describes the state of an electron that is injected with the prescribed energy $E > 0$ from the right lead into an electronic device, modelled on the interval $[0,1]$. The corresponding (complex valued) wave function is denoted by $\psi(x)$, where $|\psi(x)|^2$ is related to the spatial probability density of the electron.
The boundary conditions in (2.2) are the so called open or *transparent boundary conditions*, permitting an electron wave to enter or leave the device without reflections [63]. For this we assumed that the given electrostatic potential V is constant outside the device. To allow for an injection at $x = 1$, we have to require that $a(1) > 0$. In fact, $E > V(x)$ characterises the oscillatory, classically allowed regime, whereas $E < V(x)$ characterises the evanescent, classically forbidden regime. Fig. 2.1 sketches a tunneling structure similar to the one we shall consider, including both regimes.

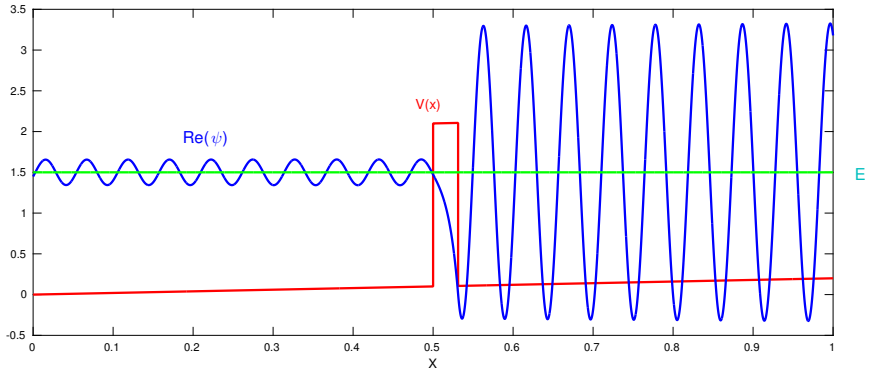

Figure 2.1: Tunnelling structure with injection of a plane wave from the right ($x = 1$). Red curve: piecewise linear potential $V(x)$ with applied bias. Blue curve: $\Re(\psi(x))$, real part of the wave function that is partly transmitted, but mainly reflected in this example; $\varepsilon = 0.01$. Green line: energy of the injected plane wave with $E < \max V(x)$.

The goal of this chapter is to introduce a numerical method coupling the oscillatory and evanescent regimes of our device via WKB-ansatz functions for both situations. On the one hand, for $a(x) > 0$, the solution is highly oscillatory, with the small (local) wave length $\lambda(x) = \frac{2\pi\varepsilon}{\sqrt{a(x)}}$. On the other hand, for $a(x) < 0$, the wave function ψ is (essentially) exponentially de/increasing, typically exhibiting a thin boundary layer with thickness of the order $\mathcal{O}\big(\frac{\varepsilon}{\sqrt{|a(x)|}}\big)$. A key aspect of this work is that $a(x)$ takes both signs, such that we have to cope with a classical multi-scale problem, combining different types of arduousnesses and multi-scale behaviours. Numerically, we aim at recovering these fine structures of the solution, *without* having to use a fine spatial grid. For this we shall develop a (non-overlapping) domain decomposition method (DDM) to separate the oscillatory and evanescent regions, as they require very different numerical approaches.

In the oscillatory regime we shall use the marching scheme from [14], and in the evanescent regime a FEM like in [**?**]. In the first case, the key idea is to eliminate analytically the dominant oscillations of the solution to (2.1). The transformed problem then has a much smoother solution, in the sense that the amplitude of the residual oscillations is much smaller than in the original problem – often by many orders of magnitude. Hence, the new problem can be solved numerically on a coarse grid, still yielding a very accurate approximation. In the evanescent regime, the key idea of the WKB-FEM method is to use WKB-ansatz functions (of exponential type), rather than the standard polynomials. The strategy is the same as in the oscillatory region: filter out the boundary layers via well-chosen basis functions. Since WKB-basis functions are asymptotic solutions to (2.1) (as $\varepsilon \to 0$), this method is very accurate on coarse grids.

For the solvability of the model (2.2), the following simple result holds:

Proposition 1. *[15] Let $a \in L^\infty(0,1)$ with $a(0) \neq 0$ and $a(1) > 0$.*[4] *Then the boundary value problem (2.2) has a unique solution $\psi \in W^{2,\infty}(0,1) \hookrightarrow C^1[0,1]$.*

Let us remark finally that turning points (zeros of the function a) are excluded in our analysis, so that we shall concentrate on devices with abrupt jumps in a. The reason for this is that the WKB-approximation presented below is not valid at turning points.

The WKB-technique

Both parts of the hybrid numerical method we shall introduce in §III are based on WKB functions. Hence, let us first review the well-known WKB-approximation (cf. [60])

[4] Here and in the sequel, $a(0)$ and $a(1)$ are not meant as the point values of the function a (which would not be defined for an L^∞–function), but rather as the const. pot. in the left and right leads.

for the singularly perturbed ODE (2.1). In the standard approach, for the oscillatory regime (i.e. $a>0$), the WKB-ansatz

$$\psi(x) \sim \exp\left(\frac{1}{\varepsilon}\sum_{p=0}^{\infty}\varepsilon^p\phi_p(x)\right), \tag{2.3}$$

is inserted in (2.1) and after comparison of the ε^p-terms, leads to

$$\begin{aligned}
\phi_0(x) &= \pm\mathbf{i}\int_0^x\sqrt{a(y)}\,dy+const.,\\
\phi_1(x) &= \ln a(x)^{-1/4}+const.,\\
\phi_2(x) &= \mp\mathbf{i}\int_0^x\beta(y)\,dy+const., \qquad \beta:=-\frac{1}{2|a|^{1/4}}(|a|^{-1/4})''.
\end{aligned} \tag{2.4}$$

Truncating the ansatz (2.3) after $p=0,1$, or 2, yields the asymptotic approximation $\psi(x)\approx C\varphi_p^{os}(x)$, with the following *oscillatory WKB-functions*:

$$\begin{aligned}
\varphi_0^{os}(x) &= \exp\left(\pm\frac{1}{\varepsilon}\int_0^x\sqrt{a(y)}\,dy\right),\\
\varphi_1^{os}(x) &= \frac{\exp\left(\pm\frac{1}{\varepsilon}\int_0^x\sqrt{a(y)}\,dy\right)}{\sqrt[4]{a(x)}},\\
\varphi_2^{os}(x) &= \frac{\exp\left(\pm\frac{1}{\varepsilon}\int_0^x\left[\sqrt{a(y)}-\varepsilon^2\beta(y)\right]dy\right)}{\sqrt[4]{a(x)}}.
\end{aligned} \tag{2.5}$$

Proceeding analogously for the evanescent regime (i.e. $a<0$) yields the following *evanescent WKB-functions* (of the three lowest orders in ε):

$$\begin{aligned}
\varphi_0^{ev}(x) &= \exp\left(\pm\frac{1}{\varepsilon}\int_0^x\sqrt{|a(y)|}\,dy\right),\\
\varphi_1^{ev}(x) &= \frac{\exp\left(\pm\frac{1}{\varepsilon}\int_0^x\sqrt{|a(y)|}\,dy\right)}{\sqrt[4]{|a(x)|}},\\
\varphi_2^{ev}(x) &= \frac{\exp\left(\pm\frac{1}{\varepsilon}\int_0^x\left[\sqrt{|a(y)|}+\varepsilon^2\beta(y)\right]dy\right)}{\sqrt[4]{|a(x)|}}.
\end{aligned} \tag{2.6}$$

In the hybrid numerical method analysed in §III we shall use the first order WKB ansatz functions φ_1^{ev} for the FEM in the evanescent region. And in the oscillatory region we shall use the second order WKB functions φ_2^{os} to transform (2.1) into a smoother problem that can be solved accurately and efficiently on a coarse grid. The choice of a first order WKB-method in the evanescent region is due to the reduction of the complexity of the numerical scheme. Furthermore the choice of a second order WKB-method in the oscillatory region is done in order to use the results from [14]. Anyhow, our hybrid method is second order with respect to h and asymptotically accurate with respect to ε. More accurate methods can naturally be developped by working more and choosing φ_2^{ev} as FEM-basis functions.

II DOMAIN DECOMPOSITION OF THE SCHRÖDINGER BOUNDARY VALUE PROBLEM

Let us now consider the Schrödinger BVP (2.2) with a given coefficient function $a(x)$ as illustrated in Figure 2.2: It consists of three regimes, two oscillatory regions at the interval boundaries and an evanescent region in the middle. Since we exclude turning points here, a is assumed to have jump discontinuities (and sign changes) at the interfaces $x = x_c$ and $x = x_d$, satisfying:

Hypothesis a1 *Let* $a \in L^\infty(0,1)$ *with* $a|_{(x_c,x_d)} < 0$, $a|_{(0,x_c)\cup(x_d,1)} > 0$, $a(0) > 0$, *and* $a(1) > 0$.

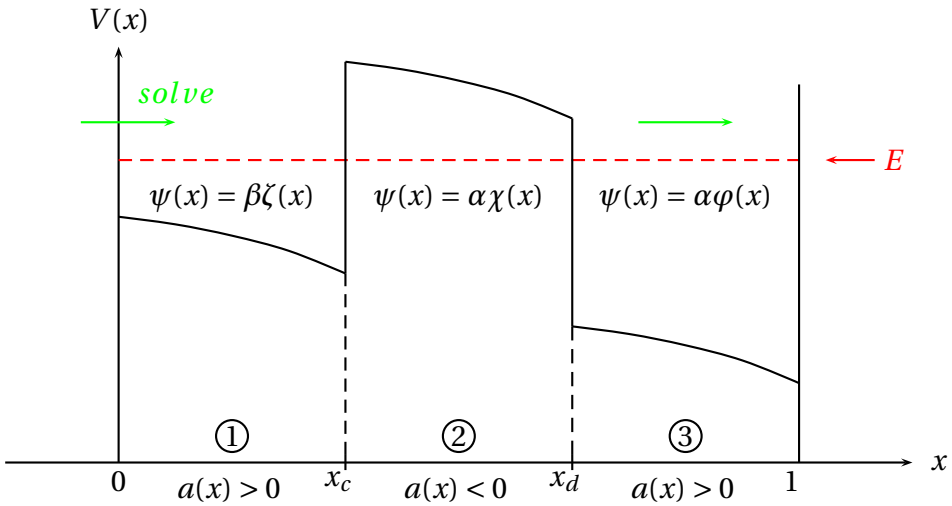

Figure 2.2: Tunnelling structure: While electrons are injected from the right boundary with energy E, the decomposed problem has to be solved from left to right (as an IVP–BVP–IVP). $a(x) := E - V(x)$.

Following the basic idea from [14] we shall solve the BVP (2.2) as an IVP-BVP-IVP problem in the opposite direction of the injection direction, i.e. starting at $x = 0$. In contrast to [14], (2.2) includes the evanescent region (2), cf. Fig. 2.2, which still has to be formulated as a BVP. For efficiency reasons it would be more intersting to solve the whole problem as an IVP, by using the marching method. However, the solution in the evanescent region is a linear combination of exponentially in/decreasing functions. Stability reasons impose then the solution of a BVP in that region. This leads to the following domain decomposition and coupling for the auxiliary wave functions ζ, χ, φ:

Step 1 – IVP for ζ in region (1):

$$\begin{cases} \varepsilon^2\zeta''(x) + a(x)\zeta(x) = 0\,, \quad x \in (0, x_c)\,, \\ \zeta(0) = 1\,, \qquad\qquad \text{(auxiliary Dirichlet BC)} \\ \varepsilon\zeta'(0) = -i\sqrt{a(0)}\,. \qquad \text{(due to the left BC in (2.2))} \end{cases} \tag{2.7}$$

Step 2 – BVP for χ in region (2):

$$\begin{cases} \varepsilon^2\chi''(x) + a(x)\chi(x) = 0\,, \quad x \in (x_c, x_d)\,, \\ \zeta'(x_c)\chi(x_c) - \zeta(x_c)\chi'(x_c) = 0\,, \quad \text{(Robin BC for } \chi \text{ implies continuity of } \frac{\psi'}{\psi} \text{ at } x_c) \\ \varepsilon\chi'(x_d) = 1\,. \qquad\qquad \text{(auxiliary Neumann BC)} \end{cases} \tag{2.8}$$

Step 3 – IVP for φ in region (3):

$$\begin{cases} \varepsilon^2\varphi''(x) + a(x)\varphi(x) = 0\,, \quad x \in (x_d, 1)\,, \\ \varphi(x_d) = \chi(x_d)\,, \qquad \text{(implies continuity of } \psi \text{ at } x_d) \\ \varphi'(x_d) = \chi'(x_d)\,. \qquad \text{(implies continuity of } \psi' \text{ at } x_d) \end{cases} \tag{2.9}$$

Step 4 – scaling of the auxiliary wave functions:

$$\psi(x) := \begin{cases} \beta\zeta(x)\,, & x \in (0, x_c)\,, \\ \alpha\chi(x)\,, & x \in (x_c, x_d)\,, \\ \alpha\varphi(x)\,, & x \in (x_d, 1)\,, \end{cases} \tag{2.10}$$

with the scaling parameters $\alpha, \beta \in \mathbb{C}$ still to be defined.

This procedure can be explained as follows: First we note that the BCs of (2.7) imply $\varepsilon\zeta'(0) + i\sqrt{a(0)}\zeta(0) = 0$, just as in the left BC of the BVP (2.2). Hence, the IVP (2.7) coincides on region (1) with the BVP (2.2), except for the auxiliary Dirichlet BC $\zeta(0) = 1$. The true solution of (2.2) satisfies instead $\psi(0) = \beta$ with some a-priori unknown $\beta \in \mathbb{C}$. Hence, the auxiliary wave function ζ is related to ψ by the scaling $\psi\big|_{[0,x_c]} = \beta\zeta$, as postulated in the first line of (2.10). Clearly, this implies $\frac{\psi'}{\psi} = \frac{\zeta'}{\zeta}$ on $[0, x_c]$. In the above Step 2, the Robin BC allows to carry over this relation to region (2): $\frac{\psi'}{\psi} = \frac{\chi'}{\chi}$, and the auxiliary wave function χ is related to ψ by the scaling $\psi\big|_{[x_c,x_d]} = \alpha\chi$, with some $\alpha \in \mathbb{C}$ to be determined. The initial conditions for the auxiliary wave function φ in Step 3 imply C^1–continuity of ψ when using again the scaling $\psi\big|_{[x_d,1]} = \alpha\varphi$.

So far, the wave function ψ defined in (2.10) neither satisfies continuity at x_c nor the right BC from (2.2). Therefore we define the scaling parameters $\alpha, \beta \in \mathbb{C}$ via

$$\alpha\,[\varepsilon\varphi'(1) - i\sqrt{a(1)}\,\varphi(1)] = -2i\sqrt{a(1)}\,, \qquad \text{(due to the right BC in (2.2))} \quad (2.11)$$

$$\beta\,\zeta(x_c) = \alpha\,\chi(x_c)\,. \qquad \text{(implies continuity of } \psi \text{ at } x_c) \quad (2.12)$$

Remark 2. *The key aspect of the above algorithm is to prescribe in the BVP (2.8) the continuity of $\frac{\zeta'}{\zeta}$ to $\frac{\chi'}{\chi}$ at x_c. Note that this continuity is invariant under the scaling (2.10). Hence it is inherited by $\frac{\psi'}{\psi}$, implying (with the continuity of ψ) the required C^1–continuity of ψ. The simpler alternative to prescribe in (2.8) continuity of ζ to χ would typically be paired with a discontinuity of ζ' to χ' at $x = x_c$ (as a result of solving the BVP). Then, the scaling of (2.10) would lead to an unwanted discontinuity of ψ' at $x = x_c$.*

Lemma 3. *Let Hypothesis* **a1** *be satisfied. Then:*

(i) The IVPs (2.7), resp. (2.9) admit $\forall\,\varepsilon > 0$ unique solutions $\zeta \in W^{2,\infty}(0, x_c) \subset C^1[0, x_c]$, resp. $\varphi \in W^{2,\infty}(x_d, 1) \subset C^1[x_d, 1]$.

(ii) The BVP (2.8) has $\forall\,\varepsilon > 0$ a unique solution $\chi \in W^{2,\infty}(x_c, x_d) \subset C^1[x_c, x_d]$.

(iii) The scaling parameters $\alpha, \beta \in \mathbb{C} \setminus \{0\}$ are well-defined by (2.11), (2.12).

Proof. Part (i) is straightforward. For (ii), let us first consider the IVP (2.7). Its unique solution ζ has the property: $\zeta(x_c)$ and $\zeta'(x_c)$ are linearly independent over $\mathbb{R}$. Otherwise, the backward IVP (starting at x_c) would yield "final values" $\zeta(0)$ and $\zeta'(0)$ that are linearly dependent over $\mathbb{R}$, which is in contradiction with the initial condition in (2.7).

To solve the BVP (2.8), let χ_1, χ_2 be a (real valued) basis of solutions for that Schrödinger equation on (x_c, x_d), with

$$\chi_1(x_c) = 1\,, \qquad \chi_1'(x_c) = 0\,,$$
$$\chi_2(x_c) = 0\,, \qquad \chi_2'(x_c) = 1\,.$$

Setting $\chi = c_1\chi_1 + c_2\chi_2$ with some $c_1, c_2 \in \mathbb{C}$, the BCs of (2.8) give rise to the following linear equation:

$$\begin{pmatrix} \zeta'(x_c) & -\zeta(x_c) \\ \varepsilon\chi_1'(x_d) & \varepsilon\chi_2'(x_d) \end{pmatrix} \begin{pmatrix} c_1 \\ c_2 \end{pmatrix} = \begin{pmatrix} 0 \\ 1 \end{pmatrix}. \quad (2.13)$$

The determinant of this system satisfies $\varepsilon[\zeta'(x_c)\chi_2'(x_d) + \zeta(x_c)\chi_1'(x_d)] \neq 0$, since $\chi_{1,2}'(x_d) \in \mathbb{R}$, but $\zeta(x_c)$ and $\zeta'(x_c)$ are linearly independent over $\mathbb{R}$. Hence, (2.13) is uniquely solvable for c_1, c_2, thus providing the unique solution to (2.8).

For part (iii) we shall first argue that (2.11) yields a well-defined $\alpha \in \mathbb{C} \setminus \{0\}$. For this, prove that $\varepsilon\varphi'(1) \neq i\sqrt{a(1)}\,\varphi(1)$, using the quantum mechanical current of model (2.2):

$$j(x) := \varepsilon\Im[\bar{\psi}(x)\,\psi'(x)]\,. \quad (2.14)$$

Assume now that $\varepsilon\varphi'(1) = i\sqrt{a(1)}\,\varphi(1)$. Then, (2.10) implies on the one hand

$$j(1) = \varepsilon|\alpha|^2\,\Im[\bar{\varphi}(1)\,\varphi'(1)] = |\alpha|^2\,\sqrt{a(1)}\,|\varphi(1)|^2 \geq 0\,. \tag{2.15}$$

But, on the other hand, (2.7) yields

$$j(0) = \varepsilon|\beta|^2\Im[\bar{\zeta}(0)\,\zeta'(0)] = -|\beta|^2\,\sqrt{a(0)}\,|\zeta(0)|^2 \leq 0\,.$$

Since the current in a stationary quantum model is constant in x, this implies $j \equiv 0$. Since $a(1) > 0$ and $\alpha \neq 0$ (otherwise $\psi(1) = \psi'(1) = 0$ would contradict the BC at $x = 1$ in (2.2)), (2.15) shows that $\varphi(1) = 0$, and hence –by our assumption– $\varphi'(1) = 0$. But this leads to a contradiction in the BC at $x = 1$ in (2.2). Hence, (2.11) yields indeed a unique $\alpha \in \mathbb{C} \setminus \{0\}$.

Finally, (2.12) yields a well-defined $\beta \in \mathbb{C}$ since $\zeta(x_c)$ and $\zeta'(x_c)$ are linearly independent over $\mathbb{R}$. Moreover, $\beta \neq 0$ since $\chi(x_c) = c_1 \neq 0$ (otherwise the first line of (2.13) would also yield $c_2 = 0$). ∎

The above lemma shows that the *domain decomposition algorithm* (2.7)-(2.12) yields a unique function ψ that is piecewise in $W^{2,\infty}$ and piecewise (on the three regions) a solution to the Schrödinger equation (2.2). Moreover, one has the proposition:

Proposition 4. *Let Hypothesis* **a1** *be satisfied. Then the function ψ obtained from* (2.7)-(2.12) *belongs to $W^{2,\infty}(0,1)$ and is the unique solution of* (2.2) *(as guaranteed by Proposition 1).*

Proof. The matching conditions in (2.8) and (2.12) imply C^1–continuity of ψ at x_c, and the initial conditions in (2.9) imply C^1–continuity of ψ at x_d. Hence, $\psi \in C^1[0,1]$, and this proves the claim. ∎

III HYBRID WKB-METHOD AND ERROR ESTIMATES

Let us now present the hybrid WKB-method we developed and give the corresponding error-estimate.

Variational formulation and FEM for the evanescent region BVP

We start by introducing the variational formulation of the evanescent region problem (2.8), on which the FEM shall be based. As pointed out previously, we consider in the current work only situations with an abrupt potential jump, avoiding turning points, such that we shall suppose:

Hypothesis a2 *Let $V \in W^{2,\infty}(x_c,x_d)$, $0<\varepsilon<1$ be arbitrary and $E>0$ satisfy*

$$0 < \tau_{ev} \le -a(x) := V(x) - E \le M_{ev}\,, \quad \forall\, x \in (x_c,x_d)\,.$$

We are now searching for a weak solution of (2.8) in the Hilbert space

$$\mathcal{V} := H^1(x_c,x_d)\,, \quad (\chi,\theta)_{\mathcal{V}} := (\chi,\theta)_{L^2(x_c,x_d)} + \varepsilon^2(\chi',\theta')_{L^2(x_c,x_d)}\,.$$

This ε–dependent norm gives rise to the following weighted Sobolev embedding, where the Gagliardo-Nirenberg inequality for bounded domains is used in the first estimate:

$$\begin{aligned} \varepsilon\|\chi\|^2_{C[x_c,x_d]} &\le C\|\chi\|_{L^2(x_c,x_d)}\left(\varepsilon\|\chi'\|_{L^2(x_c,x_d)}\right) + C\varepsilon\|\chi\|^2_{L^2(x_c,x_d)} \\ &\le C\left(\|\chi\|^2_{L^2(x_c,x_d)} + \varepsilon^2\|\chi'\|^2_{L^2(x_c,x_d)}\right) = C\|\chi\|^2_{\mathcal{V}}\,. \end{aligned} \tag{2.16}$$

The variational formulation reads now: Find $\chi \in \mathcal{V}$, solution of

$$b(\chi,\theta) = L(\theta)\,, \quad \forall\theta \in \mathcal{V}\,, \tag{2.17}$$

with the sesquilinear form $b : \mathcal{V}\times\mathcal{V} \to \mathbb{C}$ and the antilinear form $L : \mathcal{V} \to \mathbb{C}$ defined as

$$\begin{aligned} b(\chi,\theta) &:= \varepsilon^2\int_{x_c}^{x_d}\chi'(x)\overline{\theta}'(x)\,dx - \int_{x_c}^{x_d} a(x)\,\chi(x)\overline{\theta}(x)\,dx + \varepsilon\sqrt{|a(x_c)|}\,\chi(x_c)\overline{\theta}(x_c)\,, \quad \forall\chi,\theta\in\mathcal{V} \\ L(\theta) &:= \varepsilon\overline{\theta}(x_d)\,, \quad \forall\theta\in\mathcal{V}\,. \end{aligned} \tag{2.18}$$

The BVP (2.8) is a standard elliptic problem, meaning that the forms $b(\cdot,\cdot)$ and $L(\cdot)$ are continuous and $b(\cdot,\cdot)$ is coercive, *i.e.* there exists a constant $C>0$ independent of ε, such that for all $\chi,\theta\in\mathcal{V}$ one has

$$|b(\chi,\theta)| \le C\,\|\chi\|_{\mathcal{V}}\,\|\theta\|_{\mathcal{V}}\,, \quad |L(\theta)| \le C\sqrt{\varepsilon}\,\|\theta\|_{\mathcal{V}}\,, \quad b(\theta,\theta) \ge \min\{1,\tau_{ev}\}\,\|\theta\|^2_{\mathcal{V}}\,.$$

The Lax-Milgram theorem implies then for each $\varepsilon>0$ the existence and uniqueness of a weak solution $\chi\in\mathcal{V}$ of (2.17).

The multi-scale WKB-FEM method we shall use for an efficient resolution of the evanescent region problem (2.8) is now based on (2.17) as well as on a specific choice of WKB-basis functions from (2.6), in particular φ_1^{ev}. In more detail, the Hilbert space $\mathcal{V}$ will be approximated by an appropriate finite-dimensional Hilbert space $\mathcal{V}_h \subset \mathcal{V}$, spanned by well chosen basis functions, and the continuous problem (2.17) will be approximated by the following discrete problem: Find $\chi_h \in \mathcal{V}_h$, solution of

$$b(\chi_h,\theta_h) = L(\theta_h)\,, \quad \forall\theta_h\in\mathcal{V}_h\,. \tag{2.19}$$

To introduce the finite-dimensional space $\mathcal{V}_h$, let us partition the interval $[x_c,x_d]$ into $x_c = x_1 < x_2 < \cdots < x_N = x_d$ and denote the mesh size by $h_n := x_{n+1} - x_n$ as well as $h := \max_{n=1,\cdots,N-1}\{h_n\}$. The appropriate Hilbert space $\mathcal{V}_h$ is then defined as

$$\mathcal{V}_h := \left\{ \theta_h \in \mathcal{V} \;\middle|\; \theta_h(x) = \sum_{n=1}^{N} z_n\zeta_n(x)\,, \quad z_n\in\mathbb{C} \right\},$$

with the WKB-hat functions defined as

$$\zeta_n(x) := \begin{cases} v_{n-1}(x), & x \in [x_{n-1}, x_n], \\ w_n(x), & x \in [x_n, x_{n+1}], \\ 0, & \text{otherwise}. \end{cases} \tag{2.20}$$

Here we used the notation

$$\begin{aligned} w_n(x) &:= \alpha_n(x)\, q_n(x) \quad ; \quad v_n(x) := \beta_n(x)\, q_{n+1}(x), \\ \alpha_n(x) &:= -\frac{\sinh \sigma_{n+1}(x)}{\sinh \gamma_n} \quad ; \quad \beta_n(x) := \frac{\sinh \sigma_n(x)}{\sinh \gamma_n}, \\ \sigma_n(x) &:= \frac{1}{\varepsilon}\int_{x_n}^{x} \sqrt{|a(y)|}\, dy \quad ; \quad \gamma_n := \frac{1}{\varepsilon}\int_{x_n}^{x_{n+1}} \sqrt{|a(y)|}\, dy, \\ q_n(x) &:= \frac{(V(x_n)-E)^{1/4}}{(V(x)-E)^{1/4}}. \end{aligned} \tag{2.21}$$

To summarize, the FEM for the evanescent region BVP (2.8) corresponds to the formulae (2.19)-(2.21).

IVP and marching method for the oscillatory region (2.9)

In this subsection we shall first investigate the IVP (2.9) on the continuous level, in particular rewrite it in vectorial form, via a non-standard transformation that is appropriate for the subsequent numerical WKB-marching method. For the next analysis let us make the following assumptions on the potential:

Hypothesis a3 *Let $V \in C^5[x_d, 1]$ and $E > 0$ satisfy the bounds*

$$0 < \tau_{os} \le a(x) := E - V(x) \le M_{os}, \quad \forall x \in [x_d, 1].$$

Following [14] it is convenient to pass from the second-order differential equation to a system of first-order, introducing the following notation for $\varphi(x)$ on $[x_d, 1]$:

$$U(x) = \begin{pmatrix} u_1 \\ u_2 \end{pmatrix} := \begin{pmatrix} a^{1/4}\varphi(x) \\ \frac{\varepsilon(a^{1/4}\varphi)'(x)}{\sqrt{a(x)}} \end{pmatrix} = \begin{pmatrix} a^{1/4}\varphi(x) \\ \varepsilon\big(\frac{1}{4}a^{-5/4}a'\varphi + a^{-1/4}\varphi'\big)(x) \end{pmatrix}. \tag{2.22}$$

The norm of U is equivalent to the norm of the vector $(\varphi, \varepsilon\varphi')^\top$. Indeed, the transformation matrix between these two vectors reads

$$A(x) := \begin{pmatrix} a^{1/4}(x) & 0 \\ \frac{\varepsilon}{4}a^{-5/4}(x)a'(x) & a^{-1/4}(x) \end{pmatrix} \quad \text{i.e.} \quad U(x) = A(x)\begin{pmatrix} \varphi \\ \varepsilon\varphi' \end{pmatrix}, \tag{2.23}$$

where the matrix A and its inverse are bounded, uniformly w.r.t. x and ε.
Let $\varphi_{ex} \in W^{2,\infty}(x_d, 1)$ be the exact solution of (2.9) as guaranteed by Lemma 3. In the

above vector notation it will be denoted by $U_{ex}(x)$ or simply $U(x)$, and it is the unique solution to

$$\begin{cases} U'(x) = \left[\frac{1}{\varepsilon}A_0(x) + \varepsilon A_1(x)\right] U(x), \quad x_d < x < 1, \\ U(x_d) = A(x_d+)\,(\chi_{ex}(x_d), 1)^\top, \end{cases} \tag{2.24}$$

with the two matrices

$$A_0(x) := \sqrt{a(x)}\begin{pmatrix} 0 & 1 \\ -1 & 0 \end{pmatrix}; \quad A_1(x) := \begin{pmatrix} 0 & 0 \\ 2\beta(x) & 0 \end{pmatrix}.$$

Here, $\beta = -\frac{1}{2a^{1/4}}(a^{-1/4})''$ was already defined in (2.4), and the matrix elements $a(x_d+)$ resp. $a'(x_d+)$ of $A(x_d+)$ denote the right-sided limit of a resp. a' at the jump discontinuity x_d.

Let us now come to the discretization of the IVP (2.24). Following [14] the numerical method consists of two parts, first an analytic transformation of (2.24) into a less oscillatory problem, and second the discretization of the smooth problem on a coarse grid in an ε-uniform manner. The analytic WKB-transformation reviewed here is related to using oscillatory WKB-functions of second order, $\varphi_2^{os}(x)$ (see (2.5)).

Part 1 – analytic transformation: The starting point is the vectorial IVP (2.24). The vector function $U \in \mathbb{C}^2$ is then transformed to the new unknown $Z \in \mathbb{C}^2$ by introducing

$$Z(x) = \begin{pmatrix} z_1 \\ z_2 \end{pmatrix} := \exp\left(-\frac{i}{\varepsilon}\Phi^\varepsilon(x)\right) P\, U(x), \quad \forall x \in [x_d, 1],$$

with the matrices

$$P := \frac{1}{\sqrt{2}}\begin{pmatrix} i & 1 \\ 1 & i \end{pmatrix} \quad ; \quad \Phi^\varepsilon(x) := \begin{pmatrix} \phi^\varepsilon(x) & 0 \\ 0 & -\phi^\varepsilon(x) \end{pmatrix},$$

and the (real valued) phase function

$$\phi^\varepsilon(x) := \int_{x_d}^{x} \left(\sqrt{a(y)} - \varepsilon^2\beta(y)\right) dy. \tag{2.25}$$

This change of unknown leads to the smooth ODE-system

$$\begin{cases} \frac{dZ}{dx} = \varepsilon N^\varepsilon Z, \quad x_d < x < 1, \\ Z(x_d) := P\, U_{ex}(x_d). \end{cases} \tag{2.26}$$

Here, the 2×2–matrix function

$$N^\varepsilon(x) := \beta(x)\exp(-\frac{i}{\varepsilon}\Phi^\varepsilon)\begin{pmatrix} 0 & 1 \\ 1 & 0 \end{pmatrix}\exp(\frac{i}{\varepsilon}\Phi^\varepsilon) = \beta(x)\begin{pmatrix} 0 & e^{-\frac{2i}{\varepsilon}\phi^\varepsilon(x)} \\ e^{\frac{2i}{\varepsilon}\phi^\varepsilon(x)} & 0 \end{pmatrix},$$

is off-diagonal and bounded independently on ε, which is the main advantage as compared to (2.24). This finishes the analytical transformation, and the goal of the second part is to provide an ε-uniform discretization of (2.26) that is second order w.r.t. the mesh size.

Part 2 – numerical discretization: First we partition the interval $[x_d, 1]$ into $x_d = x_N < x_{N+1} < \cdots < x_M = 1$. As in §III.1 we denote the mesh size by $h_n := x_{n+1} - x_n$ as well as $h := \max_{n=1,\cdots,M-1}\{h_n\}$.

Given the initial condition $Z_N := P\,U_N \in \mathbb{C}^2$ and $U_N := U_{ex}(x_d) \in \mathbb{C}^2$, the marching scheme for the resolution of (2.26) reads as follows (see [14]):

$$Z_{n+1} = (I + A_n^1 + A_n^2)\, Z_n\,, \qquad n = N, ..., M-1\,, \tag{2.27}$$

with the 2×2–matrices

$$\begin{aligned}
A_n^1 :=& \\
&-i\varepsilon^2 \begin{pmatrix} 0 & \beta_0(x_n)e^{-\frac{2i}{\varepsilon}\phi(x_n)} - \beta_0(x_{n+1})e^{-\frac{2i}{\varepsilon}\phi(x_{n+1})} \\ \beta_0(x_{n+1})e^{\frac{2i}{\varepsilon}\phi(x_{n+1})} - \beta_0(x_n)e^{\frac{2i}{\varepsilon}\phi(x_n)} & 0 \end{pmatrix} \\
&+\varepsilon^3 \begin{pmatrix} 0 & \beta_1(x_{n+1})e^{-\frac{2i}{\varepsilon}\phi(x_{n+1})} - \beta_1(x_n)e^{-\frac{2i}{\varepsilon}\phi(x_n)} \\ \beta_1(x_{n+1})e^{\frac{2i}{\varepsilon}\phi(x_{n+1})} - \beta_1(x_n)e^{\frac{2i}{\varepsilon}\phi(x_n)} & 0 \end{pmatrix} \\
&+i\varepsilon^4\beta_2(x_{n+1}) \begin{pmatrix} 0 & -e^{-\frac{2i}{\varepsilon}\phi(x_n)} H_1(-\frac{2}{\varepsilon}S_n) \\ e^{\frac{2i}{\varepsilon}\phi(x_n)} H_1(\frac{2}{\varepsilon}S_n) & 0 \end{pmatrix} \\
&-\varepsilon^5\beta_3(x_{n+1}) \begin{pmatrix} 0 & e^{-\frac{2i}{\varepsilon}\phi(x_n)} H_2(-\frac{2}{\varepsilon}S_n) \\ e^{\frac{2i}{\varepsilon}\phi(x_n)} H_2(\frac{2}{\varepsilon}S_n) & 0 \end{pmatrix},
\end{aligned}$$

$$\begin{aligned}
A_n^2 \;:=\; & -i\varepsilon^3(x_{n+1}-x_n)\frac{\beta(x_{n+1})\beta_0(x_{n+1}) + \beta(x_n)\beta_0(x_n)}{2} \begin{pmatrix} 1 & 0 \\ 0 & -1 \end{pmatrix} \\
& -\varepsilon^4\beta_0(x_n)\beta_0(x_{n+1}) \begin{pmatrix} H_1(-\frac{2}{\varepsilon}S_n) & 0 \\ 0 & H_1(\frac{2}{\varepsilon}S_n) \end{pmatrix} \\
& +i\varepsilon^5\beta_1(x_{n+1})[\beta_0(x_n) - \beta_0(x_{n+1})] \begin{pmatrix} H_2(-\frac{2}{\varepsilon}S_n) & 0 \\ 0 & -H_2(\frac{2}{\varepsilon}S_n) \end{pmatrix}.
\end{aligned}$$

Here we used the notation

$$\beta_0(y) := \frac{\beta}{2(\sqrt{a} - \varepsilon^2\beta)}(y); \qquad \beta_{k+1}(y) := \frac{1}{2\phi'(y)}\frac{d\beta_k}{dy}(y)\,, \quad k = 0, 1, 2,$$

$$H_1(\eta) := e^{i\eta} - 1\,, \qquad H_2(\eta) := e^{i\eta} - 1 - i\eta\,,$$

and the discrete phase increments

$$S_n := \phi(x_{n+1}) - \phi(x_n) = \int_{x_n}^{x_{n+1}} \left(\sqrt{a(y)} - \varepsilon^2 \beta(y)\right) dy\,.$$

Remark that for notational reasons we omitted in the aforementioned description of the scheme the ε-index. Furthermore we assumed that the two functions ϕ and β (the latter involving the derivatives a', a'') are explicitly "available". Alternatively, ϕ, a' and a'' could be approximated numerically. Note that the marching procedure (2.27) is obtained by combining the truncation of a Picard iteration (explicit formula for $Z(x)$) with the discretization of highly oscillating integrals via IPP.

Finally we have to transform back to the U-solution vector via

$$U_n = P^{-1}\, e^{\frac{i}{\varepsilon}\Phi^\varepsilon(x_n)}\, Z_n\,, \qquad n = N+1, ..., M\,. \tag{2.28}$$

This concludes the presentation of the WKB-marching algorithm, which corresponds to (2.27)-(2.28).

Convergence results for the overall hybrid WKB method

The following error-estimate result for our WKB-hybrid scheme is the main result of the paper [15] and will be only cited here.

Theorem 5. (Convergence WKB-hybrid) *Let Hypotheses* **a2** *and* **a3** *be satisfied and let the phase ϕ^ε be explicitly calculable via (2.25). Then ψ_h, the numerical solution to the hybrid scheme (2.19)-(2.21); (2.27)-(2.28) satisfies the following error estimates, as compared to the exact solution ψ_{ex} of the DDM (2.7)-(2.12):*

$$\|\tilde{e}_h\|_\infty \le C\sqrt{h}\,\min\{\varepsilon^{3/2}, h^{3/2}\}\,, \qquad \varepsilon\|\tilde{e}'_h\|_\infty \le C\varepsilon\sqrt{h}\,\min\{\sqrt{\varepsilon}, \sqrt{h}\}\,, \tag{2.29}$$

with the notation $\tilde{e}_h(x) := \psi_{ex}(x) - \psi_h(x)$ for the evanescent region; , $\tilde{e}_{h,n} := \psi_{ex}(x_n) - \psi_{h,n}$ and $\tilde{e}'_{h,n} := \psi'_{ex}(x_n) - \psi'_{h,n}$ for the oscillatory region, and finally

$$\|\tilde{e}_h\|_\infty := \max\{\|\tilde{e}_h\|_{L^\infty(x_c,x_d)}\,;\, \max_{n=N,...,M} |\tilde{e}_{h,n}|\}.$$

Remark 6. *As one can observe from the estimate (2.29), our hybrid-method is second order in h and asymptotically correct for $\varepsilon \to 0$.*

IV NUMERICAL TESTS OF THE HYBRID WKB-METHOD

The aim of this section is to present the numerical results obtained with the WKB-coupling scheme and to compare these results with the error analysis established in

Section III.3. In particular, we present the results for 3 zones (oscillating-evanescent-oscillating) corresponding to the flow of electrons through a tunnelling structure similar to the one in Fig. 2.1, with a piecewise linear and, respectively, piecewise quadratic potential $V(x)$, chosen such that the phase $\phi^\varepsilon(x)$ is explicitly calculable. The reason for such a choice is to avoid having to care about an $\frac{h^\gamma}{\varepsilon}$ –error term appearing in the marching method [14]. In this case, our scheme is an asymptotically correct scheme for fixed $h > 0$ and $\varepsilon \to 0$.

Example 1: We start with the piecewise linear potential graphed in Fig. 2.1. Note the small applied bias with $V(0) = 0$, $V(1) = 0.2$.

In Fig. 2.3 we plotted the numerical errors of the coupling method associated to the wave function ψ (left plot) and to its derivative $\varepsilon\psi'$ (right plot), as functions of the mesh size h (in log−log scale) and for three different ε-values. In the oscillating regions we chose the second order method (2.27)-(2.28) and in the evanescent region the FEM (2.19). The plotted errors are the L^∞-errors between the numerical solution on the whole interval $[0,1]$ and a reference solution, computed with the same scheme but on a finer grid of 2^{18} points. It can be observed that the slopes in these two plots are approximatively one (for $h \gtrsim 3\cdot 10^{-5}$) and improving to 1.5 for smaller values of h. For $\varepsilon = 0.1$ the slope of the ψ–error even improves up to 2 for the smallest values of h. This behaviour is in accordance with our numerical analysis in Theorem 5.

The ε-dependence seems to be like $\mathcal{O}(\sqrt{\varepsilon})$ (for large values of ε), improving to $\mathcal{O}(\varepsilon)$ (for small values of ε), and even $\mathcal{O}(\varepsilon^{3/2})$ (for small values of ε and large h). Summarizing, the error of ψ shows to be of order $\mathcal{O}(\min\{h^2, \sqrt{\varepsilon}h^{3/2}, \varepsilon h, \varepsilon^{3/2}\sqrt{h}\})$, which corresponds exactly to the estimates given in Theorem 5. The error of $\varepsilon\psi'$ shows to be of order $\mathcal{O}(\min\{\sqrt{\varepsilon}h^{3/2}, \varepsilon h, \varepsilon^{3/2}\sqrt{h}\})$, which is even slightly better than the estimate from Theorem 5 (in the sense of including also an $\mathcal{O}(\sqrt{\varepsilon}h^{3/2})$–behaviour).

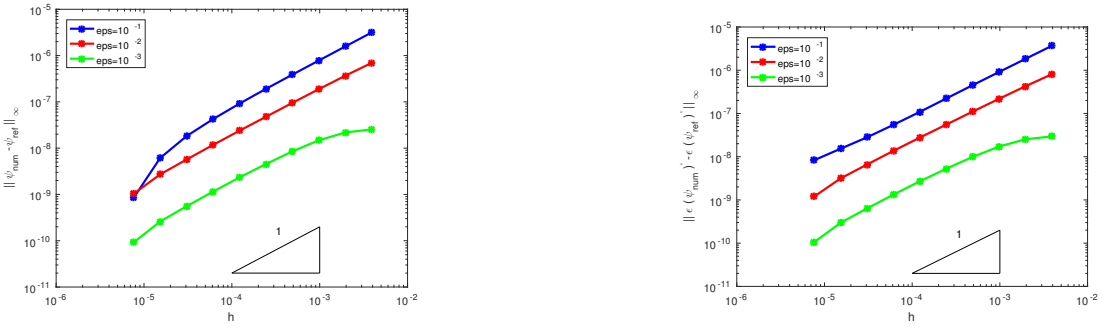

Figure 2.3: Absolute error (in the L^∞-norm and log−log scale) between the computed solution and a reference solution (obtained with $h = 2^{-18} \approx 4\cdot 10^{-6}$), for a piecewise linear potential. Left: $||\psi_{ref} - \psi_{num}||_\infty$. Right: $||\varepsilon\psi'_{ref} - \varepsilon\psi'_{num}||_\infty$.

We mention that the obtained numerical errors are mainly those introduced by the WKB-FEM of the evanescent region. Indeed, in this evanescent region, the numerical error of the WKB-FEM is larger than the one obtained from the second order WKB

marching method of the oscillating region [14].

Example 2: Next we consider a piecewise quadratic potential given by

$$a(x) := c_1(x+c_2)^2\,, \quad \forall x \in [0, x_c] \cup [x_d, 1]\,; \quad a(x) := -c_1(x+c_2)^2\,, \quad \forall x \in (x_c, x_d)\,,$$

with $x_c = 0.5$, $x_d = 0.5 + 2^{-5} = 0.53125$ and

$$E = 1.5\,, \quad V_1 = V(1) = 0.2\,, \quad c_2 = -\frac{E + \sqrt{E^2 - V_1 E}}{V_1}\,, \quad c_1 = \frac{E}{c_2^2}\,.$$

The corresponding error plots are similar to those of Fig. 2.3 and are plotted as well as commented in the paper [15].

Let us consider however in this case the condition number associated to solving the discrete variational problem (2.19) in the (intermediate) evanescent region. In Fig. 2.4 we plot this condition number as a function of h, for three different values of ε. For $\varepsilon = 10^{-1}, 10^{-2}$ it grows like $\mathcal{O}(h^{-2})$ when $h \to 0$, and for $\varepsilon = 10^{-3}$ it grows like $\mathcal{O}(h^{-1})$ (on the shown interval of h-values). We remark that this behaviour is not a problem in practice: For large ε, the solution ψ_{ex} is *not* highly oscillatory and hence does not need a high spatial resolution. For small values of ε, even a fine resolution would only lead to moderate condition numbers. Indeed, one observes a decrease of the condition number when ε gets smaller. This important feature is somehow related to the *asymptotic-preserving* property of the scheme.

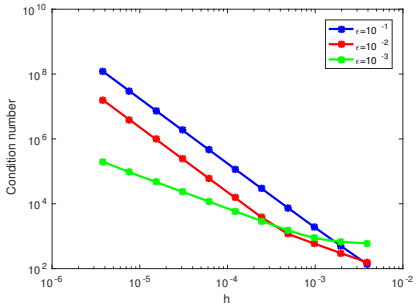

Figure 2.4: Condition number for the discrete BVP in Ex. 2, as a function of h, for three values of ε.

To summarize, these numerical tests show clearly that the WKB-hybrid method presented in this chapter provides an accurate solution of the 1D Schrödinger equation in the semi-classical regime, and this even on coarse grids, chosen independently on the parameter ε (Planck constant). Hence the WKB-method is an asymptotic-preserving scheme, fact which was also confirmed via a detailed numerical analysis in [15]. To complete the scheme, one should next treat also turning point situations.

CHAPTER 3

TWO-BODY SCHRÖDINGER EQUATION MODELLING THE INTERACTION OF A HEAVY PARTICLE WITH A LIGHT ONE.

Chapter based on the articles:
R. Adami, C. Negulescu [1]
C. Negulescu [2]
R. Adami, M. Hauray, C. Negulescu [3]

Systems with multiple time scales are frequently encountered in molecular dynamics, chemistry, plasma physics, *etc.* One of the major problems in these fields is the presence of both fast and slow processes in the problem. Small time steps have hence to be chosen to have stable numerical methods and follow accuratly the rapid dynamics, however this implies necessarly extremly large computational resources and has to be avoided if possible. A multi-scale treatment can hence be of rescue.

In the centre of this chapter stands the linear, time-dependent two-body Schrödinger equation, describing a quantum system (modelled by a heavy particle) interacting with the surrounding environment (modelled by a light particle). The interaction of a quantum system with the environment leads to the suppression of interference patterns in the quantum system, which are typical quantum mechanical features. This supression phenomenon is the so-called “quantum decoherence” and is nowadays considered as the key concept in the description of the transition from the quantum to the classical world. Its study is the central problem of this chapter. Asymptotic techniques are used to cope with the rather different dynamics of the heavy and light particles.

[1] "A numerical study of quantum decoherence", CiCP (Communications in Computational Physics) 12 (2012), no. 1, 85–108.

[2] "Numerical error analysis of a splitting method for the resolution of the anisotropic Schroedinger equation", submitted.

[3] "Decoherence for a heavy particle interacting with a light one: new analysis and numerics", CMS (Communications in Mathematical Sciences) 14 (2016), no. 5, 1373–1415.

I THE MATHEMATICAL PROBLEM

Quantum decoherence is nowadays considered as the key concept in the description of the transition from the quantum to the classical world [23, 25, 27, 51, 52, 58, 75].

As it is well-known, the axioms of quantum mechanics allow superposition states, namely, normalized sums of admissible wave functions are once more admissible wave functions. It is then possible to construct non-localized states that lack a classical interpretation, for instance, by summing two states localized far apart from each other. The observable mark of such a quantum mechanical superposition state is the presence of interference fringes in the probability distribution associated to the state (see e.g. [34]). We stress that this phenomenon does not have a classical explanation: classically, a probability distribution evolving freely in the phase space of a single particle follows the free Liouville equation, so, by linearity, two colliding probability densities sum up without creating an interference pattern.

Nonetheless, at human scale no interference is revealed, so the question arises, on how does the interference pattern disappear. Such a phenomenon is called *decoherence* and its explanation lies in the fact that macroscopic objects undergo a continuous interaction with an external environment (such as air molecules, fields), which causes the loss of the phase relations between the different states in the superposition. Thus, the state of the system becomes a statistical mixture in which the quantum effects are suppressed. In this sense, the system loses its quantum nature and then its state admits a classical interpretation.

Understanding decoherence is important not only in the foundations of quantum mechanics, but also in applied physics. For example, in quantum computation (QC), electron spin resonance (ESR), and nuclear magnetic resonance (NMR) it is of paramount importance to preserve the quantum behaviour, so decoherence is not desired and efforts are made in order to avoid it [89, 95]. On the other hand, in quantum interference effect transistors (QuIET) decoherence is exploited to control the quantum current flow [92]. In such devices, decoherence acts like a switch to modulate the current flow, the device being switched "off" in the completely coherent state and "on" when interference disappears.

We remark that the transition from the quantum to the classical regime due to decoherence is different from the semi-classical limit, where the classical behaviour is recovered exploiting the smallness of Planck's constant. Let us stress three main differences to this regard: first, decoherence requires an open system, i.e. a system that interacts with an environment; second, decoherence acts at the length-scale of the interference pattern, whereas a typical semi-classical procedure consists in evaluating a macroscopic observable on a fast oscillating probability distribution; third, decoherence is a dynamical effect: it grows with time, whereas the semi-classical limit can be performed in the stationary framework too. Furthermore, at least qualitatively, $\hbar$ plays no role in the mechanism of decoherence: nevertheless, from a quantitative point of view, in many models of physical relevance the time-scale of the decoherence owes its

shortness to the smallness of $\hbar$ (see e.g. [75]).

Our aim in this chapter is to analyze the dynamics of a quantum system composed of a heavy and a light particle, interacting with each other. We consider the heavy particle as the "system", and monitor the decoherence induced on it by the light one, that plays the role of the "environment". According to the axioms of non-relativistic quantum mechanics, the evolution of the two-particle wave function $\psi_\varepsilon(t,X,x)$ is driven by the time-dependent Schrödinger equation

$$\begin{cases} i\partial_t\psi_\varepsilon = -\dfrac{1}{2M}\Delta_X\psi_\varepsilon - \dfrac{1}{2\varepsilon M}\Delta_x\psi_\varepsilon + \dfrac{1+\varepsilon}{\varepsilon}V(x-X)\,\psi_\varepsilon, \quad \forall (t,X,x)\in\mathbb{R}^+\times\mathbb{R}^{2d}, \\ \psi_\varepsilon(0,X,x) = \psi_\varepsilon^0(X,x), \end{cases} \tag{3.1}$$

where we used units in which $\hbar = 1$, M is the mass and X the spatial coordinate of the heavy particle, while εM is the mass and x the spatial coordinate of the light one. So ε is the ratio between the mass of the light particle and the mass of the heavy one, and we study the regime $\varepsilon \ll 1$, which we call the *small mass ratio* regime.

The interaction is described by the potential $\frac{1+\varepsilon}{\varepsilon}V$; the uncommon coupling constant is chosen to be of order ε^{-1} so that even a single collision leaves an observable mark on the heavy particle; furthermore, the factor $1+\varepsilon$ hardly affects the dynamics and simplifies some expressions. We shall always choose a *factorized* initial state, i.e. ψ_ε^0 will be the product of functions depending only on the variable X and the variable x, respectively, *i.e.*

$$\psi_\varepsilon^0(X,x) = \varphi(X)[U_0(-\varepsilon^{-\gamma})\chi](x), \tag{3.2}$$

where φ (heavy part.) and χ (light part.) are regular functions and $\gamma\in(0,1)$. The presence of the free propagator $U_0(-\varepsilon^{-\gamma})$ in the definition of the initial state of the light particle is useful to describe a situation in which the light particle comes from infinity and reaches $x=0$ in a time of order $\varepsilon^{1-\gamma}$. Physically, this means that initially the two particles are uncorrelated. We shall always assume that ψ_ε^0, and consequently $\psi_\varepsilon(t)$, is normalized in $L^2(\mathbb{R}^{2d})$.

The numerical resolution of system (3.1) poses extremely challenging problems. It is an example of a multi-scale problem, due to the small parameter $0<\varepsilon\ll 1$. The light particle has a rapid dynamics (rapid dispersion), whereas the heavy one responds on relatively long time scales. The decoherence effect, which is the phenomenon we want to study, appears clearly in the limit $\varepsilon\to 0$, as explained in [5]. For very large ε-values, deformation-effects eclipse the desired decoherence effect. However, very small ε-values lead to sever numerical problems. We are thus in a sort of dilemma: On the one hand, for large ε-values we have precise, but uninteresting results (with deformation) and on the other hand, very interesting decoherence results can be studied for $0<\varepsilon\ll 1$, but much work and attention is needed to avoid numerical difficulties and to get precise results. This leads naturally to the idea of an asymptotic study of the solution as the parameter ε tends to zero, and this strategy will be adopted in the sequel.

II A MULTI-SCALE ASYMPTOTIC RESOLUTION OF THE TWO-BODY SCHRÖDINGER SYSTEM (3.1)

To simplify the following composition, let us fix at the beginning some notation.

- We denote the free Hamiltonian operator in $L^2(\mathbb{R}^d)$ by

$$H_0 := -\frac{1}{2}\Delta, \quad H_0 : H^2(\mathbb{R}^d) \subset L^2(\mathbb{R}^d) \to L^2(\mathbb{R}^d),$$

which is self-adjoint in $L^2(\mathbb{R}^d)$ and generates the free Schrödinger propagator, denoted in the following by $U_0(t)$. At fixed t, $U_0(t)$ acts as the convolution with the integral kernel

$$U_0(t,x) = \frac{1}{(2\pi i t)^{d/2}} e^{i\frac{|x|^2}{2t}}, \qquad x \in \mathbb{R}^d.$$

- Whenever a tensor product appears, the first factor refers to the heavy particle or to its state, while the second refers to the light particle or to its state. The convention applies to operators and wave functions. Given a wave function χ_X for the light particle, where the coordinate X of the heavy particle enters as a parameter, $\varphi \otimes \chi_X$ will denote the wave function defined by

$$[\varphi \otimes \chi_X](X,x) := \varphi(X)\chi_X(x).$$

- We denote by H_V the Hamiltonian

$$H_V := -\frac{1}{2}\Delta + V,$$

where V is the multiplication by $V(x)$. In all cases we consider, H_V is self-adjoint, and $U_V(t)$ denotes the unitary group generated by H_V, i.e.

$$U_V(t) := e^{-iH_V t}.$$

- We denote by S the scattering operator corresponding to the potential V, *i.e.*

$$S_V := \lim_{t,t'\to+\infty} S_V(t,t'), \quad \text{where} \quad S_V(t,t') := U_0(-t')U_V(t+t')U_0(-t), \tag{3.3}$$

and the limit holds in the strong operator topology. In all cases we consider, S_V is well-defined, unitary and relates incoming and outgoing, scattered particles.

- Consider the self-adjoint Hamiltonian operator H_V, its unitary group U_V and the related scattering operator S_V. Then, the shifts by any $X \in \mathbb{R}^d$, denoted respectively by H_V^X, U_V^X and S_V^X, are also well-defined and share the properties of the unshifted ones. More explicitly,

$$H_V^X := -\frac{1}{2}\Delta + V(\cdot - X), \qquad U_V^X(t) := e^{-iH_V^X t},$$
$$S_V^X := \lim_{t,t'\to+\infty} S_V^X(t,t'), \quad \text{where} \quad S_V^X(t,t') := U_0(-t')U_V^X(t+t')U_0(-t).$$

When no confusion is possible, we will forget the subscript V and use the shorthand notation H, S, U and H^X, U^X, S^X.

- The two-particle free Hamiltonian operator and the Hamiltonian operator containing the interaction among the two particles shall be denoted respectively by

$$H_\varepsilon^f := -\frac{1}{2}\Delta_X - \frac{1}{2\varepsilon}\Delta_x, \qquad H_\varepsilon := -\frac{1}{2}\Delta_X - \frac{1}{2\varepsilon}\Delta_x + \frac{1+\varepsilon}{\varepsilon}V(|X-x|).$$

Both are unbounded self-adjoint operators on $L^2(\mathbb{R}^{2d})$. The associated unitary groups will be represented respectively by $U_\varepsilon^f(t)$ and $U_\varepsilon(t)$.

The unitary group generated by H_ε^f factorizes as

$$U_\varepsilon^f(t) \;=\; U_0(t) \otimes U_0(t/\varepsilon).$$

- The space of self-adjoint trace-class operators (see [82]) on $L^2(\mathbb{R}^d)$ or $L^2(\mathbb{R}^{2d})$ is denoted by $\mathscr{L}^1$ and the norm of a generic element ρ in that space is given by

$$\|\rho\|_{\mathscr{L}^1} \;:=\; \mathrm{Tr}|\rho|, \quad \forall \rho \in \mathscr{L}^1,$$

where Tr denotes the trace functional (see [82]). The subspace of the positive elements of $\mathscr{L}^1$ is denoted by $\mathscr{L}^1_+$.

Asymptotic approximations

Let us now provide in this section an approximate solution to the problem (3.1)-(3.2), valid in the regime $\varepsilon \ll 1$ and permitting considerable computational savings both in memory and time, as compared to standard methods. The main idea of our asymptotic approximation is based on the fact that the characteristic evolution time is of order one for the heavy particle and of order ε for the light one, so the light particle diffuses almost instantaneously, while, during the interaction, the heavy particle hardly moves. Thus, the main effect of the interaction on the heavy particle is the reduction of the quantum interference among the two bumps. This, roughly speaking, is the content of the celebrated Joos-Zeh's heuristic formula (see e.g. formula (3.43) in [58]), which establishes that the state of the heavy particle has hardly changed, while the state of the light particle is transformed by the action of a suitable scattering operator. We stress that the small mass ratio hypothesis is the key aspect of this approximation.

In Theorem 7 the case of a pure state (i.e. a wave function) is considered, and we give an approximate solution in which the evolution of the heavy particle is decoupled from the evolution of the light one, provided that the initial state has been suitably modified. In Theorem 10 we generalize the result to the case of a mixed state (i.e. a density operator), in which the problem (3.1)-(3.2) is replaced by the operator differential equation (3.6). Theorem 10 provides an approximate density operator for the

heavy particle whose dynamics is governed by a free evolution problem with modified initial data. The modification of the initial data is given by the action of the collision operator $\mathscr{I}_\chi$.

Theorem 7. *[6] Let us assume suitable regularity conditions on the potential V as well as on the initial wave-functions φ and χ. Furthermore, let $\psi_\varepsilon(t)$ denote the solution to (3.1)-(3.2) with $M=1$; moreover let $\psi_\varepsilon^a(t)$ denote the solution to the free two-body Schrödinger equation*

$$\begin{cases} i\,\partial_t \psi_\varepsilon^a = -\frac{1}{2}\Delta_X \psi_\varepsilon^a - \frac{1}{2\varepsilon}\Delta_x \psi_\varepsilon^a = H_\varepsilon^f \psi_\varepsilon^a \\ \psi_\varepsilon^a(0) = \varphi \otimes U_0(-\varepsilon^{-\gamma})\, S^X \chi. \end{cases} \tag{3.4}$$

Then, the error introduced by approximating ψ_ε by ψ_ε^a is estimated as

$$\|\psi_\varepsilon(t) - \psi_\varepsilon^a(t)\|_2 \leq C_1\left(\frac{1+\varepsilon}{\varepsilon}\, t - \varepsilon^{-\gamma}, \varepsilon^{-\gamma}\right) + C_2\,\varepsilon + C_3\,\varepsilon^{1-\gamma}, \tag{3.5}$$

with $\lim_{\tau,\tau'\to+\infty} C_1(\tau,\tau') = 0$ and the constants $C_2, C_3 > 0$ dependent only on φ, χ and V.

This theorem states that for small ε-values, one can replace the resolution of the two-body interacting Schrödinger system (3.1) by the free Schrödinger equation (3.4) however with a modified initial condition, which contains now the whole information about the heavy-light interaction. The light particle is instantaneously scattered by the heavy particle, and this one evolves then freely, after this spontaneous interaction at $t=0$.

Let us now generalize Theorem 7 to the formalism of density operators. Such a step is necessary in order to describe the dynamics of the heavy particle when interacting with several light particles: indeed, as we can see from (3.4), the initial condition for the asymptotic model is not factorized, so after one collision the heavy particle lies in a mixed state that has to be described by the appropriate density operator.

Assume that the initial state of the heavy particle is given by the density operator $\rho^M(0) \in \mathscr{L}^1_+$, while, as before, the light particle at time zero lies in the state represented by the wave function $U_0(-\varepsilon^{-\gamma})\chi$. Then, the density operator $\rho_\varepsilon(t)$ that represents the state of the two-body system at time t solves the Von Neumann equation

$$\begin{cases} i\partial_t \rho_\varepsilon(t) &= [H_\varepsilon, \rho_\varepsilon(t)] \\ \rho_\varepsilon(0) &:= \rho^M(0) \otimes |U_0(-\varepsilon^{-\gamma})\chi\rangle\langle U_0(-\varepsilon^{-\gamma})\chi|, \end{cases} \tag{3.6}$$

where the symbol $[A_1, A_2]$ denotes the commutator of the operators A_1 and A_2.

For the sake of studying the dynamics of the heavy particle, the interesting quantity is the density operator of the heavy particle, which is denoted by $\rho_\varepsilon^M(t)$ and defined as

$$\rho_\varepsilon^M(t) \;:=\; \mathrm{Tr}_m \rho_\varepsilon(t) = \sum_j \langle \chi_j | \rho_\varepsilon(t) | \chi_j \rangle, \tag{3.7}$$

where $\{\chi_j\}_{j\in\mathbb{N}}$ is a complete orthonormal set for the space $L^2(\mathbb{R}^d)$, and Tr_m denotes the so-called *partial trace w.r.t. the light particle*.

Let us be more precise on how to compute such a partial trace. As $\rho_\varepsilon(t)$ is compact, it can be represented as an integral operator whose kernel can be denoted, with a slight abuse of notation, by $\rho_\varepsilon(t,X,X',x,x')$. The integral kernel of the reduced density matrix for the heavy particle then reads

$$\rho_\varepsilon^M(t,X,X') := \int_{\mathbb{R}^d} \rho_\varepsilon(t,X,X',x,x)\,dx. \tag{3.8}$$

There is no closed equation for the time evolution of ρ_ε^M, but, as we shall see, as ε goes to zero and for any $t \neq 0$, the operator $\rho_\varepsilon^M(t)$ converges to an operator $\rho^{M,a}(t)$ that satisfies a closed equation. In order to state this result properly, we need to introduce a further operator on $\mathscr{L}_1$ which we call the *collision operator*.

Definition 8 (Collision operator)**.** *Under suitable regularity conditions, we define the* collision operator

$$\mathscr{I}_\chi : \mathscr{L}^1(\mathbb{R}^d) \to \mathscr{L}^1(\mathbb{R}^d), \quad \rho^M \mapsto \mathrm{Tr}_m\big(\rho^M \otimes |S^X\chi\rangle\langle S^{X'}\chi|\big). \tag{3.9}$$

Remark 9. It can be verified that the operator $\mathscr{I}_\chi$ is well-defined and completely positive (in particular it preserves positivity). Moreover, in terms of integral kernels, the action of the collision operator reads

$$[\mathscr{I}_\chi\rho](X,X') = \rho(X,X')\,I_\chi(X,X'), \tag{3.10}$$

where the *collision function* I_χ is defined by

$$I_\chi(X,X') := \langle S^{X'}\chi | S^X\chi\rangle, \qquad X,X' \in \mathbb{R}^d. \tag{3.11}$$

Notice that I_χ reaches its maximum modulus at $X = X'$, where it equals one.

Theorem 10. *[6] Assume sufficient regularity for the potential V and the initial condition. Denote furthermore by $\rho_\varepsilon(t)$ the solution to equation (3.6) and by $\rho^{M,a}(t)$ the unique solution to the problem*

$$\begin{cases} i\partial_t\rho^{M,a}(t) &= [H_0, \rho^{M,a}(t)] \\ \rho^{M,a}(0) &:= \mathscr{I}_\chi\rho^M(0). \end{cases} \tag{3.12}$$

Then, the error introduced by replacing ρ_ε^M by the solution $\rho^{M,a}$ is given by

$$\|\rho_\varepsilon^M(t) - \rho^{M,a}(t)\|_{\mathscr{L}^1} \le \widetilde{C}_1\left(\frac{1+\varepsilon}{\varepsilon}\,t - \varepsilon^{-\gamma}, \varepsilon^{-\gamma}\right) + \widetilde{C}_2\,\varepsilon + \widetilde{C}_3\,\varepsilon^{1-\gamma}, \tag{3.13}$$

with $\lim_{\tau,\tau'\to+\infty}\widetilde{C}_1(\tau,\tau') = 0$ and the constants $\widetilde{C}_2, \widetilde{C}_3 > 0$ dependent only on φ, χ and V.

This theorem, which is the main theorem of this work, states that one can replace the resolution of the two-body interacting system (3.6) by the freely evolving system (3.12) for the heavy particle, which embodies the information on the heavy-light interaction in the collision operator $\mathscr{I}_\chi$ occurring in the initial condition only. Therefore, one can get rid of any variable related to the light particle and thus of the fast time scale. The initial multi-scale problem then reduces to a one-scale problem, allowing a considerable gain in efficiency as compared to the method employed in [7].

One-dimensional systems. Computation of $\mathscr{I}_\chi$

Now, we restrict to one-dimensional problems and provide a general expression for the collision function I_χ (see (3.15), (3.16), (3.17)) whose form shows that it depends on the reflection and transmission amplitudes associated to the potential V and on the wave function of the light particle. Consider a particle moving on a line under the action of the potential V. We define the *transmission amplitude* t_k and the *reflection amplitude* r_k as the two complex coefficients s.t. the action of the scattering operator S, defined in (3.3), reads

$$(S\chi)(x) = \frac{1}{\sqrt{2\pi}} \int_{\mathbb{R}} \left[t_k \widehat{\chi}(k) + r_{-k} \widehat{\chi}(-k) \right] e^{ikx}\, dk, \quad \forall\, x \in \mathbb{R}, \tag{3.14}$$

for any $\chi \in L^2(\mathbb{R})$. We stress that definition (3.14) corresponds to the following formal action on plane waves

$$S(e^{ikx}) = r_k e^{-ikx} + t_k e^{ikx},$$

which, in turn, agrees with the definition of reflection and transmission amplitudes usually found in physics textbooks.

Proposition 11. *[6] For a one-dimensional two-particle system, endowed with an interaction potential V, the collision function I_χ defined in (3.11) can be expressed as*

$$I_\chi(X, X') = 1 - \Theta_\chi(X - X') + i\,\Gamma_\chi(X) - i\,\Gamma_\chi(X'), \tag{3.15}$$

with the definitions

$$\Theta_\chi(Y) := \int_{\mathbb{R}} \left(1 - e^{2ikY}\right) |r_k|^2 |\widehat{\chi}(k)|^2\, dk, \tag{3.16}$$

$$\Gamma_\chi(X) := i \int_{\mathbb{R}} e^{2ikX}\, \overline{r_{-k}}\, t_k\, \overline{\widehat{\chi}(-k)}\, \widehat{\chi}(k)\, dk. \tag{3.17}$$

In the case in which the initial state of the incoming light particle is represented by a Gaussian wave function, *i.e.*

$$\chi(x) = \frac{1}{(2\pi\sigma^2)^{1/4}} e^{-\frac{(x-x_l)^2}{4\sigma^2} + ipx}, \tag{3.18}$$

where $x_l \in \mathbb{R}$ is the centre of the wave packet, σ its spread, and p its mean momentum, one has

$$\widehat{\chi}(k) = \left(\frac{2\sigma^2}{\pi}\right)^{1/4} e^{-\sigma^2(k-p)^2 - i(k-p)x_l}.$$

We shall make this choice of state for the light particle in Section III, when dealing with numerical simulations. In this case, definitions (3.16) and (3.17) yield simplified expressions

$$\begin{aligned} \Theta_{\sigma,p}(Y) &= \sigma\sqrt{\tfrac{2}{\pi}} \textstyle\int_{\mathbb{R}} \left(1 - e^{2ikY}\right) |r_k|^2 e^{-2\sigma^2(k-p)^2}\, dk, \\ \Gamma_{\sigma,p}(X) &= i\sigma\sqrt{\tfrac{2}{\pi}} e^{-2\sigma^2 p^2} \textstyle\int_{\mathbb{R}} t_k \overline{r_{-k}}\, e^{-2\sigma^2 k^2 + 2ik(X - x_l)}\, dk, \end{aligned} \tag{3.19}$$

which are more manageable for our simulations.

Particular potentials of interest.

Here, we briefly introduce three particular potentials that we used in the numerical simulations, and give the corresponding reflection and transmission amplitudes, necessary for the computation of I_χ via (3.15), (3.16), (3.17).

Dirac's delta potential In the case $V = \alpha\delta_0$, with $\alpha > 0$, the reflection and transmission amplitudes are given by

$$r_k = -\frac{\alpha}{\alpha - i|k|}, \qquad t_k = -\frac{i|k|}{\alpha - i|k|}, \quad \forall k \in \mathbb{R}. \tag{3.20}$$

Potential barrier A further potential for which the scattering matrix can be explicitly computed is the potential barrier, i.e.

$$V(x) := V_0 \mathbb{1}_{[-a,a]}, \qquad V_0 = \frac{\alpha}{2a} \quad a > 0,$$

where $\mathbb{1}$ denotes the characteristic function and $\alpha > 0$ measures the strength of the interaction. Letting $E = \frac{k^2}{2}$ denote the energy of the incoming wave and defining $k_0 := \sqrt{2(E - V_0)} \in \mathbb{C}$, the transmission and reflection amplitudes have the forms

$$t_k = \frac{4kk_0 e^{-2ika}}{(k+k_0)^2 e^{-2ik_0 a} - (k-k_0)^2 e^{2ik_0 a}}, \quad \forall k \in \mathbb{R}\setminus\{0\}, \tag{3.21}$$

$$r_k = \frac{(k^2 - k_0^2)e^{-2ika}(e^{-2ik_0 a} - e^{2ik_0 a})}{(k+k_0)^2 e^{-2ik_0 a} - (k-k_0)^2 e^{2ik_0 a}}, \quad \forall k \in \mathbb{R}\setminus\{0\}. \tag{3.22}$$

Numerical approximation for more general potentials In the case of more general potentials, there is no analytic expression for the amplitudes r_k and t_k, however, we can compute them numerically.

We assume that the potential V is rapidly decreases at infinity, and choose a sufficiently large a such that we can approximate V by 0 on $\mathbb{R}\setminus[-a,a]$. To calculate the reflection and transmission amplitudes, we look for generalized eigenfunctions ψ_k of the Hamiltonian $-\frac{1}{2}\Delta + V$ associated to the eigenvalue $E = \frac{k^2}{2}$. Thanks to our approximation, these eigenfunctions are combinations of the plane-waves e^{ikx} and e^{-ikx} outside the interval $[-a,a]$. For $k > 0$ we look for solutions satisfying

$$\psi_k(x) := \begin{cases} e^{ik(x+a)} + r_k e^{-ik(x+a)} & \text{for } x < -a, \\ t_k e^{ik(x-a)} & \text{for } x > a. \end{cases} \tag{3.23}$$

In order to find the values of t_k and r_k, one must solve the stationary Schrödinger equation associated with transparent boundary conditions in the interval $[-a,a]$

$$\begin{cases} -\frac{1}{2}\psi_k''(x) + V\psi_k = E\psi\,, \quad x\in[-a,a], \\ \psi_k'(-a) + ik\psi_k(-a) = 2ik, \\ \psi_k'(a) - ik\psi_k(a) = 0. \end{cases} \tag{3.24}$$

Transparent boundary conditions express the fact that the wave function as well as its derivative are continuous at $\pm a$. Using the continuity of the wave function and of its derivative at $x=\pm a$, it can be checked that the boundary conditions in (3.24) are indeed satisfied if and only if conditions (3.23) are satisfied for some r_k and t_k. The reflection and transmission amplitudes are then given by

$$t_k := \psi_k(a)\,, \quad r_k := \psi_k(-a) - 1\,, \quad \forall k>0. \tag{3.25}$$

For a wave coming from the right, i.e. $k<0$, the procedure is analogous.

III NUMERICAL SIMULATIONS

In this section we shall finally use the approximations introduced in Section II and II.2 in order to efficiently resolve the two-body Schrödinger equation (3.1)-(3.2) in the regime $\varepsilon \ll 1$. The final aim is to quantify and study numerically the decoherence effect induced on the heavy particle by the interaction with the light one.

Model and initial data

According to Theorem 10, for small values of ε we can replace the resolution of the two-body Schrödinger equation (3.1)-(3.2) or, equivalently, of equation (3.6) for density operators, by the resolution of system (3.12) for the reduced density operator of the heavy particle. Rephrasing the latter as an equation for the integral kernel $\rho^{M,a}(t,X,X')$ of the operator $\rho^{M,a}(t)$, one gets

$$\begin{cases} i\,\partial_t \rho^{M,a}(t,X,X') = -\dfrac{1}{2M}(\Delta_X - \Delta_{X'})\rho^{M,a}(t,X,X')\,, \quad \forall (X,X')\in\mathbb{R}^2\,,\ \forall\, t\in\mathbb{R}^+ \\ \rho^{M,a}(0,X,X') = \rho_0^M(X,X')\, I_\chi(X,X'), \end{cases} \tag{3.26}$$

where the collision function I_χ is given by formulas (3.15), (3.16), (3.17), and $\rho_0^M(X,X')$ is the integral kernel of the operator ρ_0^M, which represents the state of the heavy particle before the collision. We set

$$\rho_0^M(X,X') := \varphi(X)\,\overline{\varphi(X')}, \tag{3.27}$$

where

$$\varphi(X) := N\big(\varphi_-(X) + \varphi_+(X)\big) \tag{3.28}$$

with

$$\varphi_\pm(X) := \frac{1}{(2\pi)^{1/4}\sqrt{\sigma_H}} e^{-\frac{(X\mp X_0)^2}{4\sigma_H^2}} e^{\mp i p_H X} \tag{3.29}$$

$$N := \sqrt{2}\left(1+e^{-\frac{X_0^2}{2\sigma_H^2}} e^{-2\sigma_H^2 p_H^2}\right)^{\frac{1}{2}}. \tag{3.30}$$

The parameters X_0, p_H and σ_H are positive and defined in Table 3.1.

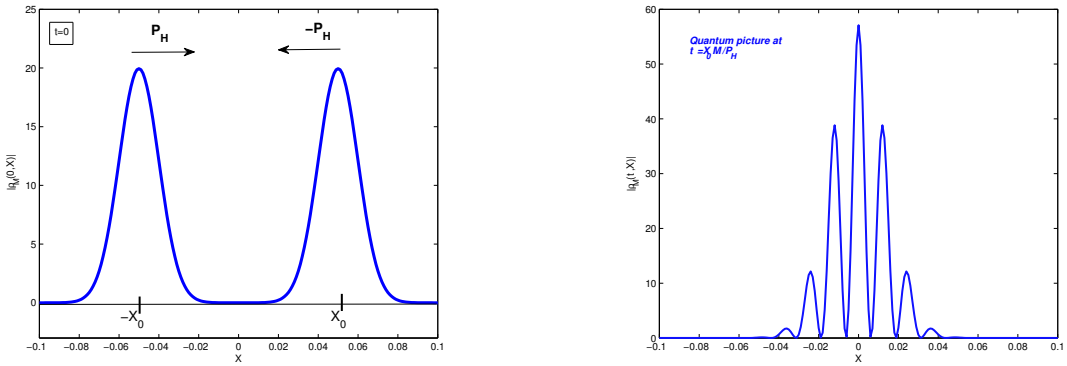

Figure 3.1: Left: Probability density associated to the initial state of the heavy particle. Right: Probability density associated to the state of the heavy particle in the case of no interaction, at the time of maximal overlap of the two bumps

Then, the integral kernel (3.27) can be rewritten as

$$\begin{aligned}\rho_0^M(0,X,X') &= N^2\left[\varphi_-(X)+\varphi_+(X)\right]\left[\overline{\varphi_-(X')}+\overline{\varphi_+(X')}\right] \\ &= N^2\left[\varphi_-(X)\overline{\varphi_-(X')}+\varphi_-(X)\overline{\varphi_+(X')}+\varphi_+(X)\overline{\varphi_-(X')}+\varphi_+(X)\overline{\varphi_+(X')}\right].\end{aligned} \tag{3.31}$$

The two terms $\varphi_\pm(X)\overline{\varphi_\pm(X')}$ are called *diagonal*, while the two terms $\varphi_\pm(X)\overline{\varphi_\mp(X')}$ are called *antidiagonal*. In fact, in view of definition (3.29) the products $\varphi_\pm(X)\overline{\varphi_\pm(X')}$ rapidly decay outside of a diagonal region $\{|X-X'|\simeq\sigma_H\}$, while the products $\varphi_\pm(X)\overline{\varphi_\mp(X')}$ are essentially supported in the region $\{|X+X'|\simeq\sigma_H\}$.

Physically, the density matrix "before the collision" ρ_0^M or, equivalently, the initial wave function (3.28), describes a state consisting of a quantum superposition of two localized bumps centred respectively at $\pm X_0$ and moving against each other with relative speed $2p_H/M$, as illustrated in the left plot of Figure 3.1. If no light particle or, more generally, no interaction is present, then one should use $\rho_0^M(X,X')$ as initial data in (3.26). Thus, at time MX_0/p_H the non-diagonal terms in (3.31) give rise to an interference pattern, shown in the right plot of Figure 3.1. The emergence of interference is due to the non-diagonal terms in (3.31). On the other hand, due to the collision, the initial data in (3.26) is replaced by $\rho_0^{M,a}(X,X') = I_\chi(X,X')\rho_0^M(X,X')$. We will see in Section III.3 that the presence of the factor I_χ damps the interference.

Numerical domain and discretization

Here we give some brief explanation about the numerical resolution of equation (3.26).

First, we truncate the spatial domain $\mathbb{R}^2$ to a bounded simulation domain $\Omega_X^2 := (-H,H)\times(-H,H)$ and impose boundary conditions on $\partial\Omega_X$. To simplify computations, we choose homogeneous Neumann boundary conditions, which prescribe that the particle is reflected at the boundaries. However, if the domain is sufficiently large, the presence of the boundaries has negligible influence on the dynamics of the heavy particle.

Second, we discretize equation (3.26). For the discretization in time we employ the Peaceman-Rachford scheme which is unconditionally stable and second-order accurate. Let us explain in more detail the steps in the scheme. We start by discretizing the time interval $[0,T]$ and the simulation domain of the heavy particle $\Omega_X = (-H,H)$. Let us introduce the time and space steps

$$\Delta t = \frac{T}{L} > 0, \qquad h_X := \frac{2H}{J-1} > 0, \qquad \text{with } L, J \in \mathbb{N},$$

and define the homogeneous discretization $t_l := l\Delta t$, $X_j = -H + (j-1)h_X$, so that

$$0 = t_0 \le \cdots \le t_l \le \cdots \le t_L = T, \quad -H = X_1 \le \cdots \le X_j \le \cdots \le X_J = H.$$

Then, defining the operators $A, B : \mathscr{H} \subset L^2(\Omega_X) \to L^2(\Omega_X)$

$$A := -\frac{1}{2M}\Delta_X, \quad B := \frac{1}{2M}\Delta_{X'}, \quad \mathscr{H} := \{\phi \in H^2(\Omega_X) \;/\; \partial_n\phi = 0, \text{ on } \partial\Omega_X\},$$

where ∂_n denotes the outward normal to the boundary $\partial\Omega_X$, the Peaceman-Rachford scheme for the system (3.26) writes

$$\rho^{l+1} = (iId - \frac{\Delta t}{2}A)^{-1}(iId + \frac{\Delta t}{2}B)(iId - \frac{\Delta t}{2}B)^{-1}(iId + \frac{\Delta t}{2}A)\rho^l, \qquad l = 0,\cdots,L-1, \tag{3.32}$$

where ρ^l (resp. ρ^l_{ij}) denotes the approximation of $\rho^{M,a}(t_l)$ (resp. $\rho^{M,a}(t_l,X_i,X_j)$). Notice that (3.32) is a sequence of Euler-explicit, Crank-Nicolson and Euler-implicit steps. Equivalently, one performs a sequential resolution of two 1D systems

$$(iId - \frac{\Delta t}{2}B)\rho^{l+1/2} = (iId + \frac{\Delta t}{2}A)\rho^l, \quad (iId - \frac{\Delta t}{2}A)\rho^{l+1} = (iId + \frac{\Delta t}{2}B)\rho^{l+1/2}.$$

Finally, we discretize the operators A and B in space via a standard second-order centered method.

The parameters employed in the simulations are summarized in Table 3.1.

Let us remark here that the scheme is an alternating-direction implicit (ADI) omethod, i.e. the actions of the two operators A and B, acting respectively on the variable X and X', are separated, so that, compared to a direct resolution of (3.26) via the Crank-Nicolson method, the computational costs are drastically reduced.

$2*H$	$2*10^{-1}$	J	201
T	$1.92*10^{-2}$	L	$120*20+1$
$\hbar$	1	p_H	$3.4*M$
M	100	p	$1.25; 2.5; 3.5*10^2$
σ_H, σ	$10^{-2}, 2*10^{-2}$	X_0, x_l	$5*10^{-2}, 2*10^{-1}$
α	$0, \cdots, 40*10^2$		

Table 3.1: Parameters used in the numerical simulations.

Numerical results and interpretation

Here we present some numerical results obtained via the method introduced in the previous section for the resolution of the evolution equation (3.26). We shall consider in this lecture only the Dirac's delta interaction potential, the cases of a potential barrier or a Gaussian potential are presented and commented in [6]. Furthermore, we shall also sketch the case with multiple light particles.

Dirac's delta potential

Let us here consider the case $V(x) = \alpha\delta_0(x)$, with $\alpha \in \mathbb{R}^+$. The left plot in Figure 3.2 shows the quantity $|\rho_0^M(X, X')|$ (i.e. the state of the heavy particle before the collision with the light one). Notice that the non-trivial values of $\rho_0^M(X, X')$ are concentrated in four bumps. In accordance with the terminology introduced in Section III.1, the two bumps located around the diagonal $X = X'$ are called *diagonal* while the two others, located around the set $X = -X'$, are called *antidiagonal*. The diagonal bumps give the probability density associated to the state of the heavy particle, while the antidiagonal bumps are responsible for the interference. Diagonal and antidiagonal bumps share the same shape and the same size.

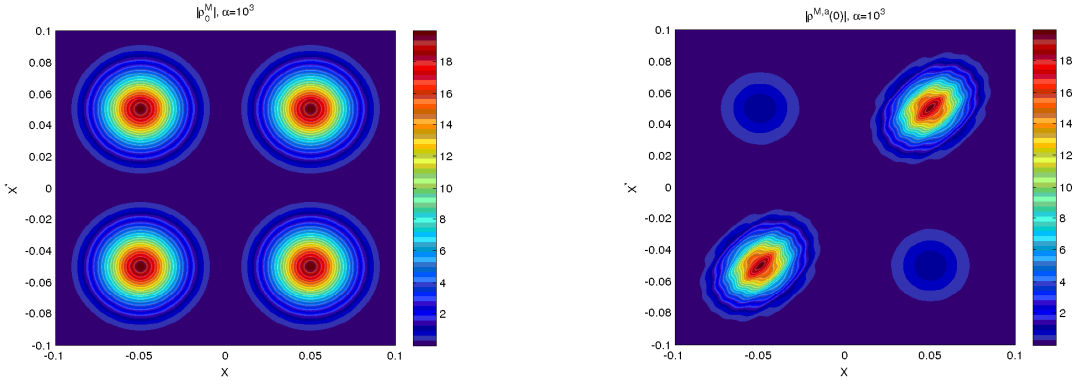

Figure 3.2: Test case: Dirac potential with $\alpha = 10^3$. Left: Plot of $|\rho_0^M(X, X')|$ before the collision; Right: Plot of $|\rho^{M,a}(0, X, X')|$ immediately after the collision.

The right plot in Figure 3.2 displays $|\rho^{M,a}(0,X,X')| = |I_\chi(X,X')\rho_0^M(X,X')|$ (i.e. the state of the heavy particle immediately after the collision) in the test case $\alpha = 10^3$. It is easily seen that, as an effect of the collision with the light particle, the antidiagonal bumps are damped, thus providing the expected attenuation of the interference.

To understand this Figure better, we devoted Fig. 3.3 to the collision function I_χ. In the left plot we show $|I_\chi(X,X')|$ corresponding to the right plot of Figure 3.2, while in the right plot of Figure 3.3 we give $|I_\chi(X,-X)|$ for different values of α. One can observe that, as the strength of the potential varies, the band width of $|I_\chi(X,-X)|$ remains unchanged; on the other hand, notice that the more the potential is intense, the more the quantity $|I_\chi(X,-X)|$ is reduced for large values of X. It is precisely this reduction which causes the damping of the antidiagonal bumps in Figure 3.2.

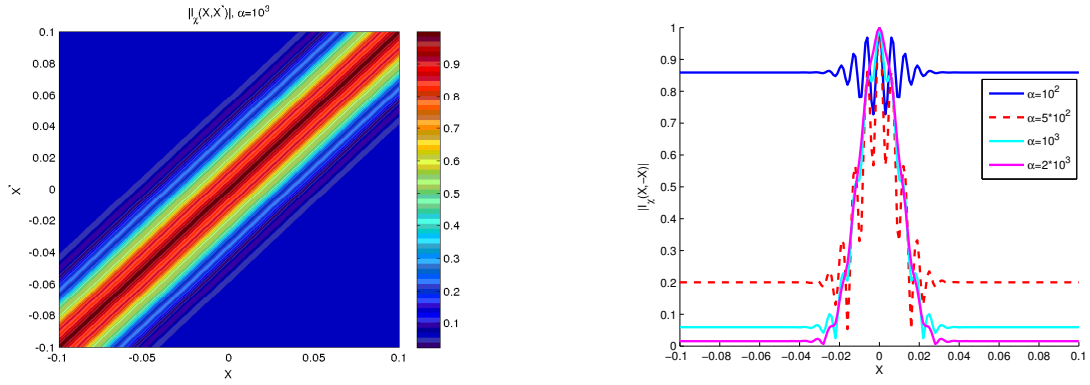

Figure 3.3: Left: Plot of $|I_\chi(X,X')|$ for $\alpha = 10^3$. Right: Plot of $|I_\chi(X,-X)|$ for several values of α.

In order to examine how the decoherence effect varies with the momentum of the light particle, in Figure 3.4 we plot $|I_\chi(0.05,-0.05)|$ for several values of α and three different momenta p of the light particle. We observe that the larger the momentum is, the smaller the decoherence effect on the heavy particle is. This can be explained by the fact that most of the light particle is transmitted when its momentum is large.

Finally, in Figure 3.5 we display the probability density $\rho^{M,a}(t_*,X,X)$ associated to the state of the heavy particle at the time $t_* = X_0 M/p_H$ of maximal overlap of the two diagonal bumps. The left plot in Figure 3.5 corresponds to a collision with a light particle arriving from the right with mean momentum $p = -2.5 * 10^2$, for several potential strengths α. One sees that the probability density associated to the state of the heavy particle splits into a component that exhibits complete interference and a bump that travels with mean momentum $p_H + p > p_H$ towards the right without experiencing interference. We refer to the component that displays interference as the *coherent part*, while the component in which interference is absent is referred to as the *decoherent part*.
In the right plot, the light particle has momentum $p = 0$ and is located at the centre $x_l = 0$. The interference pattern exhibits a clear decoherence effect. In particular, notice

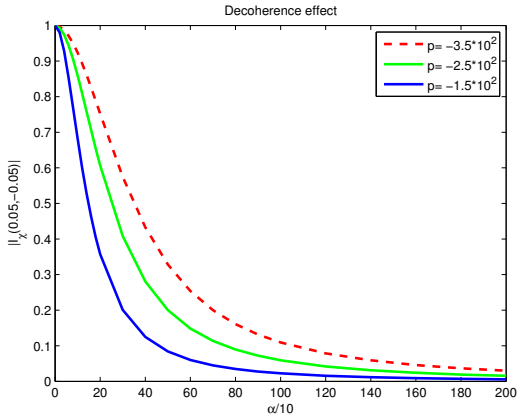

Figure 3.4: The quantity $|I_\chi(0.05,-0.05)|$ as a function of α for three different values of the momentum of the light particle.

that inside the pattern there are no points with zero probability. The corresponding plot is similar to the ones exhibited in [7] through a direct use of the Joos-Zeh formula. In fact, this plot too can be understood as the simultaneous presence of a coherent and of a decoherent part, except that here, since the momentum of the decoherent part is zero, the two components share the same support. A theoretical explanation of the appearance of the decoherent bumps is given in [6].

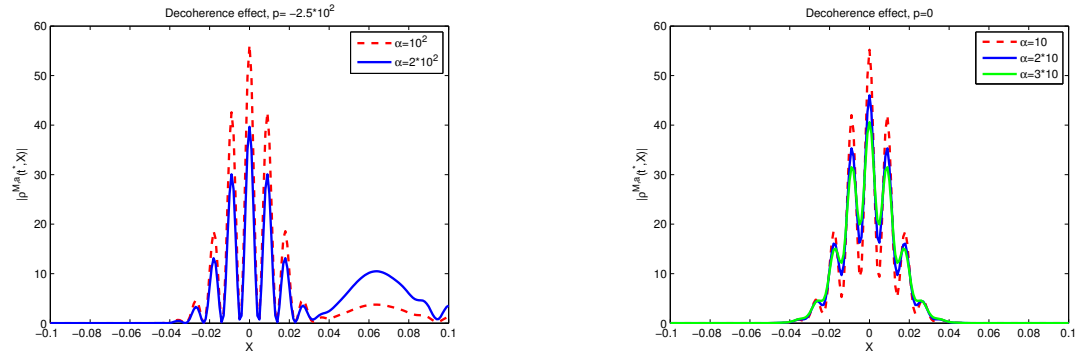

Figure 3.5: Attenuation of the interference pattern of the heavy particle, in the case that the light particle comes from the right with $p = -2.5 * 10^2$ (left Fig.) resp. $p = 0$ (right Fig.)

Several light particles

We suppose now that many light particles are injected one-by-one into the computational domain, in such a way that the heavy particle undergoes a finite sequence of collisions at times $t_k := 4k\Delta t$. At any collision, the state of the light particle is supposed to be the same, i.e., the k.th colliding light particle lies in the state represented

by the wave function $U_0(t_k - \varepsilon^{-\gamma})\chi$. During any time interval (t_k, t_{k+1}), between two collisions, the heavy particle evolves freely. The state of the heavy particle after each collision $\rho(t_k^+)$ is then related to the state before collision $\rho(t_k^-)$ by

$$\rho(t_k^+) = \mathscr{F}_\chi[\rho(t_k^-)].$$

On the left plot of Figure 3.6 we show the probability density $\rho^{M,a}(t^*, X, X)$ associated to the state of the heavy particle at the time of maximal overlap. The plot refers to the case of a Dirac's delta potential with strength $\alpha = 10$, momentum of the light particle $p = 0$ and $N = 1, 2, 3$ collisions. As expected, multiple collisions enforce the destruction of the interference pattern.

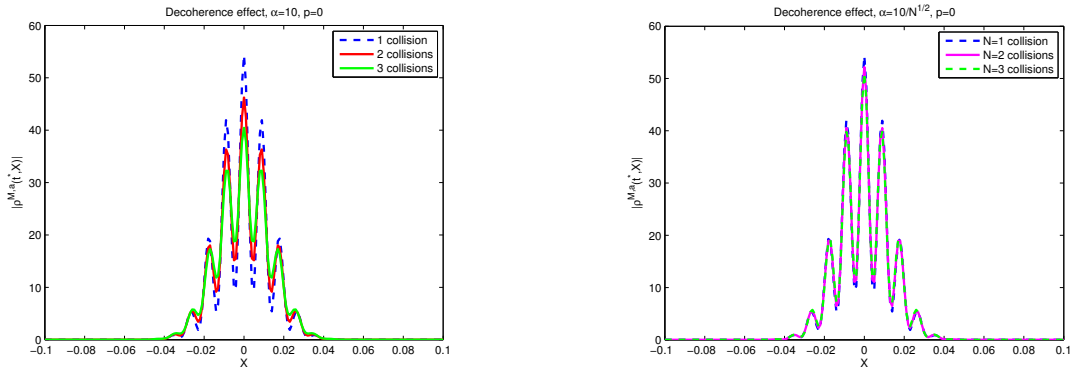

Figure 3.6: Attenuation of the interference pattern of the heavy particle in the case of several collisions. Test case: Dirac's delta potential, $p = 0$. Left: Fixed $\alpha = 10$ and several collisions $N = 1, 2, 3$. Right: $N = 1, 2, 3$ with $\alpha = 10/\sqrt{N}$.

All these numerical simulations permitted us to study the dynamics of a quantum heavy particle undergoing a repulsive interaction with one or several light particles, in the aim to better understand the so-called decoherence phenomenon. If one is interested in the study of infinitly many incoming light particles, then a significant re-scaling of the potential should be done, namely of strength $\alpha/\sqrt{N}$ with fixed α: with this scaling, the decoherence effect should remain of order one (see the right plot in Figure 3.6). A detailed mathematical study of this effect in the case $N \to \infty$ would be an interesting forthcoming work.

CHAPTER 4

NONLINEAR SCHRÖDINGER EQUATION WITH DELTA-DIRAC POINT INTERACTION.

Chapter based on the article:
R. Carlone, R. Figari, C. Negulescu [1]

Nonlinear Schrödinger equations arise in several fields of application, as have been mentioned in the ouverture of this course. The modelling of crystals with defects or the scattering mechanism from impurities in a crystal, motivates the introduction of a special class of short-range nonlinearites, concentrated in a bounded region, as for example the Delta-Dirac point interactions or so-called δ-potentials. These artificial potentials are very interesting, as they approximate more complexe, realistic potentials, and permit explicit computations.

The core of this chapter concerns the modelling of the quantum beating-effect of the nitrogen nucleus N of an ammonia molecule (NH_3), performed in the double-well potential created by the hydorgen atoms. The beating-effect is a periodic motion of the N-atom, passing from one well to the other via tunneling effect and is a typical quantum feature. We are interested in this chapter in the study of the destruction of this N-beating effect, as a consequence of the nonlinearity of the problem, and the ensuing localization of the N-atom in one well (classical picture).

The model we shall use for the investigation of this phenomenon is a nonlinear Schrödinger equation with 2-point δ-interactions, which sketches the ammonia double-well potential. Highly oscillatory integrals are central to this study and constitute essentially the most challenging part from a numerical point of view. They have to be treated with adequate, efficient methods in order to get accurate results and investigate the delicate long-time behaviour of the N-atom wave-function.

[1] "The quantum beating effect and its suppression", submitted.

I THE MATHEMATICAL PROBLEM

Quantum beating may nowadays refer to many, often quite different, phenomena studied in various domains of quantum physics, ranging from quantum electrodynamics to particle physics, from solid state physics to molecular structure and dynamics. A paradigmatic example in the latter field is the inversion in the ammonia molecule observed experimentally in 1935. The ammonia molecule (NH_3) is pyramidally shaped. Three hydrogen atoms form the base and the nitrogen atom is located in one of the two distinguishable states (enantiomers) on one side or the other with respect to the base (chirality). Experimentally it was tested that microwave radiation could induce a periodic transition from one state to the other, phenomenon called "quantum beating" and which appears to be a typical quantum mechanical feature. However, in non-isolated systems, for ex. in particular organic compounds containing ammonia-molecules, the pyramidal inversion is suppressed, as a consequence of a too large pressure, and the N-nucleus becomes localized in one of the two wells. Thus we observe in such non-isolated systems a rather classical behaviour, which is due to the interaction of the ammonia-molecule with the environment (decoherence phenomenon).

A theoretical explanation of the quantum beating phenomenon was obtained by modeling the nitrogen atom as a quantum particle evolving in a double-well potential created by the three hydrogen atoms [41, 46, 86]. The beating effect appears then as a manifestation of superpositions of the ground state and the lowest exited state, concentrating periodically inside one well or the other. To reduce complexity, one can use two-point interactions instead of the two-well potential, description which renders the theoretical as well as computational aspects of the problem more easier to handle. Such point-interactions represent a non-trivial however entirely solvable limit model for potentials with very short range.

In order to introduce now the quantum-beating model we shall investigate in the present chapter, let us first briefly recall the definition of point interaction hamiltonians in $L^2(\mathbb{R})$ (see [12] for further details). For two point scatterers placed in $Y = \{y_1, y_2\}$ and with strength $\underline{\gamma} = \{\gamma_1, \gamma_2\}$, $\gamma_i \in \mathbb{R}$, the formal hamiltonian reads

$$H_{\underline{\gamma},Y}\,\psi := \text{“} -\Delta\psi + \gamma_1\delta_{y_1}\psi + \gamma_2\delta_{y_2}\psi \text{“},$$

where the Planck constant $\hbar$ has been taken equal to one and the particle mass m equal to $1/2$. The wave-function $\psi(t,x)$ represents here the probability of finding at instant t the nitrogen atom at the position x, the H-atoms being situated at the origin $x = 0$.
A mathematical rigorous definition of $H_{\underline{\gamma},Y}$ in dimension $d = 1$ has been given in the early days of quantum mechanics, when such kind of hamiltonians were extensively used to investigate the dynamics of a quantum particle in various kinds of short range scatterer arrays. A complete characterization of point interaction hamiltonians in dimension $d = 2,3$ was only made available in the second half of last century [12].

We shall detail in this work the case $d = 1$, corresponding to our physical context. Assume that the two points are placed symmetrically with respect to the origin with $|y_i| = a > 0$. Then

$$D(H_{\underline{\gamma},Y}) := \left\{ \psi \in L^2(\mathbb{R}) \mid \psi = \phi^\lambda - \sum_{i,j=1}^{2} \left(\Gamma_{\underline{\gamma}}^\lambda\right)_{ij}^{-1} \phi^\lambda(y_j) G^\lambda(\cdot - y_i), \quad \phi^\lambda \in H^2(\mathbb{R}) \right\}, \tag{4.1}$$

$$\left(H_{\underline{\gamma},Y} + \lambda\right)\psi = \left(-\frac{d^2}{dx^2} + \lambda\right)\phi^\lambda, \tag{4.2}$$

are domain and action of a selfadjoint operator in $L^2(\mathbb{R})$, which acts as the free laplacian on functions supported outside the two points $y_{1,2} = \pm a$. In (4.1) the Green function G^λ and the matrix $\Gamma_{\underline{\gamma}}^\lambda$ are defined by

$$G^\lambda(x) := \frac{e^{-\sqrt{\lambda}|x|}}{2\sqrt{\lambda}}, \qquad \left(\Gamma_{\underline{\gamma}}^\lambda\right)_{ij} := \frac{1}{\gamma_i}\delta_{ij} + G^\lambda(y_i - y_j), \tag{4.3}$$

and the positive real $\lambda \in \mathbb{R}^+$ is large enough to make the matrix $\Gamma_{\underline{\gamma}}^\lambda$ invertible. It is immediate to check that the derivative of $G^\lambda(x)$ has a jump in the origin, equal to -1. This in turn implies that every function ψ belonging to the domain $D(H_{\underline{\gamma},Y})$ satisfies the "boundary" or "interface" conditions in the points $y_{1,2} = \pm a$, *i.e.*

$$\psi'(y_j^+) - \psi'(y_j^-) = \gamma_j \psi(y_j), \qquad j = 1,2. \tag{4.4}$$

Additionally, let us also mention here the important property that the self-adjoint operator $H_{\underline{\gamma},Y}$ admits for $\gamma_{1,2} \neq 0$ at most two eigenvalues which are negative and simple. To be more precise, one has that $-\lambda \in \sigma_p(H_{\underline{\gamma},Y}) \cap (-\infty, 0)$ if and only if $\det \Gamma_{\underline{\gamma}}^\lambda = 0$ and the corresponding eigenfunction is of the form

$$\varphi^\lambda(x) = \sum_{j=1}^{2} c_j G^\lambda(x - y_j), \quad c_j \in \mathbb{R},$$

where (c_1, c_2) is an eigenvector of the matrix $\Gamma_{\underline{\gamma}}^\lambda$, corresponding to the eigenvalue zero.

To summarize, the dynamics generated by $H_{\underline{\gamma},Y}$ is thus characterized by a free dynamics outside the two scatterers and the fulfilment at any time of the boundary conditions (4.4). Our aim in this work is now to investigate the behaviour of the solutions to the non-autonomous evolution problem

$$\begin{cases} \mathbf{i}\partial_t \psi = H_{\underline{\gamma}(t),Y}\,\psi, & \forall (t,x) \in \mathbb{R}^+ \times \mathbb{R}, \\ \psi(0,x) = \psi_0(x) \in D(H_{\underline{\gamma}(0),Y}), & \forall x \in \mathbb{R}, \\ \gamma_j(t) := \gamma |\psi(t,y_j)|^{2\sigma}, & \gamma < 0, \quad \sigma \geq 0, \end{cases} \tag{4.5}$$

where the time dependence of $\underline{\gamma}$ is non-linearly determined by the values of the solution itself in the points $y_{1,2} = \pm a$.

An alternative way to examine the Cauchy problem (4.5) is to write down the solution under the form of a Duhamel's formula, with a forcing term concentrated on the two points $y_{1,2} = \pm a$. In detail, let $U(\tau, y)$ be the integral kernel of the unitary group $\mathscr{U}(t) := e^{\mathbf{i}t\Delta}$, defined as

$$U(\tau, y) := \frac{e^{\mathbf{i}\frac{|y|^2}{4\tau}}}{\sqrt{4\mathbf{i}\pi\tau}}, \quad (\mathscr{U}(t)\xi)(x) = \int_{-\infty}^{\infty} U(t; x-y)\,\xi(y)\,dy \qquad \forall \xi \in L^2(\mathbb{R}).$$

Then from Duhamel's formula, one gets

$$\psi(t,x) = (\mathscr{U}(t)\psi_0)(x) - \mathbf{i}\gamma \sum_{j=1}^{2} \int_0^t U(t-s; x-y_j)|\psi(s,y_j)|^{2\sigma}\psi(s,y_j)\,ds, \tag{4.6}$$

yielding in the scatteres $y_{1,2} = \pm a$ the formula

$$\psi(t,y_i) = (\mathscr{U}(t)\psi_0)(y_i) - \mathbf{i}\gamma \sum_{j=1}^{2} \int_0^t U(t-s; y_i-y_j)|\psi(s,y_j)|^{2\sigma}\psi(s,y_j)\,ds. \tag{4.7}$$

It is easy to check that a function of the form (4.6) satisfies the non-linear boundary conditions at all times (see [8] for details). Following now a standard use in higher dimensional cases, we shall introduce in this work the two functions $q_1(t) \equiv \psi(t,-a)$ and $q_2(t) \equiv \psi(t,a)$, which satisfy the following coupled nonlinear Volterra integral equations, called also "charge equations"

$$\begin{cases} q_1(t) + \dfrac{\gamma}{2}\sqrt{\dfrac{\mathbf{i}}{\pi}}\displaystyle\int_0^t \frac{q_1(s)\,|q_1(s)|^{2\sigma}}{\sqrt{t-s}}\,ds + \frac{\gamma}{2}\sqrt{\frac{\mathbf{i}}{\pi}}\int_0^t \frac{q_2(s)\,|q_2(s)|^{2\sigma}}{\sqrt{t-s}}\,e^{\mathbf{i}\frac{a^2}{t-s}}\,ds \\ \qquad\qquad = (\mathscr{U}(t)\,\psi_0)(-a), \\ q_2(t) + \dfrac{\gamma}{2}\sqrt{\dfrac{\mathbf{i}}{\pi}}\displaystyle\int_0^t \frac{q_2(s)\,|q_2(s)|^{2\sigma}}{\sqrt{t-s}}\,ds + \frac{\gamma}{2}\sqrt{\frac{\mathbf{i}}{\pi}}\int_0^t \frac{q_1(s)\,|q_1(s)|^{2\sigma}}{\sqrt{t-s}}\,e^{\mathbf{i}\frac{a^2}{t-s}}\,ds \\ \qquad\qquad = (\mathscr{U}(t)\,\psi_0)(a). \end{cases} \tag{4.8}$$

Let us underline that $\vartheta(t,x) := (\mathscr{U}(t)\,\psi_0)(x)$ is the solution of the free 1D Schrödinger equation

$$\begin{cases} \mathbf{i}\partial_t\vartheta = -\partial_{xx}\vartheta, \quad \forall (t,x) \in \mathbb{R}^+ \times \mathbb{R}, \\ \vartheta(0,x) = \psi_0(x), \quad \forall x \in \mathbb{R}. \end{cases} \tag{4.9}$$

The solution of the Cauchy problem (4.5) is now simply reduced to the computation of the free evolution $(\mathscr{U}(t)\,\psi_0)(\pm a)$ and the solution of the two coupled nonlinear Volterra integral equations (4.8). The whole wave-function ψ is then recovered via (4.6). This strategy shall permit us to do considerable savings in memory and time, as will be noticed in Sections II and III. Indeed, system (4.8) is only time-dependent, and the free Schrödinger equation (4.9) can be simply solved via a spectral method.

In order to better understand how the beating effect occurs and the reasons why one expects suppression of this phenomenon by nonlinear perturbation, we study in Sections I.1 and I.2 a symmetric and anti-symmetric linear case in some detail.

Linear point interactions - Symmetric double well

Let us consider the symmetric linear case, corresponding to $\sigma = 0$ and $\gamma_1 = \gamma_2 = \gamma$. We will show that the eigenstates relative to the lowest eigenvalues are explicitly computable for the hamiltonian we consider.

First of all, if we consider only a one point interaction in $y = 0$ of strength γ, then the Hamiltonian

$$H_{\gamma,0} := \text{“} - \partial_{xx} + \gamma\,\delta_0'', \qquad \gamma < 0\,, \tag{4.10}$$

admits a unique bound state $(-\lambda, G^\lambda)$, meaning $H_{\gamma,0}\,G^\lambda = -\lambda\,G^\lambda$ (in the distributional sense), with eigenvalue $E = -\lambda < 0$ and eigenfunction G^λ given by

$$G^\lambda(x) := \frac{e^{-\sqrt{\lambda}\,|x|}}{2\sqrt{\lambda}}\,, \qquad \lambda = \gamma^2/4 > 0\,. \tag{4.11}$$

The stationary solutions to the evolution equation

$$\mathbf{i}\,\partial_t\psi = -\partial_{xx}\psi + \gamma\,\delta_0\,\psi\,, \tag{4.12}$$

are hence of the form $\psi(t,x) = N\,e^{\mathbf{i}\lambda\,t}G^\lambda(x)$, with $N > 0$ a normalization constant.

Coming now to our two-point interaction case, the Hamiltonian $H_{\underline{\gamma},Y}$ admits two bound state $(-\lambda_f, \phi_f)$ and $(-\lambda_e, \phi_e)$. To be more precise, $-\lambda$ will be a negative eigenvalue of $H_{\underline{\gamma},Y}$ if and only if $\det(\Gamma^\lambda_{\underline{\gamma}}) = 0$. In the case of two point interactions of the same strength this condition reads

$$\det\begin{pmatrix} \frac{1}{\gamma} + \frac{1}{2\sqrt{\lambda}} & \frac{e^{-2\sqrt{\lambda}\,a}}{2\sqrt{\lambda}} \\ \frac{e^{-2\sqrt{\lambda}\,a}}{2\sqrt{\lambda}} & \frac{1}{\gamma} + \frac{1}{2\sqrt{\lambda}} \end{pmatrix} = 0 \quad \Longleftrightarrow \quad 1 + \xi/\gamma = \pm e^{-\xi\,a}\,, \quad \text{with } \xi := 2\sqrt{\lambda}\,. \tag{4.13}$$

For $\gamma < -\frac{1}{a}$ there are two solutions $\lambda_{f,e} > 0$ to the previous equation. The indices "f,e" stand for “fundamental” resp. first “excited” state. The associated eigenfunctions are

$$\phi_f(x) = N_f\left(G^{\lambda_f}(x+a) + G^{\lambda_f}(x-a)\right), \tag{4.14}$$

$$\phi_e(x) = N_e\left(G^{\lambda_e}(x+a) - G^{\lambda_e}(x-a)\right), \tag{4.15}$$

where N_f and N_e are easily computable normalization factors.

In Fig. 4.1 we plotted the two eigenstates $\phi_f(x)$ and $\phi_e(x)$, corresponding to the ground state (symmetric function) and the first excited state (anti-symmetric function). Notice that the two eigenstates are relative to energies getting closer and closer as the value of $|\gamma|$ increases. In the same limit the absolute values of the two eigenfunctions tend to coincide.

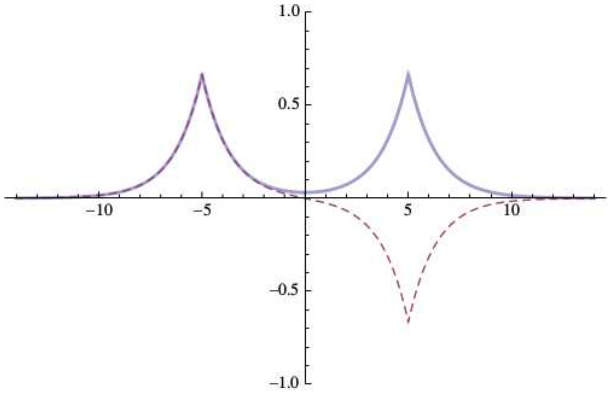

Figure 4.1: Plot of the functions $\phi_f(x)$ in blue and $\phi_e(x)$ with a dashed line

The stationary solutions corresponding to these eigenstates are given by

$$\psi_f(t,x) = e^{\mathbf{i}\lambda_f t}\phi_f(x)\,, \quad \psi_e(t,x) = e^{\mathbf{i}\lambda_e t}\phi_e(x)\,. \tag{4.16}$$

A superposition of the two stationary states,

$$\psi_0(x) = \alpha\,\phi_f(x) + \beta\,\phi_e(x)\,, \qquad \alpha,\beta \in \mathbb{R}\,,$$

evolves as

$$\psi(t,x) = \alpha\, e^{\mathbf{i}\lambda_f t}\phi_f(x) + \beta\, e^{\mathbf{i}\lambda_e t}\phi_e(x)\,.$$

An initial condition with $\alpha \neq 0$ and $\beta \neq 0$ gives rise to a beating dynamics. If one of both parameters α,β is zero, we are in a stationary state as (4.16).
The special superposition

$$\psi^L_{beat,0}(x) := \frac{1}{\sqrt{2}}\left(\phi_f(x) + \phi_e(x)\right), \tag{4.17}$$

is concentrated in the left well and will evolve in time as

$$\psi^L_{beat}(t,x) = \frac{1}{\sqrt{2}}\left(e^{\mathbf{i}\lambda_f t}\phi_f(x) + e^{\mathbf{i}\lambda_e t}\phi_e(x)\right), \tag{4.18}$$

with a probability density given by

$$\mathscr{P}(t,x) = \frac{1}{2}\left[|\phi_f(x)|^2 + |\phi_e(x)|^2 + 2\,\phi_f(x)\phi_e(x)\cos\left((\lambda_f - \lambda_e)\,t\right)\right]. \tag{4.19}$$

It is now clear that ψ^L_{beat} is an oscillating function with period $T_B = \dfrac{2\pi}{\lambda_f - \lambda_e}$ concentrated successively on the left and on the right well, justifying hence the definition of (4.18) as a beating state.

Linear point interactions - Asymmetric double well

Let us now investigate the changes in the beating mechanism when the two zero range potentials have different strengths $\gamma_1 \neq \gamma_2$, $\gamma_1 < \gamma_2$. In this asymmetric case the equation for finding the eigenvalues of the Hamiltonian $H_{\underline{\gamma},Y}$ is:

$$\det \Gamma^{\lambda}_{(\gamma_1,\gamma_2)} = \det \begin{pmatrix} \frac{1}{\gamma_1} + \frac{1}{2\sqrt{\lambda}} & \frac{1}{2\sqrt{\lambda}} e^{-2\sqrt{\lambda}a} \\ \frac{1}{2\sqrt{\lambda}} e^{-2\sqrt{\lambda}a} & \frac{1}{\gamma_2} + \frac{1}{2\sqrt{\lambda}} \end{pmatrix} = 0\,, \tag{4.20}$$

leading to

$$\left(\frac{1}{\gamma_1} + \frac{1}{2\sqrt{\lambda}}\right)\left(\frac{1}{\gamma_2} + \frac{1}{2\sqrt{\lambda}}\right) - \left(\frac{1}{2\sqrt{\lambda}}\right)^2 e^{-4\sqrt{\lambda}a} = 0\,. \tag{4.21}$$

Defining $\xi := 2\sqrt{\lambda}$ the last equation can be rewritten as

$$\frac{\xi^2}{\gamma_1\gamma_2} + \xi\left(\frac{1}{\gamma_1} + \frac{1}{\gamma_2}\right) + 1 = e^{-2\xi a}\,. \tag{4.22}$$

The number of positive solutions to (4.22) depends on the values of the parameters γ_i and on the distance $2a$. Straightforward computations show that (4.22) admits two distinct positive solutions (ξ_0, ξ_1) in the case that both $\gamma' s$ are negative, $1/|\gamma_2| < 2\,a$ and that $|\gamma_1| \gg |\gamma_2|$. The corresponding eigenvalues are denoted in this case by (λ_0, λ_1).

The eigenfunction relative to the lowest eigenvalue $E_0 = -\lambda_0 < 0$ as well as the first excited state $E_1 > E_0$, $E_1 = -\lambda_1 < 0$, have the form (see Theorem 2.1.3 in [12])

$$\phi_0(x) = N_0 \left[\, G^{\lambda_0}(x+a) + \alpha_0\, G^{\lambda_0}(x-a)\right], \qquad \alpha_0 := \sqrt{\frac{\gamma_2}{\gamma_1}}\sqrt{\frac{2\sqrt{\lambda_0}+\gamma_1}{2\sqrt{\lambda_0}+\gamma_2}}, \tag{4.23}$$

$$\phi_1(x) = N_1 \left[\, G^{\lambda_1}(x+a) - \alpha_1\, G^{\lambda_1}(x-a)\right], \qquad \alpha_1 := \sqrt{\frac{\gamma_2}{\gamma_1}}\sqrt{\frac{2\sqrt{\lambda_1}+\gamma_1}{2\sqrt{\lambda_1}+\gamma_2}}, \tag{4.24}$$

where $N_0 > 0, N_1 > 0$ are normalization constants.

Special choices of γ_1, γ_2 permit to render ϕ_0 orthogonal to ϕ_1 in the sense that $\phi_0(x)\,\phi_1(x) \approx 0$, leading to a suppression of the oscillating term in (4.19) and, as a consequence, the beating will be locked only around one interaction point. This symmetry-breaking and hence beating-destructing phenomenon will be investigated numerically in Section III. Starting from an initial condition of the form

$$\psi_{asy,0}(x) := \alpha\,\phi_0(x) + \beta\,\phi_1(x)\,, \quad \alpha, \beta \in \mathbb{R}\,, \tag{4.25}$$

the exact time-evolution of this state is given by

$$\psi_{asy}(t,x) := \alpha\, e^{\mathbf{i}\lambda_0 t}\,\phi_0(x) + \beta\, e^{\mathbf{i}\lambda_1 t}\,\phi_1(x)\,. \tag{4.26}$$

Nonlinear point interactions

A detailed analytical study of the non linear case $\sigma > 0$ (which is no longer explicitly solvable) can be found in [8, 9]. The authors obtained general results about existence of solutions either local or global in time and proved existence of blow up solutions for σ larger than 2.
In Section III we present the numerical simulation results for the evolution of a beating state, i.e., an initial state giving rise in the linear case to a beating motion of the particle, namely

$$\psi_0(x) := \alpha\phi_f(x) + \beta\phi_e(x), \quad \alpha, \beta \in \mathbb{R}. \tag{4.27}$$

Our aim is to study how the nonlinearity influences the beating phenomenon. As we already mentioned we expect that even if the initial condition is almost-symmetric, the nonlinearity will have the effect of braking the symmetry. The numerical simulations will be based on the resolution of the Volterra system (4.8), as mentioned above.

Let us further observe that from [8] (Theorem 6) we know that, if $0 \leq \sigma < 1$ and for an initial data $\psi_0 \in H^1(\mathbb{R})$, the Cauchy problem has a unique solution which is global in time. Moreover in [8] (Theorem 23) it is proved that if $\gamma < 0$ and $\sigma \geqslant 1$, there exist initial data such that the solutions of the Cauchy problem will blow-up in finite time.

II THE NUMERICAL DISCRETIZATION OF THE VOLTERRA-SYSTEM

Let us come now to the numerical part of this work, namely the discretization and later on simulation of the Volterra-system (4.8), in order to investigate the delicate phenomenon of beating. Linear (symmetric and asymmetric) as well as nonlinear cases will be treated, starting from an initial condition under one of the forms

$$\psi^L_{beat,0}(x) := \alpha\phi_f(x) + \beta\phi_e(x), \quad \psi_{asy,0}(x) := \alpha\phi_0(x) + \beta\phi_1(x), \tag{4.28}$$

with some given constants $\alpha, \beta \in \mathbb{R}$ and (ϕ_f, ϕ_e) resp. (ϕ_0, ϕ_1) defined in (4.14)-(4.15) resp. (4.23)-(4.24).

The discretization of the Volterra-system (4.8) passes through the discretization of two different kind of integrals, an Abel-integral, which is of the form

$$\mathscr{A}b(t) := \int_0^t \frac{g(s)}{\sqrt{t-s}}\, ds, \tag{4.29}$$

and a highly-oscillating integral of the form

$$\mathscr{H}o(t) := \int_0^t \frac{g(s)}{\sqrt{t-s}}\, e^{\mathbf{i}\frac{a^2}{t-s}}\, ds. \tag{4.30}$$

Besides, the free Schrödinger equation (4.9) has to be solved to compute the right hand side of the Volterra system, *i.e.* $(\mathscr{U}(t)\psi_0)(\pm a)$, and one has also to take care of the nonlinearity, which will be treated iteratively by means of a linearization. The treatment of all these four steps shall be presented in the following subsections.

For the numerics we shall consider the truncated time-space domain $[0,T]\times[-L_x,L_x]$ and impose periodic boundary conditions in space. We shall furthermore fix a homogeneous discretization of this domain, defined as

$$0=t_1<\cdots<t_l<\cdots<t_K=T\,,\qquad t_l:=(l-1)\Delta t\,,\qquad \Delta t:=T/(K-1);$$
$$-L_x=x_1<\cdots<x_i<\cdots<x_N=L_x\,,\quad x_i:=-L_x+(i-1)\Delta x\,,\quad \Delta x:=2L_x/(N-1)\,.$$

The free Schrödinger evolution

We shall present now two different resolutions of the Schrödinger equation (4.9), a numerical resolution via the Fast Fourier Transform (fft,ifft) assuming periodic boundary conditions in space and an analytic, explicit resolution by means of the continuous Fourier Transform and based on the specific initial condition we choose.

The numerical resolution starts from the partial Fourier-Transform (in space) of (4.9)

$$\begin{cases}\partial_t\hat\theta_k(t)=-\mathbf{i}\,k^2\hat\theta_k(t)\,,\quad\forall k\in\mathbb{Z}\,,\quad\forall t\in\mathbb{R}^+\,,\\ \hat\theta_k(0)=\hat\psi_{0,k}\,,\quad\forall k\in\mathbb{Z}\,,\end{cases}$$

where

$$\hat\psi_{0,k}:=\frac{1}{2L_x}\int_{-L_x}^{L_x}\psi_0(x)e^{-\mathbf{i}\omega x k}\,dx\,,\quad \omega:=\frac{\pi}{L_x}\,,$$

and hence

$$\hat\theta_k(t)=e^{-\mathbf{i}k^2t}\hat\theta_k(0)\,,\quad\forall(t,k)\in\mathbb{R}^+\times\mathbb{Z}\,. \tag{4.31}$$

Remark that we supposed here periodic boundary conditions in the truncated space-domain $[-L_x,L_x]$, where the appearance of the discrete Fourier-variable $k\in\mathbb{Z}$. Using the fft- as well as ifft-algorithms permits hence to get from (4.31) a numerical approximation of the solution $\vartheta(t,x)$ of the free Schrödinger equation (4.9).

Analytically, we shall situate us in the whole space $\mathbb{R}$ and shall perform the same steps explicitly, taking advantage of the initial condition, which has the form

$$\psi_0(x):=\alpha\phi_f(x)+\beta\phi_e(x)\,,\quad\forall x\in\mathbb{R}\,,\quad\alpha,\beta\in\mathbb{R}\,, \tag{4.32}$$

where we recall that (see (4.3), (4.14), (4.15))

$$\phi_f(x)=N_f\left[G^{\lambda_f}(x+a)+G^{\lambda_f}(x-a)\right]\,,\quad \phi_e(x)=N_e\left[G^{\lambda_e}(x+a)-G^{\lambda_e}(x-a)\right]\,.$$

Thus one has with the definition of the Fourier-transform and its inverse

$$\hat{\phi}(\nu) := \frac{1}{\sqrt{2\pi}} \int_{-\infty}^{\infty} \phi(x)\, e^{-\mathbf{i}x\nu}\, dx, \quad \phi(x) = \frac{1}{\sqrt{2\pi}} \int_{-\infty}^{\infty} \hat{\phi}(\nu)\, e^{\mathbf{i}x\nu}\, d\nu,$$

that

$$\hat{\psi}_0(\nu) = \alpha\, \hat{\phi}_f(\nu) + \beta\, \hat{\phi}_e(\nu) \quad \Rightarrow \quad \hat{\vartheta}(t,\nu) = \alpha\, \hat{\phi}_f(\nu)\, e^{-\mathbf{i}\nu^2 t} + \beta\, \hat{\phi}_e(\nu)\, e^{-\mathbf{i}\nu^2 t} \quad (t,\nu) \in \mathbb{R}^+ \times \mathbb{R}.$$

Let us now compute explicitly the Fourier transform of ϕ_0 and ϕ_1 and finally the inverse Fourier transform of $\hat{\vartheta}(t,\nu)$. For this, remark that one has

$$\hat{G}^{\lambda}(\nu) = \frac{1}{\sqrt{2\,\pi}}\, \frac{1}{\lambda + \nu^2}, \quad \forall \nu \in \mathbb{R},$$

leading to

$$\hat{\phi}_f(\nu) = \frac{2N_f}{\sqrt{2\,\pi}}\, \frac{\cos(\nu\, a)}{\lambda_f + \nu^2}, \quad \hat{\phi}_e(\nu) = -\frac{2\,\mathbf{i}\,N_e}{\sqrt{2\,\pi}}\, \frac{\sin(\nu\, a)}{\lambda_e + \nu^2}.$$

Now, in the aim to resolve numerically the Volterra-system (4.8), one needs only to compute the solution of (4.9) in the points $y_{1,2} = \pm a$, which means

$$\vartheta(t,-a) = \frac{\alpha\, N_f}{2\pi} \int_{-\infty}^{\infty} \frac{1 + e^{-2\mathbf{i}a\nu}}{\lambda_f + \nu^2}\, e^{-\mathbf{i}\nu^2 t}\, d\nu + \frac{\beta\, N_e}{2\pi} \int_{-\infty}^{\infty} \frac{1 - e^{-2\mathbf{i}a\nu}}{\lambda_e + \nu^2}\, e^{-\mathbf{i}\nu^2 t}\, d\nu.$$

$$\vartheta(t,a) = \frac{\alpha\, N_f}{2\pi} \int_{-\infty}^{\infty} \frac{1 + e^{2\mathbf{i}a\nu}}{\lambda_f + \nu^2}\, e^{-\mathbf{i}\nu^2 t}\, d\nu - \frac{\beta\, N_e}{2\pi} \int_{-\infty}^{\infty} \frac{1 - e^{2\mathbf{i}a\nu}}{\lambda_e + \nu^2}\, e^{-\mathbf{i}\nu^2 t}\, d\nu,$$

To compute these two integrals, we shall take advantage of the following two formulae

$$I_A^{\lambda} := \int_{-\infty}^{\infty} \frac{1}{\lambda + \nu^2}\, e^{-\mathbf{i}\nu^2 t}\, d\nu = \frac{\pi}{\sqrt{\lambda}}\, e^{\mathbf{i}\lambda t} \left[1 - \operatorname{erf}(\sqrt{\mathbf{i}\lambda\, t})\right],$$

$$I_B^{\lambda} := \int_{-\infty}^{\infty} \frac{e^{\pm 2\mathbf{i}a\nu}}{\lambda + \nu^2}\, e^{-\mathbf{i}\nu^2 t}\, d\nu = \int_{-\infty}^{\infty} \frac{\cos(2\,a\nu)}{\lambda + \nu^2}\, e^{-\mathbf{i}\nu^2 t}\, d\nu,$$

where erf(·) is the so-called error-function, defined by

$$\operatorname{erf}(x) := \frac{2}{\sqrt{\pi}} \int_0^x e^{-t^2}\, dt.$$

After some straightforward computations, one gets

$$I_B^{\lambda} = \frac{\pi}{2\sqrt{\lambda}}\, e^{\mathbf{i}\lambda t} \left\{ e^{2\sqrt{\lambda}a} \left[1 - \operatorname{erf}\left(\sqrt{\mathbf{i}\lambda\, t} + \frac{a}{\sqrt{\mathbf{i}\, t}}\right)\right] + e^{-2\sqrt{\lambda}a} \left[1 - \operatorname{erf}\left(\sqrt{\mathbf{i}\lambda\, t} - \frac{a}{\sqrt{\mathbf{i}\, t}}\right)\right] \right\}.$$

With the two expressions I_A^{λ} and I_B^{λ} one has now

$$(\mathscr{U}(t)\,\psi_0)(-a) = \vartheta(t,-a) = \frac{\alpha\, N_f}{2\pi} \left[I_A^{\lambda_f} + I_B^{\lambda_f}\right] - \frac{\beta\, N_e}{2\pi} \left[I_A^{\lambda_e} + I_B^{\lambda_e}\right],$$

$$(\mathscr{U}(t)\,\psi_0)(a) = \vartheta(t,a) = \frac{\alpha\, N_f}{2\pi} \left[I_A^{\lambda_f} + I_B^{\lambda_f}\right] + \frac{\beta\, N_e}{2\pi} \left[I_A^{\lambda_e} + I_B^{\lambda_e}\right],$$

which permits to have the right-hand side of the Volterra-system (4.8) analytically.
Let us observe that the same computations hold also for the asymmetric initial condition (4.25) with (ϕ_f, ϕ_e) replaced by (ϕ_0, ϕ_1), as well as (N_f, N_e) by (N_0, N_1).

The Abel integral

Let us now present a discretization of an Abel-integral of the form (4.29), based on a Gaussian quadrature. The time interval $[0,T]$ is discretized in a homogeneous manner, as proposed above, such that one can now approximate $\mathscr{A}b(t_l)$ for $l=1,\cdots,K$ as follows

$$\mathscr{A}b(t_l)=\int_0^{t_l}\frac{g(s)}{\sqrt{t_l-s}}\,ds=\sum_{k=1}^{l-1}\int_{t_k}^{t_{k+1}}\frac{g(s)}{\sqrt{t_l-s}}\,ds=\sum_{k=1}^{l-1}\sqrt{\Delta t}\int_0^1\frac{g(t_k+\xi\Delta t)}{\sqrt{l-k-\xi}}\,d\xi\,.$$

Now, introducing the notation

$$r_k^{(l)}:=l-k\,,\quad \varphi_k(\xi):=g(t_k+\xi\Delta t)\,,\quad p_k^{(l)}(\xi):=\frac{1}{\sqrt{r_k^{(l)}-\xi}}\,,$$

we will use a Gaussian quadrature formula with one point and the weight-function $p_k^{(l)}(\xi)$ to approximate the last integral as follows

$$\int_0^1 p_k^{(l)}(\xi)\,\varphi_k(\xi)\,d\xi=w_k^{(l)}\,\varphi_k(\xi_k^{(l)})\,,$$

with the "Gauss-points" given by

$$w_k^{(l)}:=\int_0^1\frac{1}{\sqrt{r_k^{(l)}-\eta}}\,d\eta\,,\quad \xi_k^{(l)}:=\frac{1}{w_k^{(l)}}\int_0^1\frac{\eta}{\sqrt{r_k^{(l)}-\eta}}\,d\eta\,. \tag{4.33}$$

This leads to

$$\mathscr{A}b(t_l)\approx\sqrt{\Delta t}\sum_{k=1}^{l-1}w_k^{(l)}\,g(t_k+\Delta t\,\xi_k^{(l)})\,.$$

As the function g is known only at the grid points t_k, we shall linearize g in the cell $[t_k,t_{k+1}]$ to find finally the approximation formula we used for the Abel-integral

$$\mathscr{A}b(t_l)\approx\mathscr{A}b_{num}(t_l):=\sqrt{\Delta t}\sum_{k=1}^{l-1}w_k^{(l)}\left[\xi_k^{(l)}\,g_{k+1}+(1-\xi_k^{(l)})\,g_k\right],\quad\forall\,l=1,\cdots,K,\tag{4.34}$$

where $w_k^{(l)}$ and $\xi_k^{(l)}$ are given by (4.33) and $g_k:=g(t_k)$. Let us remark here that the function $g(s)$ is known up to the instant t_{l-1}, such that we have to keep in mind that there is a term in this last formula, which is unknown, *i.e.* g_l, and which has to be computed at this present step via the Volterra-system. This procedure shall be explained in subsection II.4, however let us here introduce some notation, to simplify the subsequent analysis. We shall denote

$$\mathscr{A}b^1_{num}(t_l):=\sqrt{\Delta t}\sum_{k=1}^{l-2}w_k^{(l)}\left[\xi_k^{(l)}\,g_{k+1}+(1-\xi_k^{(l)})\,g_k\right]+\sqrt{\Delta t}\,w_{l-1}^{(l)}\,(1-\xi_{l-1}^{(l)})\,g_{l-1}\,,\quad\forall\,l=1,\cdots,K,$$

and

$$\mathscr{A}b^2_{num}(t_l):=\sqrt{\Delta t}\,w_{l-1}^{(l)}\,\xi_{l-1}^{(l)}\,g_l\,,$$

such that (4.34) becomes simply

$$\mathscr{A}b(t_l)\approx\mathscr{A}b_{num}(t_l)=\mathscr{A}b^1_{num}(t_l)+\sqrt{\Delta t}\,w_{l-1}^{(l)}\,\xi_{l-1}^{(l)}\,g_l\,,\quad\forall\,l=1,\cdots,K.\tag{4.35}$$

The Highly-oscillating integral

Let us come now to the treatment of the highly oscillatory integral (4.30), which is the most delicate part of our numerical scheme. Indeed, as one can observe from Fig. 4.2, the integrand function (here with $g \equiv 1$, $t = a = 1$) is a rapidly varying function such that its integration has to be done with care. We shall present here different procedures

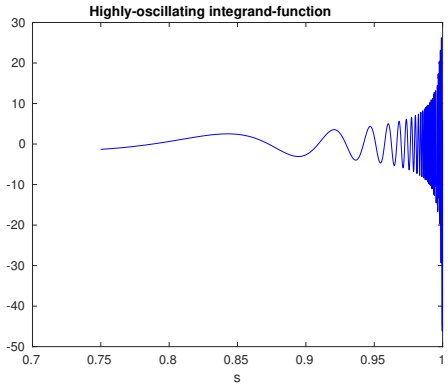

Figure 4.2: Evolution in time of the integrand function $h(s) := \frac{1}{\sqrt{1-s}}\, e^{\mathbf{i}\frac{1}{1-s}}$ with $s \in [0,1]$.

for its computation or approximation. The first procedure is more analytical and based on integral-tables [1]. The second one is a numerical approach and uses integration-by-parts to cope with the high oscillations.

The analytic procedure starts with linearizing the function g in the cell $[t_k, t_{k+1}]$,

$$g(s) = \frac{g_{k+1} - g_k}{\Delta t}\,(s - t_k) + g_k\,, \quad \forall s \in [t_k, t_{k+1}]\,,$$

in order to approximate

$$\begin{aligned}
\mathscr{H}o(t_l) &:= \int_0^{t_l} \frac{g(s)}{\sqrt{t_l - s}}\, e^{\mathbf{i}\frac{a^2}{t_l - s}}\, ds \\
&\approx \sum_{k=1}^{l-1} \left[\frac{g_{k+1} - g_k}{\Delta t} \int_{t_k}^{t_{k+1}} \frac{s - t_k}{\sqrt{t_l - s}}\, e^{\mathbf{i}\frac{a^2}{t_l - s}}\, ds + g_k \int_{t_k}^{t_{k+1}} \frac{1}{\sqrt{t_l - s}}\, e^{\mathbf{i}\frac{a^2}{t_l - s}}\, ds \right] \\
&= \sum_{k=1}^{l-1} \left[\frac{g_{k+1} - g_k}{\Delta t}\, I_1^{k,l} + g_k\, I_2^{k,l} \right], \quad \forall l = 1, \cdots, K\,,
\end{aligned}$$

where we denoted

$$I_1^{k,l} := \int_{t_k}^{t_{k+1}} \frac{s - t_k}{\sqrt{t_l - s}}\, e^{\mathbf{i}\frac{a^2}{t_l - s}}\, ds\,, \qquad I_2^{k,l} := \int_{t_k}^{t_{k+1}} \frac{1}{\sqrt{t_l - s}}\, e^{\mathbf{i}\frac{a^2}{t_l - s}}\, ds\,.$$

The $I_1^{k,l}$-integral can be further developped as follows

$$I_1^{k,l} = \int_{t_k}^{t_{k+1}} \frac{s - t_l}{\sqrt{t_l - s}}\, e^{\mathbf{i}\frac{a^2}{t_l - s}}\, ds + (t_l - t_k) \int_{t_k}^{t_{k+1}} \frac{1}{\sqrt{t_l - s}}\, e^{\mathbf{i}\frac{a^2}{t_l - s}}\, ds = -I_3^{k,l} + (t_l - t_k)\, I_2^{k,l}\,,$$

where we introduced

$$I_3^{k,l} := \int_{t_k}^{t_{k+1}} \sqrt{t_l - s}\, e^{\mathbf{i}\frac{a^2}{t_l - s}}\, ds.$$

The integrals $I_2^{k,l}$ and $I_3^{k,l}$ have now explicit expressions. Indeed, one can find, using [1], that

$$I_2^{k,l} = 2\int_{D_{k+1}}^{D_k} e^{\mathbf{i}a^2/\xi^2}\, d\xi = 2\left[\sqrt{-\mathbf{i}\pi}\, a\, \mathrm{erf}\left(\frac{\sqrt{-\mathbf{i}}\, a}{\xi}\right)\right]_{D_{k+1}}^{D_k}, \quad D_k := \sqrt{t_l - t_k}; \tag{4.36}$$

and

$$I_3^{k,l} = 2\int_{D_{k+1}}^{D_k} \xi^2\, e^{\mathbf{i}a^2/\xi^2}\, d\xi = \frac{2}{3}\left[\xi^3\right]_{D_{k+1}}^{D_k} + 4\sqrt{\mathbf{i}\pi}\,(T_{D_k} - T_{D_{k+1}}), \tag{4.37}$$

with

$$T_D = \left[\frac{\xi^3}{3}\,\mathrm{erf}\left(\frac{\sqrt{-\mathbf{i}}}{D}\,\xi\right) + e^{\frac{\mathbf{i}}{D^2}\xi^2}\,\frac{D}{3\sqrt{-\mathbf{i}\pi}}\left(\xi^2 + \mathbf{i}D^2\right)\right]_0^a, \quad \text{for } D = D_k, D_{k+1}.$$

Using now these explicit formulae (4.36)-(4.37) we get an approximate formula for the highly-oscillating intergral $\mathscr{H}o$, *i.e.*

$$\mathscr{H}o(t_l) \approx \sum_{k=1}^{l-1}\left[\frac{g_{k+1} - g_k}{\Delta t}\left(-I_3^{k,l} + (t_l - t_k) I_2^{k,l}\right) + g_k\, I_2^{k,l}\right], \quad \forall l = 1, \cdots, K, \tag{4.38}$$

This formula is quasi-analytical, and is based on the linearization of the function g. This linearization is possible, if the function g itself is not highly-oscillating. We remark here also that (4.38) involves the still unknown value g_l.

A second idea can be used to approximate these highly oscillating integrals, based more on a numerical discretization. Let us start from

$$\begin{aligned}
\mathscr{H}o(t_l) &= \int_0^{t_l} \frac{g(s)}{\sqrt{t_l - s}}\, e^{\mathbf{i}\frac{a^2}{t_l - s}}\, ds \\
&= \sum_{k=1}^{N_{it}^{(l)}-1} \int_{t_k}^{t_{k+1}} \frac{g(s)}{\sqrt{t_l - s}}\, e^{\mathbf{i}\frac{a^2}{t_l - s}}\, ds + \sum_{k=N_{it}^{(l)}}^{l-2} \int_{t_k}^{t_{k+1}} \frac{g(s)}{\sqrt{t_l - s}}\, e^{\mathbf{i}\frac{a^2}{t_l - s}}\, ds + \int_{t_{l-1}}^{t_l} \frac{g(s)}{\sqrt{t_l - s}}\, e^{\mathbf{i}\frac{a^2}{t_l - s}}\, ds \\
&=: I_{H1} + I_{H2} + I_{H3}, \quad \forall l = 1, \cdots, K.
\end{aligned}$$

This decomposition follows the evolution of the integrand-function, meaning that the index $N_{it}^{(l)} \in [1, l-1] \subset \mathbb{N}$ will delimitate the regions of smooth evolution resp. rapid variation and shall permit two different treatments of the integrals. This index is chosen in our case in the following manner:

The highly oscillating function $e^{\mathbf{i}\frac{a^2}{t_l - s}}$ has a period which diminishes monotonically as $s \to t_l$. The extrema of this function are localized at the points $s_j := t_l - \frac{a^2}{j\pi}$, $j \in \mathbb{N}$ and $s_j \to_{j\to\infty} t_l$. A function is smooth in our sens, if between two extrema we have at

least 5 time-steps. Hence, letting $J \in \mathbb{N}$ being the index, such that $5 \star \Delta t \sim s_{J+1} - s_J = \frac{a^2}{\pi}\left[\frac{1}{J} - \frac{1}{J+1}\right] \sim \frac{a^2}{\pi J^2}$, we define $N_{it}^{(l)}$ such that $t_{N_{it}^{(l)}} < s_J < t_{N_{it}^{(l)}+1}$.
Now for $k < N_{it}^{(l)}$ the integrand function is not so oscillating, and a standard quadrature-method (for example rectangle or trapez-method) can be used to approximate I_{H1}. In particular, using the trapez-method leads to

$$I_{H1} \approx \sum_{k=1}^{N_{it}^{(l)}-1} \frac{\Delta t}{2}\left[\frac{g_{k+1}}{\sqrt{t_l - t_{k+1}}}\, e^{\mathbf{i}\frac{a^2}{t_l - t_{k+1}}} + \frac{g_k}{\sqrt{t_l - t_k}}\, e^{\mathbf{i}\frac{a^2}{t_l - t_k}}\right].$$

For $k \geq N_{it}^{(l)}$ the integrand function is becoming too oscillating to use any more standard quadrature methods, such that we shall rather make use of an integration-by-parts (IPP) technique, *i.e.*

$$\begin{aligned}
\int_{t_k}^{t_{k+1}} \frac{g(s)}{\sqrt{t_l - s}}\, e^{\mathbf{i}\frac{a^2}{t_l - s}}\, ds &= \left(-\frac{\mathbf{i}}{a^2}\right)\int_{t_k}^{t_{k+1}} g(s)\,(t_l - s)^{3/2}\left(\frac{\mathbf{i}a^2}{(t_l - s)^2}\, e^{\mathbf{i}\frac{a^2}{t_l - s}}\right) ds \\
&= \frac{\mathbf{i}}{a^2}\int_{t_k}^{t_{k+1}} \left[g(s)\,(t_l - s)^{3/2}\right]' e^{\mathbf{i}\frac{a^2}{t_l - s}}\, ds - \frac{\mathbf{i}}{a^2}\left[g(s)\,(t_l - s)^{3/2}\, e^{\mathbf{i}\frac{a^2}{t_l - s}}\right]_{t_k}^{t_{k+1}} \\
&\approx \left(-\frac{\mathbf{i}}{a^2}\right)\left[g_{k+1}\,(t_l - t_{k+1})^{3/2}\, e^{\mathbf{i}\frac{a^2}{t_l - t_{k+1}}} - g_k\,(t_l - t_k)^{3/2}\, e^{\mathbf{i}\frac{a^2}{t_l - t_k}}\right]; \\
\int_{t_{l-1}}^{t_l} \frac{g(s)}{\sqrt{t_l - s}}\, e^{\mathbf{i}\frac{a^2}{t_l - s}}\, ds &\approx \frac{\mathbf{i}}{a^2}\, g_{l-1}\,(\Delta t)^{3/2}\, e^{\mathbf{i}a^2/\Delta t}.
\end{aligned}$$

Using these formulae, and remarking the telescopic summation, one gets immediately

$$I_{H2} + I_{H3} \approx \frac{\mathbf{i}}{a^2}\, g_{N_{it}^{(l)}}\,(t_l - t_{N_{it}^{(l)}})^{3/2}\, e^{\mathbf{i}\frac{a^2}{t_l - t_{N_{it}^{(l)}}}}.$$

Hence, we get altogether

$$\mathscr{H}o_{num}(t_l) = \sum_{k=1}^{N_{it}^{(l)}-1} \frac{\Delta t}{2}\left[\frac{g_{k+1}}{\sqrt{t_l - t_{k+1}}}\, e^{\mathbf{i}\frac{a^2}{t_l - t_{k+1}}} + \frac{g_k}{\sqrt{t_l - t_k}}\, e^{\mathbf{i}\frac{a^2}{t_l - t_k}}\right] + \frac{\mathbf{i}}{a^2}\, g_{N_{it}^{(l)}}\,(t_l - t_{N_{it}^{(l)}})^{3/2}\, e^{\mathbf{i}\frac{a^2}{t_l - t_{N_{it}^{(l)}}}}. \tag{4.39}$$

Remark at this point that in this case, we do not need g_l for the computation of $\mathscr{H}o(t_l)$.

The Non-linearity

The non-linearity is treated iteratively, by linearizing the non-linear term. To explain this procedure, let us first summarize what we performed up to now in the discretization of the Volterra-system (4.8). Denoting for simplicity the constant $\kappa := \frac{\gamma}{2}\sqrt{\frac{\mathbf{i}}{\pi}}$ and using the approximations (4.35) as well as (4.39), we have for $l = 1, \cdots, K$

$$\begin{cases}
q_1^l + \kappa\sqrt{\Delta t}\, w_{l-1}^{(l)}\, \xi_{l-1}^{(l)}\, q_1^l\, |q_1^l|^{2\sigma} + \kappa\, \mathscr{A}b_{num}^{1,-}(t_l) + \kappa\, \mathscr{H}o_{num}^{+}(t_l) = \vartheta(t_l, -a) \\
q_2^l + \kappa\sqrt{\Delta t}\, w_{l-1}^{(l)}\, \xi_{l-1}^{(l)}\, q_2^l\, |q_2^l|^{2\sigma} + \kappa\, \mathscr{A}b_{num}^{1,+}(t_l) + \kappa\, \mathscr{H}o_{num}^{-}(t_l) = \vartheta(t_l, a),
\end{cases} \tag{4.40}$$

where in the Abel and highly-oscillating terms we introduced a sign $\pm$ in order to underline which function $g(s) = q_{1,2}(s)\,|q_{1,2}(s)|^{2\sigma}$ they involve, in particular the one corresponding to $y_1 = -a$ or to $y_2 = +a$.
The resolution of the non-linear system (4.40) consists now in introducing the linearization-sequence $\{q_{1,2}^{l,n}\}_{n\in\mathbb{N}}$ as follows

$$q_{1,2}^{l,0} := q_{1,2}^{l-1}\,,$$

and where the terms $q_{1,2}^{l,n}$ are solution for $n \geq 1$ of the linearized Volterra-system

$$\begin{cases} q_1^{l,n} + \kappa\sqrt{\Delta t}\, w_{l-1}^{(l)}\, \xi_{l-1}^{(l)}\, q_1^{l,n}\, |q_1^{l,n-1}|^{2\sigma} + \kappa\, \mathscr{A}\, b_{num}^{1,-}(t_l) + \kappa\, \mathscr{H}\, o_{num}^{+}(t_l) = \vartheta(t_l, -a) \\ q_2^{l,n} + \kappa\sqrt{\Delta t}\, w_{l-1}^{(l)}\, \xi_{l-1}^{(l)}\, q_2^{l,n}\, |q_2^{l,n-1}|^{2\sigma} + \kappa\, \mathscr{A}\, b_{num}^{1,+}(t_l) + \kappa\, \mathscr{H}\, o_{num}^{-}(t_l) = \vartheta(t_l, a)\,. \end{cases} \tag{4.41}$$

This procedure is stopped at $k = M$, either when two subsequent iterations do not vary any more, meaning $|q_{1,2}^{l,n} - q_{1,2}^{l,n-1}| < 10^{-3}$, or when a maximal number of interations, as $k = 10$ is reached, and one defines finally

$$q_{1,2}^{l} := q_{1,2}^{l,M}\,.$$

Solving now the system (4.41) permits us to get a numerical approximation of the solution to the Volterra-system (4.8) and in the next section we shall present the simulations based on the just presented scheme.

III NUMERICAL SIMULATION OF THE BEATING PHENOMENON

Let us present in this section the numerical results obtained with the scheme presented in Section II. First we shall investigate the symmetric and asymmetric linear case and compare the obtained results with the exact solutions in order to validate the code. A particular attention is paid to the asymmetric linear case, which does not allow for a beating motion of the particle, the initial symmetry being destroyed. Secondly we shall pass to the non-linear simulations and study the destruction of the beating due to the manifestation of the non-linearity.

The symmetric linear case

In this section we set $\sigma = 0$ and consider the linear Volterra-system (4.8)-(4.9) associated with the initial condition given in (4.32), namely

$$\psi_{beat,0}^{L}(x) := \alpha\,\phi_f(x) + \beta\,\phi_e(x)\,, \quad \alpha, \beta \in \mathbb{R}\,, \tag{4.42}$$

and corresponding exact solution

$$\begin{cases} q_1(t) = \alpha\,\phi_f(-a)\, e^{\mathbf{i}\lambda_f t} + \beta\,\phi_e(-a)\, e^{\mathbf{i}\lambda_e t}\,, \\ q_2(t) = \alpha\,\phi_f(a)\, e^{\mathbf{i}\lambda_f t} + \beta\,\phi_e(a)\, e^{\mathbf{i}\lambda_e t}\,, \end{cases} \quad \forall\, t \in \mathbb{R}^+\,. \tag{4.43}$$

In the following linear tests, we performed the simulations with the parameters

$$a = 3\,, \quad \alpha = \sqrt{0.01}\,,\ \beta = \sqrt{0.99}\,, \quad \gamma = -0.5\,. \tag{4.44}$$

Figure 4.3 presents on the left the time-evolution of the numerical solutions of the Volterra-system (4.8)-(4.9), associated to the parameters presented above, and on the right the relative error between the exact solution and the numerical solution. One can firstly observe the so-called beating motion of the system between the two "stable" configurations, which correspond to the first two energy states of the nitrogen atom. Secondly, one remarks also a nice overlap of the numerical with the exact solutions. This overlap begins to deteriorate in time, effect which comes from the accumulation of the numerical errors, arising during the approximations we perform in the simulation. These linear tests permitted us to validate the linear version of our code.

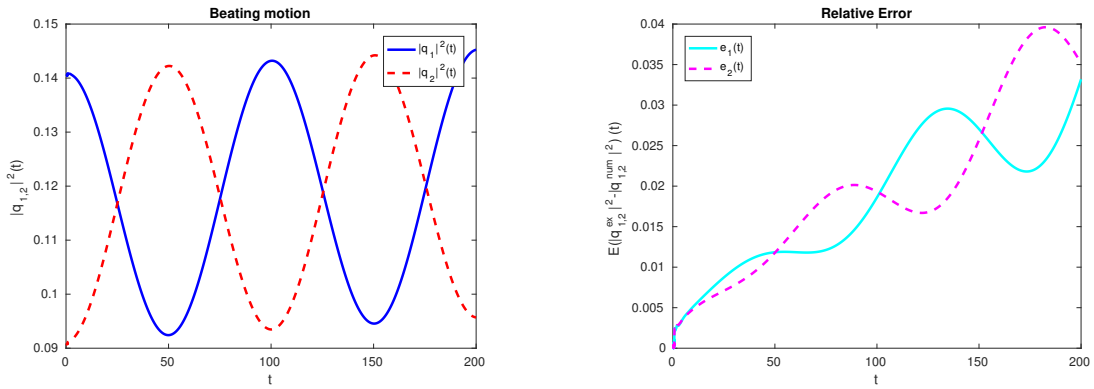

Figure 4.3: The beating effect. Left: Evolution in time of the numerical solutions $|q_1|^2(t)$ resp. $|q_2|^2(t)$. Right: Relative error: abs $\left[|q_{1,2}^{ex}|^2 - |q_{1,2}^{num}|^2\right] / ||q_{1,2}^{ex}||_\infty$.

The asymmetric linear case

In contrast to the previous case, we shall now choose an asymmetric initial condition of the form

$$\psi_{asy,0}(x) := \alpha\,\phi_0(x) + \beta\,\phi_1(x)\,, \quad \alpha, \beta \in \mathbb{R}\,,$$

with ϕ_0, ϕ_1 defined in (4.23)-(4.24). The exact solution is equally known in this case, and is given by similar a formula as (4.43) (see (4.26)). Two plots are presented in Fig. 4.4, corresponding to the two sets of parameters:

- (A) $\gamma_1 = -8,\ \gamma_2 = -4,\ a = 1/2,\ \alpha = \beta = 1/\sqrt{2}\,;$
- (B) $\gamma_1 = -10,\ \gamma_2 = -4,\ a = 5,\ \alpha = \beta = 1/\sqrt{2}\,.$

As expected, the beating motion of the nitrogen atom is completely annihilated, and this due to the asymmetric initial conditions. In Fig. 4.4 (A) one observes that the particle remains with a certain probability in each potential well, without crossing the barrier by tunneling and jumping in the other well. In each well, the particle is performing a periodic motion, permitting to show that the particle is not at rest in the well. In Fig. 4.4 (B) the parameters are more extreme and the particle seems even to be at rest in the two wells. The small oscillations one can observe in Fig. 4.4 (B) are

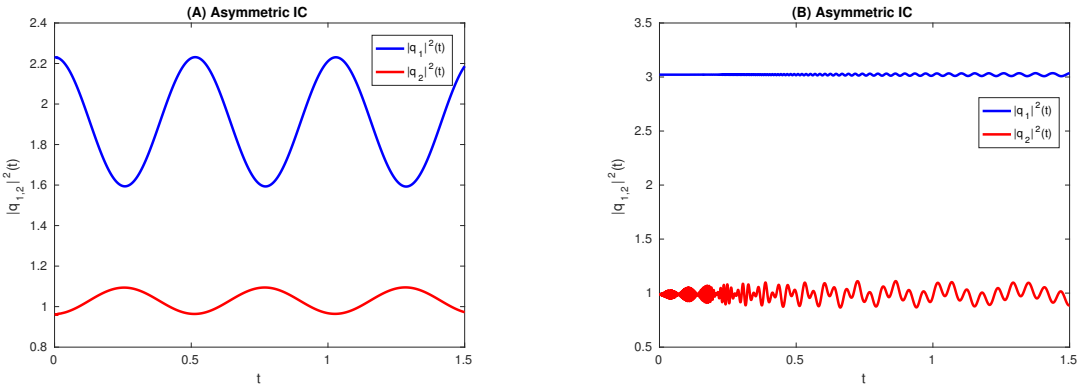

Figure 4.4: The asym. lin. case. Left: Evolution in time of the numerical solutions $|q_1|^2(t)$ resp. $|q_2|^2(t)$ with the set of parameters (A). Right: Same plots with the set of parameters (B).

due to numerical errors, the exact solution is quasi constant in time, oscillating with an amplitude of approx. 10^{-7}, as shown in the zoom of Fig. 4.5 for the unknown q_2. The relative error in this case between the exact solution and the numerical one is of 12%.

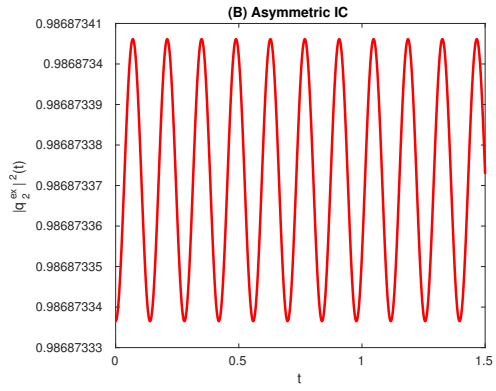

Figure 4.5: The asym. lin. case. Evolution in time of the numerical solutions $|q_2|^2(t)$ with the set of parameters (B).

The non-linear case

Let us now come to the study of the non-linear case and a detailed investigation of the destruction of the beating phenomenon. We start by choosing the same initial condition and the same parameters as in the symmetric linear case (4.42), (4.44) and go on by raising step by step the parameter $\sigma > 0$. The following Figures correspond to the following nonlinearity exponents

$$\sigma = 0.3\,;\ \sigma = 0.6\,;\ \sigma = 0.7\,;\ \sigma = 0.8\,;\ \sigma = 0.82\,;\ \sigma = 0.9\,;\ \sigma = 0.98\,.$$

What has to be mentioned here, is the choice of the parameter γ. We recall that

$$\gamma_{\pm}(t) = \gamma\,|\psi(t,\pm a)|^{2\sigma}\,.$$

Using this formula at the initial instant $t = 0$ with $\gamma_{\pm}(0)$ given as in the symmetric linear case, namely $\gamma_{\pm}(0) = -0.5$, permits after insertion of $\psi_0(\pm a)$ to choose $\gamma < 0$ as follows

$$\gamma := 2\,\gamma_{\pm}(0)\,/\,[|\psi_0(a)|^{2\sigma} + |\psi_0(-a)|^{2\sigma}]\,.$$

In the following Figures 4.6 and 4.7 we plotted the numerical solutions of the Volterra-system (4.8)-(4.9), *i.e.* $|q_1^{num}|^2(t)$ resp. $|q_2^{num}|^2(t)$ (in blue resp. red) as functions of time, and for the different non-linearity exponents given above. At the same time, we plotted in the same Figures, as a reference, the exact solutions of the symmetric linear system, *i.e.* $|q_{beat,1}|^2(t)$ resp. $|q_{beat,2}|^2(t)$ (in cyan resp. magenta). One remarks step by step, how the non-linearity destroies the beating-effect.

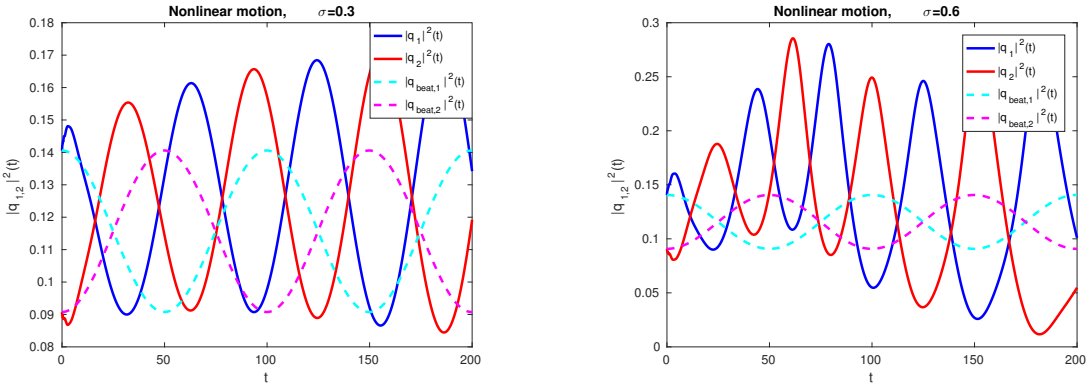

Figure 4.6: The non-linear time-evolution of the numerical solutions $|q_1^{num}|^2(t)$ resp. $|q_2^{num}|^2(t)$ (in blue/red full line) and corresponding linear beating solutions $|q_{beat,1}|^2(t)$ resp. $|q_{beat,2}|^2(t)$ (in cyan/magenta dashed line), for $\sigma = 0.3$ (left) and $\sigma = 0.6$ (right).

To conclude, let us remark that as noticed by many authors, the quantum beating mechanism is highly unstable under perturbations breaking the inversion symmetry of the problem. We also observed this feature in the present work, by analyzing the suppression of the quantum beating in a zero range, non linear, double-well potential.

We decided to perform the numerical studies of the evolution of a beating state in the presence of a non-linear perturbation of a zero-range, double-well potential, when the evolution equation is rephrased as a system of two coupled, weakly-singular Volterra integral equations. In doing this, our aim was to test the effectiveness of this reduction, in order to simplify the numerical simulations of the Schrödinger evolution equations. Furthermore, the very same reduction is possible in dimension two and three, in spite of the fact that much more singular boundary conditions have to be satisfied at any time in those cases. As a consequence, the generalization to higher dimensions is expected to be a feasible task that we want to complete in further works.

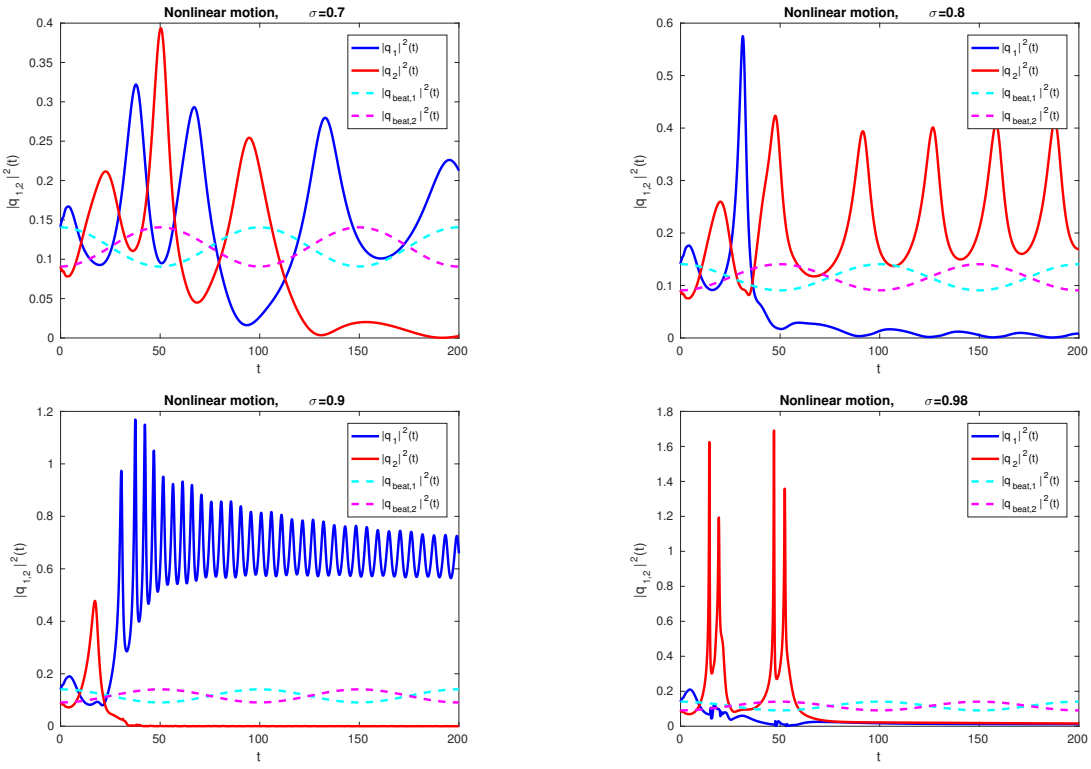

Figure 4.7: The non-linear time-evolution of the numerical solutions $|q_1^{num}|^2(t)$ resp. $|q_2^{num}|^2(t)$ (in blue/red full line) and corresponding linear beating solutions $|q_{beat,1}|^2(t)$ resp. $|q_{beat,2}|^2(t)$ (in cyan/magenta dashed line), for $\sigma = 0.7$, $\sigma = 0.8$, $\sigma = 0.9$ and $\sigma = 0.98$.

CHAPTER 5

CUBIC NONLINEAR SCHRÖDINGER EQUATION FOR THE BEC

Chapter based on the article:
W. Bao, D. Jaksch, P.A. Markowich [1]

The cubic nonlinear Schrödinger equation arises as a model for different phenomena. In particular, it describes the time-evolution of the Bose-Einstein condensate (BEC), which is a gas of atoms evolving at very low temperatures and trapped in a potential well. The particles condensate thus and occupy the single lowest energy state, being not constrained by the Pauli principle (bosons). The effects of the interactions between particles is described via a mean field potential term which gives rise to the nonlinear term in the equation. In this area the governing equation is called the "Gross-Pitaevskii" equation (GPE).

The study of the properties of BECs, like for ex. the stationary ground states, collective excitations, superconductivity, formations of vortices *etc*, passes amongst others through numerical studies. Simulations of a BEC permit in a cheap manner to explore condensed matter physics and open some new pathes for applications.
The main difficulties in the resolution of the GPE are the dimension ($3D$), the nonlinearity as well as the preservation of specific quantities. Time-splitting spectral methods are used in literature to cope with these problems and construct efficient numerical algorithms. The presentation of such schemes is the aim the present chapter.

[1] "Numerical solution of the Gross-Pitaevskii equation for Bose-Einstein condensation", JCP **187** (2003), 318–342.

I THE BOSE-EINSTEIN CONDENSATE

Superconductivity, superfluidity and Bose-Einstein condensation are very captivating phenomena, which can be explained by means of quantum mechanics. They occur only at very low temperatures, in particular below a certain critical temperature T_c, where quantum mechanical effects enter into play. One of their particularities consists in the fact that these three phenomena are different types of macroscopic quantum mechanical revelations, while other quantum mechanical manifestations occur only at atomic or sub-atomic space-scales.

Let us focus on Bose-Einstein condensates. A BEC is a state of matter in which a gas of atoms is cooled down to nearly zero temperature, at which the different atoms saddle together and take the same, lowest energy state (bosons). At this point, the atoms have all the same quantum state, can be considered as identical, obey the Bose-Einstein statistics and start to behave as a whole. Not all atoms give rise to a BEC, in particular not all atoms remain in the liquid state at so small temperatures; one of those leading to a BEC is for ex. the isotope of helium ^4He. The discovery and study of BECs in dilute gases opened new paths to the understanding of quantum mechanics. Fundamental phenomena like coherence, superfluidity, quantum phase transition, nonlinear matter-wave behaviour were studied in this new state of matter. Some typical illustrations of these phenomena are BEC interferences, vortices and vortex lattices, dark and light solitons and so on. In addition to these fundamental aspects, BEC are also thought to have some practical applications, as for example BEC atom lasers for precision measurements, etching, lithography or superposition of BECs to encode quantum bits as a basis for quantum computation. For all these multiple reasons, the study of BECs got very popular in the last years and a vast literature exists [47, 80].

The properties of a BEC at low temperatures, smaller than the critical temperature T_c, are well described by a nonlinear Schrödinger equation for the macroscopic wave function $\psi(t,x)$. Let us remark that the condensate is described by a system of N indistinguishable particles, each one being represented by the same wave-function $\psi(t,x)$, which represents the density probability to find a particle at instant t in the position x. The evolution equation of this wave-function, called also Gross-Pitaevskii equation (GPE), incorporates the trapping potential of the condensate as well as the interaction between particles, which is modelled via a nonlinear mean-field term

$$\mathbf{i}\hbar\partial_t\psi(t,x) = -\frac{\hbar^2}{2m}\Delta\psi + V(x)\psi(t,x) + W(|\psi(t,x)|^2)\,\psi(t,x), \quad \forall (t,x)\in\mathbb{R}^+\times\mathbb{R}^3, \quad (5.1)$$

where the mean-field term is defined as

$$W(\xi) := N\,U_0\,|\xi|^2, \qquad U_0 := \frac{4\pi\,\hbar^2\,a_s}{m},$$

with a_s the wave scattering length, N the number of atoms in the condensate and U_0 the effective interaction-strength between the particles. There are a lot of studies con-

cerning the numerical resolution of the time-independent Gross-Pitaevskii equation in order to investigate the ground-states of a condensate, methods based on a direct minimization of the energy functional []. Equally, there are also many studies dealing with the numerical resolution of the time-dependent equation (5.1), studies based among others on time-splitting spectral methods [16, 17, 35, 37]. These schemes are very appreciated as they have several advantages, they are explicit, unconditionally stable, time-reversible and conserve the particle density. In fact, spectral methods have particularly good accuracy properties and splitting procedures simplify drastically the resolution, permitting considerable computational time and memory savings.
The goal of this chapter will be to introduce such methods for the resolution of (5.1). However, let us first rescale the physical equation in order to identify interesting regimes to be studied.

II SCALING OF THE GROSS-PITAEVSKII EQUATION

The scaling of a physical model, as for ex. (5.1), permits to identify small parameters, describing specific regimes of the Bose-Einstein condensate. Several asymptotic studies can then be carried out, giving rise to a hierarchy of limit models. The scaling procedure starts by identifying the characteristic scales of the phenomenon. Let us thus write each quantity as follows $n = \bar{n}\, n'$, where the constant $\bar{n}$ is the characteristic scale and n' is the new adimensional variable. In the following, the external trapping potential is given under the form of a harmonic potential, *i.e.*

$$V(x,y,z) := \frac{m}{2}(\omega_x^2 x^2 + \omega_y^2 y^2 + \omega_z^2 z^2),$$

where ω_i are the trapping frequencies. With this notation, one has then

$$x := \bar{x}\, x', \quad t := \bar{t}\, t', \qquad \psi(t,x) := \bar{\psi}\, \psi'(t',x'), \quad V(x) := \bar{V}\, V'(x'), \quad W(\xi) := \bar{W}\, W'(\xi').$$

Denoting by $\omega_\star := \min\{\omega_x, \omega_y, \omega_z\}$, the characteristic length of the condensate cloud and the chosen observation time are given by

$$L := \sqrt{\frac{\hbar}{m\omega_\star}}, \qquad \bar{t} := 1/\omega_\star.$$

Now, there are some relations between all these quantities, as for example

$$\bar{\psi}^2 = \frac{1}{\bar{x}^3}, \qquad \bar{V} = m\omega_\star^2 \bar{x}^2, \qquad \bar{W} = N U_0 \bar{\psi}^2.$$

Writing now the GPE in the new dimensionless variables, yields

$$\mathbf{i}\partial_{t'}\psi'(t',x') = -\frac{\hbar}{2m}\frac{\bar{t}}{\bar{x}^2}\Delta\psi' + \frac{\bar{t}\bar{V}}{\hbar}V'(x')\psi'(t',x') + \frac{\bar{t}\bar{W}}{\hbar}W'(|\psi'(t',x')|^2)\,\psi'(t',x'). \quad (5.2)$$

Let us finally define the regime we are interested in. For this, we introduce the two scaling parameters ε and κ, defined as

$$\varepsilon := \left(\frac{L}{\bar{x}}\right)^2, \qquad \kappa := \varepsilon^{5/2} N \frac{4\pi a_s}{L} = \frac{\bar{W}\,\bar{t}^2}{m\,\bar{x}^2},$$

which represent on one hand the ratio between the characteristic condensate length and the observation scale and on the other hand the rescaled interaction-strength parameter. This last parameter can be seen as the ratio between $\bar{W}$ and the kinetic energy of the particle. Omitting the primes for simplicity reasons, the dimensionless Gross-Pitaevskii equation writes now

$$\mathbf{i}\varepsilon\partial_t\psi(t,x) = -\frac{\varepsilon^2}{2}\Delta\psi + V(x)\psi(t,x) + \kappa\,|\psi(t,x)|^2\,\psi(t,x), \quad \forall (t,x)\in\mathbb{R}^+\times\mathbb{R}^3, \tag{5.3}$$

where

$$V(x) = \frac{1}{2}(\gamma_x^2 x^2 + \gamma_y^2 y^2 + \gamma_z^2 z^2), \qquad \gamma_i := \frac{\omega_i}{\omega_\star}.$$

Two different regimes can now be clearly identified, namely

- the case where $\varepsilon \sim 1$ and $\kappa \ll 1$: weakly interacting condensate;
- the case where $\varepsilon \ll 1$ and $\kappa \sim 1$: strongly interacting condensate, semi-classical regime .

The first case is a regular perturbation case, and shall not be treated in the present lecture. The study of the second case, which is a singularly perturbed problem and hence more difficult to treat, will be the main objective of this chapter.

III SPLITTING SCHEMES

Our resolution strategy for (5.3) will be based on a spectral splitting technique, such that we shall first rapidly recall in this section the main idea of splitting methods for the resolution of abstract evolution equations of the type

$$\begin{cases} \partial_t u(t) = L\,u(t) = (A+B)\,u(t), & \forall\, t\in(0,T], \\ u(0) = u_0, \end{cases}$$

with unknown $u:[0,T]\to X$ (X Banach space) and where $L:X\to X$ can be seen as an abstract linear operator (*e.g.* differential operator), which can be decomposed into two distinct parts, the two operators A and B. Such type of problems arise in the modelling of complex physical situations involving phenomena of rather different kind (convection, diffusion, reaction, *etc*), fact which is translated in partial differential equations containing operators that are mathematically very different. This difference in the various terms make the study of these models very challenging from a theoretical as well

as numerical point of view. However, splitting techniques permit to take advantage of this difference in the operators.
Indeed, a splitting method is a strategy consisting in the decoupling of an initially given system (with operator L) into several sub-problems (with operators A resp. B), each one describing a different phenomenon. The aim is then to solve iteratively each of these sub-problems, permitting in this way the use of different analytical or numerical techniques for the respective sub-problems and gaining thus in efficiency. Indeed, one can combine specific numerical methods for each sub-problem, which are conceived for a particular type of equation (parabolic, hyperbolic, ...) in the aim to gain in computational power and reduce memory requirements. There exists a vast literature on splitting methods, we shall only give here the main ideas and refer the interested reader to [42, 48, 91].
Let us however give first some examples of models where splitting schemes can bring some advantages:

Reaction-diffusion equations:
Reaction-diffusion equations arise in biology, epidemology, physics, chemistry *etc*, and can take the form

$$\partial_t u(t,x) = \nabla \cdot (\kappa \nabla u) + f(u), \qquad \forall (t,x) \in (0,T) \times \Omega, \quad \Omega \subset \mathbb{R}^d,$$

where $u(t,x)$ is a concentration or density function, $f(u)$ describes a local, non-linear reaction (birth-death, chemical reaction) and $\kappa > 0$ is a diffusion matrix. A splitting procedure between $A = \nabla \cdot (\kappa \nabla)$ and $B = f(\cdot)$ should permit to treat the non-linearity in a different manner than the linear diffusion operator.

Convection-diffusion equations:
Models that involve a combination of convective and diffusive phenomena arise very often in fluid mechanics, astrophysics, meteorology *etc*, and have typically the form

$$\partial_t q(t,x) + \nabla \cdot f(q) - \nabla \cdot (\kappa \nabla q) = 0, \qquad \forall (t,x) \in (0,T) \times \Omega,$$

where $q(t,x)$ is a concentration (e.g. pollutant in a river), f is a possibly non-linear convective flux-term and $\kappa > 0$ a diffusion matrix. A splitting technique should permit to treat the two rather different phenomena of convection and diffusion in a different way.

Vlasov equation:
The Vlasov equation is an advection equation, describing for ex. the evolution of a gas of charged particles (plasma) in an external or self-consistent electro-magnetic field $(\mathbf{E}, \mathbf{B})$. It takes the form

$$\partial_t f + v \cdot \nabla_x f + \frac{q}{m}(\mathbf{E} + v \times \mathbf{B}) \cdot \nabla_v f = 0, \qquad \forall (t,x,v) \in (0,T) \times \mathbb{R}^{2d},$$

where the distribution function $f(t,x,v)$ stands for the density of particles located at the position $x \in \mathbb{R}^d$ and having the velocity $v \in \mathbb{R}^d$ at instant $t \geq 0$. A splitting procedure in the case without magnetic field $\mathbf{B} \equiv 0$ permits for example to decompose the system into two constant coefficient advection equations, corresponding to the operators $A = v \cdot \nabla_x$ and $B = \frac{q}{m}\mathbf{E} \cdot \nabla_v$, which can be solved explicitly.

Gross-Pitaevskii equation:
As we have seen, the Gross-Pitaevskii equation arises in several fields of application, and has generally the form

$$\mathbf{i}\hbar\partial_t\psi(t,x) = -\frac{\hbar^2}{2m}\Delta\psi + V(x)\psi(t,x) + W(|\psi(t,x)|^2)\,\psi(t,x)\,, \qquad \forall (t,x) \in \mathbb{R}^+ \times \mathbb{R}^d\,.$$

In this case, the splitting between the linear part $A = -\frac{\hbar^2}{2m}\Delta + V$ and the non-linear part $B\psi = W(|\psi(t,x)|^2)\,\psi(t,x)$ or even more simpler, between the free evolution $A = -\frac{\hbar^2}{2m}\Delta$ and the remaining potential-term, can bring several advantages, as will be seen in the following.

Directional splitting (ADI):
Diffusion equations in two or three dimensions, namely

$$\partial_t u(t,x,y,z) = \partial_x(\kappa_x\partial_x u) + \partial_y(\kappa_y\partial_y u) + \partial_z(\kappa_z\partial_z u)\,, \qquad \forall (t,x,y,z) \in \mathbb{R}^+ \times \Omega\,,$$

can be very cumbersome to solve, due to the high dimensionality. It can be then more advantageous to split the operator with respect to the different directions, and solve instead of one $3D$ diffusion problem, three $1D$ problems with $A = \partial_x(\kappa_x\partial_x)$, $B = \partial_y(\kappa_y\partial_y)$ and $C = \partial_z(\kappa_z\partial_z)$. This procedure reduces drastically the memory requirements, the computational time and can be sometimes even the only feasible method.

Splitting procedures can have several big advantages, as mentioned above. For example reduction of the dimensionality, in the ADI-case, or different numerical treatment for the different physical phenomena, like convection and diffusion, or separation of linear and non-linear parts for a better handling. Tailor-made numerical methods can then be used for each sub-system, increasing the efficiency and permitting furthermore the consideration of more complex, realistic problems involving several different physical phenomena.
There are however also some drawbacks with splitting techniques. Indeed, the splitting introduces splitting-errors in the modelling, which have to be estimated with care, in order to evaluate their magnitude as compared to the usual discretization error magnitude. Furthermore, the splitting procedure can also destroy some positivity or conservation properties of the initially given physical problem. For all these reasons, one has to do a detailed study, before applying splitting methods.

Lie and Strang splitting procedures

Let us present now the two most popular splitting methods. For simplicity reasons, we shall consider here a finite-dimensional linear framework and start from the evolution problem

$$\begin{cases} u'(t) = L\,u(t) = (A+B)\,u(t)\,, & \forall\, t \in (0,T)\,, \\ u(0) = u_0 \in \mathbb{R}^m\,, \end{cases} \tag{5.4}$$

with the unknown function $u : (0,T) \to \mathbb{R}^m$ and where $A, B \in \mathbb{R}^{m\times m}$ are two given matrices. One can imagine that these matrices are obtained via a space semi-discretization of some spatial partial differential operators. Introducing now the exponential-matrices

$$\mathscr{A}(t) := e^{tA} \in \mathbb{R}^{m\times m}\,, \quad \mathscr{B}(t) := e^{tB}\,, \quad \mathscr{L}(t) := e^{tL}\,, \quad \forall\, t \in [0,T]\,,$$

the unique exact solution of (5.4) reads $u(t) = \mathscr{L}(t)\,u_0$ for all $t \in [0,T]$.

One would like now to solve the system (5.4) in a splitted manner, for the reasons mentioned above. For this, let us introduce a time-discretization of our interval $[0,T]$:

$$0 = t_0 < \cdots < t_n < \cdots < t_K = T\,, \quad t_n = n * \Delta t\,, \quad \Delta t := T/K\,,$$

and pass from time-step t_n to t_{n+1} by solving iteratively

$$(L)_1 \begin{cases} u_1'(t) = B\,u_1(t)\,, & \forall\, t \in (t_n, t_{n+1}]\,, \\ u_1(t_n) = u_{sp}^n\,, \end{cases} \qquad (L)_2 \begin{cases} u_2'(t) = A\,u_2(t)\,, & \forall\, t \in (t_n, t_{n+1}]\,, \\ u_2(t_n) = u_1(t_{n+1})\,, \end{cases} \tag{5.5}$$

setting

$$u_{sp}^0 := u_0\,, \qquad u_{sp}^{n+1} := u_2(t_{n+1})\,. \tag{5.6}$$

The splitting procedure (5.5)-(5.6) is called *"Lie-splitting"*. If we solve the two systems (5.5) in an exact manner, the splitting-solution and the exact solution of (5.4) at time step t^{n+1} have the exact forms

$$u_{sp}^{n+1} = \mathscr{A}(\Delta t)\,\mathscr{B}(\Delta t)\,u_{sp}^n\,, \qquad u^{n+1} = \mathscr{L}(\Delta t)\,u^n\,, \quad \forall\, n \in \mathbb{N}.$$

If the two matrices commute, *i.e.* $AB = BA$ or equivalently $[A,B] = 0$, then the splitted and not-splitted solutions would be the same, namely $u_{sp}^n = u^n$ for all $n \in \mathbb{N}$, due to the fact that $e^{t(A+B)} = e^{tL}$. However, for not-commuting matrices (or operators more generally) there will be a splitting error, which shall be estimated in the next section.

The Lie-splitting is a first-order accurate method (see Section **??**), in the sense that the splitting error is of the order $\mathscr{O}(\Delta t)$. Let us thus introduce a second order splitting-procedure, called *"Strang-splitting"*, given by the following iterative resolution for the passage $t_n \to t_{n+1}$:

$$(S)_1 \begin{cases} u_1'(t) = A\,u_1(t)\,, & \forall\, t \in (t_n, t_{n+1/2}]\,, \\ u_1(t_n) = u_{sp}^n\,, \end{cases} \qquad (S)_2 \begin{cases} u_2'(t) = B\,u_2(t)\,, & \forall\, t \in (t_n, t_{n+1}]\,, \\ u_2(t_n) = u_1(t_{n+1/2})\,, \end{cases} \tag{5.7}$$

and

$$(S)_3 \begin{cases} u_3'(t) = A\,u_3(t), \quad \forall\, t \in (t_{n+1/2}, t_{n+1}], & u_{sp}^0 := u_0, \\ u_3(t_{n+1/2}) = u_2(t_{n+1}), & u_{sp}^{n+1} := u_3(t_{n+1}). \end{cases} \tag{5.8}$$

This time the error between the exact splitting solution of (5.7)-(5.8) and the exact solution of (5.4), meaning between

$$u_{sp}^{n+1} = \mathscr{A}(\Delta t/2)\,\mathscr{B}(\Delta t)\,\mathscr{A}(\Delta t/2)\,u_{sp}^n, \qquad u^{n+1} = \mathscr{L}(\Delta t)\,u^n,$$

is of the order $\mathscr{O}((\Delta t)^2)$, yielding a second-order splitting technique.

It is now very complicated or impossible to compute the exponential matrices $\mathscr{A}(t)$ resp. $\mathscr{B}(t)$ analytically, such that numerical discretization procedures have to be taken into consideration. Choosing for example the implicit Euler schemes for both systems in (5.5), yields the Lie-scheme

$$u_{sp}^{n+1} = (Id - \Delta t\,A)^{-1}\,(Id - \Delta t\,B)^{-1}\,u_{sp}^n, \quad u_{sp}^0 := u_0; \quad \forall\, n \geq 0. \tag{5.9}$$

Choosing the Euler explicit method for the first system in (5.7), the Euler implicit method for the second system (5.7) on $(t_n, t_{n+1/2})$ only and then the Euler explicit for the remainder of the interval $(t_{n+1/2}, t_{n+1})$, and finally the Euler implicit method for the third system (5.8), gives rise to the Peaceman-Rachford-scheme

$$u_{sp}^{n+1} = (Id - \frac{\Delta t}{2}A)^{-1}\,(Id + \frac{\Delta t}{2}B)\,(Id - \frac{\Delta t}{2}B)^{-1}\,(Id + \frac{\Delta t}{2}A)\,u_{sp}^n, \quad u_{sp}^0 := u_0; \quad \forall\, n \geq 0. \tag{5.10}$$

IV NUMERICAL APPROXIMATION OF THE GPE IN THE SEMI-CLASSICAL LIMIT

The goal of this section is now to introduce a time-splitting Fourier method for the numerical resolution of the following Gross-Pitaevskii equation in the semi-classical limit

$$\mathbf{i}\varepsilon\partial_t\psi(t,x) = -\frac{\varepsilon^2}{2}\Delta\psi + V(x)\psi(t,x) + \kappa|\psi(t,x)|^2\,\psi(t,x), \quad \forall (t,x) \in \mathbb{R}^+ \times \mathbb{R}^3, \tag{5.11}$$

where

$$V(x) = \frac{1}{2}(\gamma_x^2 x^2 + \gamma_y^2 y^2 + \gamma_z^2 z^2), \qquad \gamma_i \in \mathbb{R},$$

and $0 < \varepsilon \ll 1$ is a small perturbation parameter, describing the semi-classical asymptotics. For simplicity reasons, we shall rather focus on a 1D periodic case, such that our

starting problem reads

$$\begin{cases} \mathbf{i}\varepsilon\partial_t\psi(t,x) = -\dfrac{\varepsilon^2}{2}\partial_{xx}\psi + \gamma^2\dfrac{x^2}{2}\psi(t,x) + \kappa|\psi(t,x)|^2\psi(t,x), \quad \forall (t,x)\in(0,T)\times(a,b) \\ \psi(0,x) = \psi_0(x), \quad \forall x\in(a,b), \end{cases} \tag{5.12}$$

associated with periodic boundary conditions in $x = a$ and $x = b$. Let us also introduce the discretization of our domain $(0,T)\times(a,b)$, as follows

$$0 = t_0 < \cdots < t_n < \cdots < t_K = T, \quad t_n = n * \Delta t, \quad \Delta t := T/K,$$

$$a = x_0 < \cdots < x_i < \cdots < x_M = b, \quad x_i = a + i * \Delta x, \quad \Delta x := (b-a)/M.$$

The quantity ψ_i^n shall denote in the sequel a numerical approximation of the exact solution $\psi(t_n, x_i)$ for all $(n,i)\in[0,K]\times[0,M-1]\subset\mathbb{N}^2$. The periodicity conditions imply the relations

$$\psi_0^n = \psi_M^n, \qquad \psi_{-1}^n = \psi_{M-1}^n, \quad \forall n\in\mathbb{N}.$$

Our splitting procedure will be based on the following choice of the splitting-operators A and B

$$A := -\frac{\varepsilon^2}{2}\partial_{xx}, \qquad B\psi := \gamma^2\frac{x^2}{2}\psi + \kappa|\psi|^2\psi,$$

such that we shall solve in a certain iterative manner (Lie or Strang) the two systems

$$\mathbf{i}\varepsilon\partial_t\psi(t,x) = -\frac{\varepsilon^2}{2}\partial_{xx}\psi(t,x), \quad (t,x)\in(t_1,t_2)\times(a,b), \tag{5.13}$$

and

$$\mathbf{i}\varepsilon\partial_t\psi(t,x) = \gamma^2\frac{x^2}{2}\psi(t,x) + \kappa|\psi(t,x)|^2\psi(t,x), \quad (t,x)\in(t_1,t_2)\times(a,b). \tag{5.14}$$

Equation (5.13), which is linear and periodic, shall be solved via a Fourier spectral method, whereas (5.14) is solved explicitly, as the quantity $|\psi(t,x)|^2$ remains invariant in time, such that (5.14) is equivalent to

$$\mathbf{i}\varepsilon\partial_t\psi(t,x) = \gamma^2\frac{x^2}{2}\psi(t,x) + \kappa|\psi(t_1,x)|^2\psi(t,x), \quad (t,x)\in(t_1,t_2)\times(a,b). \tag{5.15}$$

Indeed, multiplying (5.14) by $\bar\psi$ and taking the imaginary part, yields immediately that $\partial_t|\psi(t,x)|^2 = 0$. Let us present now the resolution of these two sub-systems.

Fourier spectral method for (5.13)*:*
For the Fourier method, we shall choose an odd integer $M\in\mathbb{N}$ in the space-discretization,

denote $m := \frac{M-1}{2}$ and represent the x-periodic, unknown function $\psi(t,x)$ as a partial Fourier series, *i.e.*

$$\begin{aligned} \psi(t,x) &= \sum_{k=-\infty}^{\infty} \hat{\psi}_k(t)\, e^{\mathbf{i}\omega k x}, \qquad \hat{\psi}_k(t) := \frac{1}{b-a}\int_a^b \psi(t,x)\, e^{-\mathbf{i}\omega k x}\, dx, \quad \omega := \frac{2\pi}{b-a} \\ \psi(t,x_i) &\approx \sum_{k=-m}^{m} \hat{\psi}_k(t)\, e^{\mathbf{i}\omega k x_i}, \qquad \hat{\psi}_k(t) \approx \frac{1}{M}\sum_{i=0}^{M-1} \psi(t,x_i)\, e^{\mathbf{i}\omega k x_i}. \end{aligned} \tag{5.16}$$

Taking now the Fourier-transform of (5.13) yields an evolution equation for the functions $\hat{\psi}_k(t)$

$$\mathbf{i}\varepsilon\, \partial_t \hat{\psi}_k(t) = \frac{\varepsilon^2}{2}\omega^2 k^2 \hat{\psi}_k(t), \quad \forall (t,k) \in (t_1,t_2)\times\mathbb{Z},$$

which gives immediately

$$\hat{\psi}_k(t) = e^{-\mathbf{i}\frac{\varepsilon}{2}\omega^2 k^2 (t-t_1)}\, \hat{\psi}_k(t_1), \quad \forall (t,k) \in (t_1,t_2)\times\mathbb{Z},$$

permitting thus to compute $\psi_i^{t_2}$ for all $i \in [0, M-1]$, via (5.16), supposing $\psi_i^{t_1}$ known.

Exact integration of the ODE (5.15)*:*
The solution of the ODE (5.15) is immediately given by

$$\psi(t,x) = e^{-\frac{\mathbf{i}}{\varepsilon}\left[\gamma^2 x^2/2 + \kappa|\psi(t_1,x)|^2\right](t-t_1)}\, \psi(t_1,x), \quad \forall (t,x) \in (t_1,t_2)\times(a,b).$$

Global time-splitting Fourier spectral method for (5.12)*:*
Altogether, using a Strang-splitting technique, our numerical scheme for the resolution of the GPE (5.12) writes for all $n \geq 0$, $i = 0, \cdots, M-1$:

$$(Sp) \quad \begin{cases} \psi_i^{(1)} := e^{-\frac{\mathbf{i}}{\varepsilon}\left[\gamma^2 x_i^2/2 + \kappa|\psi_i^n|^2\right]\frac{\Delta t}{2}}\, \psi_i^n, & \psi_i^0 := \psi(0,x_i), \\ \psi_i^{(2)} := \displaystyle\sum_{k=-m}^{m} e^{-\mathbf{i}\frac{\varepsilon}{2}\omega^2 k^2 \Delta t}\, \hat{\psi}_k^{(1)}\, e^{\mathbf{i}\omega k x_i}, & \hat{\psi}_k^{(1)} := \frac{1}{M}\displaystyle\sum_{i=0}^{M-1} \psi_i^{(1)} e^{-\mathbf{i}\omega k x_i} \\ \psi_i^{(3)} := e^{-\frac{\mathbf{i}}{\varepsilon}\left[\gamma^2 x_i^2/2 + \kappa|\psi_i^{(2)}|^2\right]\frac{\Delta t}{2}}\, \psi_i^{(2)}, & \psi_i^{n+1} := \psi_i^{(3)}. \end{cases}$$

For comparison, one can think to use a standard Crank-Nicolson finite difference scheme for a direct resolution of (5.12), which simply writes for all $i = 0, \cdots, M-1$ and $n \geq 0$ as follows

$$\begin{aligned} (CN) \quad \mathbf{i}\varepsilon\frac{\psi_i^{n+1}-\psi_i^n}{\Delta t} = -\frac{\varepsilon^2}{4}\left[\frac{\psi_{i+1}^{n+1}-2\psi_i^{n+1}+\psi_{i-1}^{n+1}}{(\Delta x)^2} + \frac{\psi_{i+1}^{n}-2\psi_i^{n}+\psi_{i-1}^{n}}{(\Delta x)^2}\right] \\ +\gamma^2\frac{x_i^2}{2}\,\frac{\psi_i^{n+1}+\psi_i^n}{2} + \kappa|\psi_i^n|^2\,\frac{\psi_i^{n+1}+\psi_i^n}{2}. \end{aligned} \tag{5.17}$$

This method is unconditionally stable, time-reversible and conserves the total particle density. The big drawback comes from the fact that a linear system has to be solved, which in three dimensions can become very expensive.

For a detailed comparison of these two different schemes (accuracy, stability, mesh-size strategy), we refere the interested reader to the simulation results presented in [16].

BIBLIOGRAPHY

[1] M. Abramowitz, I.A. Stegun, *Handbook of mathematical functions*, Dover Publications, New-York, 2013.

[2] R. Adami, G. Dell'Antonio, R. Figari, A. Teta, *The Cauchy problem for the Schrödinger equation in dimension three with concentrated nonlinearity*, Ann. I.H. Poincaré **AN 20** (2003), pp. 477–500.

[3] R. Adami, L. Erdős, *Rate of decoherence for an electron weakly coupled to a phonon gas*, J. Stat. Phys. **132** (2008), no. 2, pp. 301–328.

[4] R. Adami, R. Figari, D. Finco, A. Teta, *On the asymptotic behaviour of a quantum two-body system in the small mass ratio limit*, J. Phys. A: Math. Gen., **37** (2004), pp. 7567–7580.

[5] R. Adami, R. Figari, D. Finco, A. Teta, *On the asymptotic dynamics of a quantum system composed by heavy and light particles*, Comm. Math. Phys. **268** (2006), no. 3, pp. 819–852.

[6] R. Adami, M. Hauray, C. Negulescu, *Decoherence for a heavy particle interacting with a light one: new analysis and numerics*, CMS (Communications in Mathematical Sciences) 14 (2016), no. 5, pp. 1373–1415.

[7] R. Adami, C. Negulescu, *A numerical study of quantum decoherence*, CiCP (Communications in Computational Physics) 12 (2012), no. 1, pp. 85–108.

[8] R. Adami, A. Teta *A Class of Nonlinear Schroedinger Equations with Concentrated Nonlinearity*, J. Funct. Ana. **180** (2001), pp. 148–175.

[9] R. Adami, A. Teta *A simple model of concentrated nonlinearity*, Op. Theory: Advanaces and Appli. **108** (1999), pp. 183–189.

[10] G. P. Agrawal, *Nonlinear Fiber optics*, Elsevire, New York, 2006.

[11] S. Albeverio, Z. Bre'zniak, L. Dabrowski, *Fundamental solutions of the Heat and Schr¨odinger equations with point interactions*, J. Func. Anal., **130** (1995), pp. 220–254.

[12] S. Albeverio, F. Gesztesy, R. Høgh-Krohn and H. Holden, *Solvable Models in Quantum Mechanics* AMS Chelsea Publishing, Providence R.I, 2005.

[13] A. Arnold, *Mathematical Properties of Quantum Evolution Equations*, in Quantum Transport - Modelling, Analysis and Asymptotics, Lecture Notes in Mathematics **1946**, Springer-Verlag, Berlin, 2008.

[14] A. Arnold, N. Ben Abdallah, C. Negulescu, *WKB-based schemes for the oscillatory 1D Schrödinger equation in the semi-classical limit*, SIAM J. Numer. Anal. 49 (2011), no. 4, pp. 1436–1460.

[15] A. Arnold, C. Negulescu, *Stationary Schrödinger equation in the semi-classical limit: Numerical coupling of oscillatory and evanescent regions*, http://arxiv.org/abs/1606.05207, submitted.

[16] W. Bao, D. Jaksch, P.A. Markowich, *Numerical solution of the Gross-Pitaevskii equation for Bose-Einstein condensation*, JCP **187** (2003), 318–342.

[17] W. Bao, S. Jin, P.A. Markowich, *Numerical study of time-splitting spectral discretizations of nonlinear Schrödinger equations in the semi-classical regimes* SIAM J. Sci. Comput. **25** (2003), no. 1, pp. 27–64.

[18] A. Batkai, P. Csomos, G. Nickel, *Operator splittings and spatial approximations for evolution equations*, J. of Evolution Equations **9** (2009), no. 3, pp. 613–636.

[19] N. Ben Abdallah, P. Degond, *On a hierarchy of macroscopic models for semiconductors*, J. Math. Phys. **37** (1996), pp. 3306–3333.

[20] N. Ben Abdallah, P. Degond, P. A. Markowich, *On a one-dimensional Schrödinger-Poisson scattering model*, ZAMP 48 (1997), pp. 35–55.

[21] N. Ben Abdallah, O. Pinaud, *Multiscale simulation of transport in an open quantum system: Resonances and WKB interpolation*, J. Comput. Phys., 213 (2006), no. 1, pp. 288–310.

[22] A. Bertoni, *Simulation of Electron Decoherence Induced by Carrier-Carrier Scattering*, J. Comp. El. 2 (2003), pp. 291–295.

[23] Ph. Blanchard, D. Giulini, E. Joos, C. Kiefer, J. Kupsch, I.-O. Stamatescu, H.D. Zeh, *Decoherence and the Appearance of a Classical World in Quantum Theory*, Springer, 1996.

[24] I. Bloch, *Quantum coherence and entanglement with ultracold atoms*, Nature **453** (2008), pp. 1016–1022.

[25] H.-P. Breuer, F. Petruccione, *The Theory of Open Quantum Systems*, Oxford University Press, Oxford, 2007.

[26] C. Cacciapuoti, R. Carlone, R. Figari, *Decoherence induced by scattering: a three dimensional model*, J. Phys. A: Math. Gen., 38, n. 22 (2005), pp. 4933—4946.

[27] A.O. Caldeira, A.J. Leggett, *Influence of damping on quantum interference: an exactly soluble model*, Phys. Rev. A **31** (1985), pp. 1059.

[28] E. Cances, C. Le Bris, Y. Maday, *Méthodes mathématiques en chimie quantique*, Springer-Verlag Berlin Heidelberg, 2006.

[29] H. Caratarius, D. Haag, D. Dast, G. Wunner, *Nonlinear Schrödinger equation for a $\mathscr{PT}$ -symmetric delta-function double well*, Journal of Physics A: Mathematical and Theoretical **45** (2012).

[30] T. Cazenave, *An introduction to nonlinear Schrödinger equations*, Instituto de Matemática, UFRJ **26**, 1993.

[31] T. Cazenave, *Semilinear Schrödinger equation*, Courant Lecture Notes in Mathematics AMS **10**, 2003.

[32] F. F. Chen *Plasma Physics and controlled fusion*, Springer Verlag New York, 2006.

[33] J. Clark, *The reduced effect of a single scattering with a low-mass particle via a point interaction*, J. Func. An. 256 (2009), no. 9, pp. 2894–2916.

[34] C. Cohen-Tannoudji, B. Diu, F. Laloë *Mécanique quantique I*, Hermann éditeurs des sciences et des arts, Paris, 1998.

[35] S. Descombes, M. Thalhammer, *An exact local error representation of exponential operator splitting methods for evolutionary problems and applications to linear Schrödinger equations in the semi-classical regime*, BIT Numer. Math. **50** (2010), pp. 729–749.

[36] G. Dujardin, E. Faou, *Normal form and long time analysis of splitting schemes for the linear Schrödinger equation with small potential*, Num. Math. **106** (2007), no. 2. pp. 223–262.

[37] G. Dujardin, E. Faou, *Long time behavior of splitting methods applied to the linear Schrödinger equation* C.R. Acad. Sci. Paris, Sér. UI. **344**, PP. 89–92.

[38] D. Dürr, R. Figari, A. Teta, *Decoherence in a two-particle model*, J. Math. Phys. 45 (2004), no. 4, pp. 1291–1309.

[39] D. Dürr, H. Spohn, *Decoherence Through Coupling to the Radiation Field*, in "Decoherence: Theoretical, Experimental and Conceptual Problems", Lect. Notes in Phys. 538 (2000), Springer, pp. 77–86.

[40] W. E *Principles of multiscale modeling*, Cambridge university press, 2011.

[41] R. Fukuizumi, A. Sacchetti, *Bifurcation and Stability for Nonlinear Schrödinger Equations with DoubleWell Potential in the Semiclassical Limit*, J. Stat. Phys. **145**, No. 6 (2011), pp. 1546–1594.

[42] L. Gauckler, C. Lubich, *Splitting integrators for nonlinear Schrödinger equations over long times*, Found. Comput. Math. **10** (2010), no. 3, pp. 275–302.

[43] B. Gaveau, R.S. Schulman, *Explicit time-dependent Schrödinger propagators*, J. Phys. A: Math. Gen. 19 (1986), 1833–1846.

[44] A.K. Ghatak, R.L. Gallawa, I.C. Goyal, *Modified Airy Function and WKB Solutions to the Wave Equation*, NIST Monograph 176, 1991.

[45] A.K. Ghatak, R.L. Gallawa, I.C. Goyal, *Accurate Solutions to Schrödinger's Equation Using Modified Airy Functions*, IEEE J. of Quantum Electr., 28 (1992), no. 2, pp. 400–403.

[46] V. Grecchi, A. Martinez, A. Sacchetti, *Destruction of the Beating Effect for a Non-Linear Schrödinger Equation*, Comm. Math. Phys. **227** (2002), pp. 191–209.

[47] A. Griffin, D. Snoke, S. Stringaro (Eds), *Bose-Einstein Condensation*, Cambridge university press, New York, 1995.

[48] E. Hansen, A. Ostermann, *Dimension splitting for evolution equations*, Numer. Math. **108** (2008), 557–570.

[49] H.A. Haus, *Waves and Fields in Optoelectronics*, Prentice-Hall. Englewood Cliffs NJ, 1984.

[50] M.H. Holmes, *Introduction to perturbation methods*, Springer-Verlag, New York, 1995.

[51] K. Hornberger, J.E. Sipe, *Collisional decoherence reexamined*, Phys. Rev. A **68** (2003), pp. 1–16.

[52] K. Hornberger, S. Uttenhaler, B. Brezger, L. Hackermüller, M. Arndt, A. Zeilinger, *Collisional decoherence observed in matter wave interpherometry*, Phys. Rev. Lett., **90** (2003), pp. 160401.

[53] K. Hornberger, B. Vacchini, Monitoring derivation of the quantum linear Boltzmann equation, Phys. Rev. A, 77, (2008), 022112 1–18.

[54] F. Ihlenburg, I. Babuška, *Finite element solution of the Helmholtz equation with high wave number. I. The h-version of the FEM*, Comput. Math. Appl., 30 (1995), no. 9, pp. 9–37.

[55] F. Ihlenburg, I. Babuška, *Finite element solution of the Helmholtz equation with high wave number. II. The h-p version of the FEM*, SIAM J. Numer. Anal., 34 (1997), no. 1, pp. 315–358.

[56] T. Jahnke, C. Lubich, *Numerical integrators for quantum dynamics close to the adiabatic limit*, Numerische Mathematik, 94 (2003), pp. 289–314.

[57] S. Jin, *Efficient Asymptotic-Preserving (AP) schemes for some multiscale kinetic equations*, SIAM J. Sci. Comp., Vol. 21 (1999), pp. 441–454.

[58] E. Joos, H.D. Zeh, *The emergence of classical properties through interaction with the environment*, Z. Phys., **B59** (1985), pp. 223–243.

[59] C. Kharif, E. Pelinovsky, A. Slunyaev, *Rogue waves in oceans*, Springer-Verlag Berlin Heidelberg, 2009.

[60] L.D. Landau, E.M. Lifschitz, *Quantenmechanik*, Akademie-Verlag, Berlin, 1985.

[61] R.E. Langer, *On the asymptotic solutions of ordinary differential equations, with an application to the Bessel functions of large order*, Transact. AMS, 33 (1931), no. 1, pp. 23–64.

[62] C. Le Bris *Systemes multi-échelles. Modélisation et simulation*, Springer Verlag Berlin-Heidelberg, 2005.

[63] C. S. Lent, D. J. Kirkner, *The Quantum Transmitting Boundary Method*, J. Appl. Phys., 67 (1990), pp. 6353–6359.

[64] K. Lorenz, T. Jahnke, C. Lubich, *Adiabatic integrators for highly oscillatory second-order linear differential equations with time-varying eigendecomposition*, BIT, 45 (2005), no. 1, pp. 91–115.

[65] Ch. Lubich, *From quantum to classical molecular dynamics: reduced models and numerical analysis*, European Mathematical Society, 2008.

[66] M. Lundstrom *Fundamentals of carrier transport*, Cambridge University Press, 2000.

[67] M. Lundstrom, J. Guo *Nanoscale transistors*, Springer Verlag, 2006.

[68] P.A. Markowich, C.A. Ringhofer, C. Schmeiser *Semiconductor equations*, Springer Verlag Wien, 1990.

[69] E. Middlemas, J. Knisley *Soliton Solutions of a Variation of the Nonlinear Schrodinger Equation*, Springer Proceedings in Mathematics & Statistics series **64** (2013), 39–53.

[70] I. Mitra, S. Roy, *Relevance of quantum mechanics in circuit implementation of ion channels in brain dynamics*, arXiv: q-bio/0606008.

[71] J.D. Murray, *Mathematical biology*, Springer-Verlag Berlin Heidelberg, 2002.

[72] A.H. Nayfeh, *Perturbation methods*, Wiley, New York, 1973.

[73] C. Negulescu, *Numerical analysis of a multiscale finite element scheme for the resolution of the stationary Schroedinger equation*, Numerische Mathematik, 108 (2008), no. 4, pp. 625–652.

[74] C. Negulescu, N. Ben Abdallah, M. Mouis, *An accelerated algorithm for 2D simulations of the quantum ballistic transport in nanoscale MOSFETs*, Journal of Computational Physics, 225 (2007), no. 1, pp. 74–99.

[75] R. Omnès, *The Interpretation of Quantum Mechanics* Princeton University Press, Princeton, 1994.

[76] M. Onorato, S. Residori, U. Bortolozzo, A. Montina ,F.T. Arecchi, *Rogue waves and their generating mechanisms in different physical contexts*, Physics report **528** (2013), no. 2, pp. 47–89.

[77] A. Osborne *Nonlinear Ocean Waves & the Inverse Scattering Transform*, International Geophysics Series, vol. 97, Academic Press, Burlington MA, 2010.

[78] A. Pazy, *Semigroups of linear operators and applications to partial differential equations*, Springer-Verlag, New-York, 1983.

[79] H.L. Pécseli, *Waves and Oscillations in Plasmas*, Taylor & Francis Group, 2013.

[80] C.J. Pethick, H. Smith, *Bose-Einstein condensation in dilute gases*, Cambridge university press, 2008.

[81] V. Petviashvili, O. Pokhotelov *Solitary waves in plasmas and in the atmosphere*, Gordon and Breach, Philadelphia, 1992.

[82] M. Reed, B. Simon, *Methods of Modern Mathematical Physics vol I: Functional Analysis*, Academic Press Inc., 1970.

[83] M. Reed, B. Simon, *Methods of Modern Mathematical Physics vol III: Scattering Theory*, Academic Press Inc., 1970.

[84] I. Rodnianski, B. Schlein, *Quantum fluctuations and rate of convergence towards mean field dynamics*, Commun. Math. Phys. 291 (2009), pp. 31–61.

[85] P. H. Rutherford *Nonlinear growth of the tearing mode*, Physics of Fluids 16 (1973), pp. 1903.

[86] A. Sacchetti, *Universal Critical Power for Nonlinear Schrödinger Equations with a Symmetric Double Well Potential*, Phys. Rev. Letters **103** (2009), pp. 194101.

[87] M. Schechter, Operator Methods in Quantum Mechanics, Courier Dover Publications, 2003.

[88] M. Schlosshauer, Decoherence and the Quantum-To-Classical Transition, Springer-Verlag, 2007.

[89] P. W. Shor, *Scheme for reducing decoherence in quantum computer memory*, Phys. Rev. A **52** (1995), no. 4, pp. 2493–2496.

[90] A.J. Smith, A.R. Baghai-Wadji, *A Numerical Technique for Solving Schrödingers Equation in Molecular Electronic Applications*, in "Smart Structures, Devices, and Systems IV", Proc. of SPIE Vol. 7268, 2008.

[91] B. Sportisse, *An analysis of operator splitting techniques in the stiff case*, Journal of Computational Physics **161** (2000), 140–168.

[92] C. A. Stafford, D. M. Cardamone, S. Mazumadar *The quantum interference effect transistor*, Nanotechnology **18** (2007), no. 42, pp. 1–6.

[93] C. Sulem, P.L. Sulem, *The nonlinear Schrödinger equation*, Springer-Verlag New-York, 1999.

[94] J. Vázquez, *The porous medium equation: mathematical theory*, Oxford University Press, USA, 2007.

[95] W. Zhang, N. Konstantinidis, K. A. Al-Hassanieh, V. V. Dobrovitski *Modelling decoherence in quantum spin systems*, J. Phys. Condens. Matter **19** (2007), no. 8, pp. 1–28.